High-Valent Perfluoronickelacycles:

Intermediates for “Green” Routes to Fluorocarbons and Their Derivatives

By

Nicole Marie Hunter

Thesis submitted to the
Faculty of Graduate and Postdoctoral Studies
University of Ottawa
in partial fulfillment of the requirements for the degree of

Master of Science

Centre for Catalysis Research and Innovation
Department of Chemistry
Ottawa-Carleton Chemistry Institute
Faculty of Science
University of Ottawa

Table of Contents

Abstract

Fluorocarbons (FCs) and their derivatives (FCDs) are heavily relied on due to their wide range of uses (e.g. solvents, surfactants, refrigerants, and pharmaceuticals). Currently, FCs and FCDs are produced on an industrial scale *via* energy-intensive processes, using hazardous materials. Hence, new catalytic chemical technologies are required to provide cleaner and greener synthetic routes to partially fluorinated materials. The exploration of fundamental organofluorometallic chemistry of base metals, such as nickel, has potential to advance the development of novel catalytic processes towards this end. It has been established previously that zero-valent nickel complexes have the ability to efficiently catalyze the hydrodimerization of polyfluoroalkenes. The reactivity of the intermediate polyfluoronickelacycles was found to be influenced by modifications in the ligand sphere. Furthermore, an increase in oxidation state of the central metal atom was proposed as an additional strategy to increase the reactivity of the M-R_F bond. In this thesis, through variation of the ligand environment and oxidation state of nickel, we have further developed the chemistry of high-valent polyfluoronickelacycles. Synthesis and characterization (NMR, EPR, UV/Vis, IR spectroscopy and electrochemistry) of new trivalent polyfluoronickelacycles are described as well as attempts to generate the corresponding tetravalent cations. Attempts to induce nucleophilic insertion of acetonitrile into the Ni-R_F bond were also investigated herein. Challenges were encountered with the isolation of the tetravalent cations due to decomposition to the corresponding divalent nickelacycle.

Table of Compounds

#	Compound	#	Compound
31	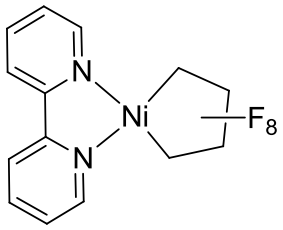	**34**	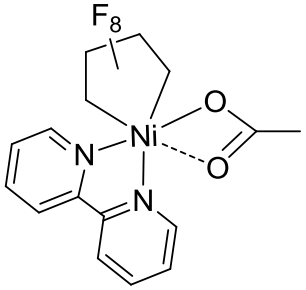
35	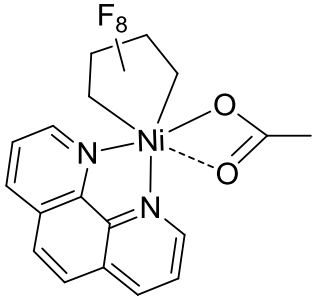	**36**	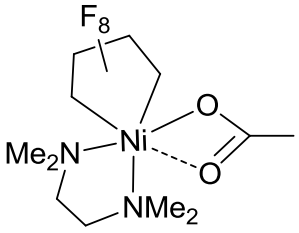
37	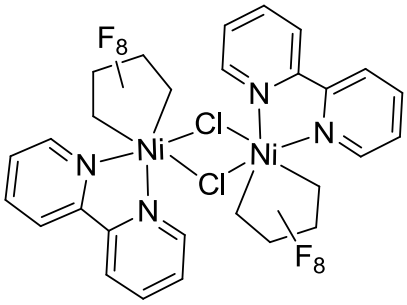	**39**	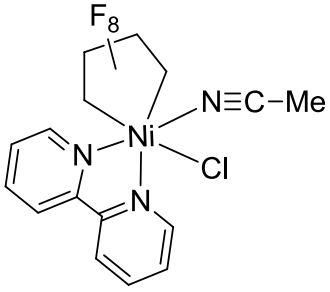
40	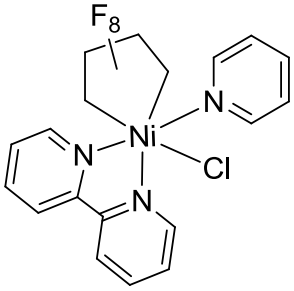		

List of Figures

List of Tables

List of Schemes

List of Abbreviations

Δ	heating or a difference (as in ΔE_p)
δ	chemical shift, in ppm
λ	wavelength
ρ_{calc}	calculated density
Å	Angstrom
Ar	aryl group
Ar_F	perfluorinated aryl group
ATR	attenuated total reflectance
bipy	2,2'-bipyridine
°C	degrees Celsius
CAN	ceric ammonium nitrate, $(NH_4)_2Ce(NO_3)_6$
CCDC	Cambridge Crystallographic Data Centre
cdt	t,t,t-cyclododeca-1,5,9-triene
cod	1,5-cyclooctadiene
CFCs	chlorofluorocarbons
CW	continuous wave
CV	cyclic voltammetry or cyclic voltammogram
DFT	density functional theory
dmad	dimethyl acetylenedicarboxylate
dmap	4-dimethylaminopyridine
DME	1,2-dimethoxyethane
EA	elemental analysis

ΔE_p	difference in peak potential (E_{pa} - E_{pc})
$E_{1/2}$	half wave potential
E_{pa}	anodic peak potential
E_{pc}	cathodic peak potential
ESI	electrospray ionization
Et	ethyl
ET	electron transfer
Et_2O	diethyl ether
EPR	electron paramagnetic resonance (electron spin resonance)
fw	formula weight
FC(s)	fluorocarbon(s)
FCD(s)	fluorocarbon derivative(s)
GOF	goodness of fit
HOMO	highest occupied molecular orbital
HPLC	high-pressure liquid chromatography
JT	Jahn-Teller
L	neutral donor ligand
LUMO	lowest unoccupied molecular orbital
Me	methyl
MS	mass spectrometry or mass spectrogram
M_W	molecular weight
N-N	bidentate nitrogen ligand
NMR	nuclear magnetic resonance

nor	norbornyl
NPA	natural population analysis
OAc	acetate
OC	open circuit
[ox]	chemical or electrochemical oxidation
PFOA	perfluorooctanoic acid
Ph	phenyl
phen	1,10-phenanthroline
^{i}Pr	isopropyl
py	pyridine
R	alkyl group
R_F	perfluorinated alkyl group
r.t.	room temperature
^{t}Bu	*tert*-butyl
TMS	trimethylsilyl
TFA	trifluoroacetic acid
TFE	tetrafluoroethylene
THF	tetrahydrofuran
tmeda	*N,N,N'N'*-tetramethylethylenediamine
UV/Vis	ultraviolet-visible
V	volume
XRD	single crystal X-ray diffraction

Acknowledgements

Firstly, I would like to thank my parents and two sisters, Denise and Kelly, for all of your support and for always being there. To my supervisor, Dr. R. Tom Baker, thank you for your guidance and for giving me this opportunity to study with you. I extend my sincere thanks to William Wright for your friendship, support, and help throughout this process. To Matt Rankin, thank you for offering your help and advice. Thanks Christian Díaz Urrutia for your insight with HPLC/MS experiments and for your friendship. I also extend my thanks to all the other members of the Baker group, especially to Stephanie Granville, Sib Mal, Timo Ott, and Amani Farhat. To Tony St-Jacques and Dr. Serge Gorelsky, thank you for all of the time and effort spent performing the DFT calculations and further computational work. To Dr. Wendy Pell, thank you for all of your help and for useful discussions pertaining to electrochemical analysis. Furthermore, thanks to Dr. Darrin Richeson for allowing me the use of your glovebox for initial electrochemical investigations. Crystallographer Dr. Ilia Korobkov is thanked for XRD analysis. Dr. Glen Facey is thanked for help with NMR experiments. Erika Wee and Dr. Tito Scaiano are thanked for spectrophotometer access. Thank you Dr. Sushil Misra and Mohammed Alsawafta for your collaboration and help in running EPR measurements at Concordia University. My thanks is extended to Dr. Xavier Ottenwaelder and Mohammed Askari for allowing me the use of your glovebox for sample preparation and for welcoming me to Montreal. Further thanks to Dr. Sushil Misra and Anna Nalepa for low temperature (10 K) EPR measurements and Max-Plank Institute fur Bioanorganische Chemie, Mulheim an der Ruhr, Germany for providing facilities.

1. Introduction

1.1. Importance of Fluorocarbons and their Environmental Impact

Fluorocarbons (FCs) and their derivatives (FCDs) are produced on a massive industrial scale and are heavily relied on due to their wide range of uses as solvents, surfactants, refrigerants, propellants, anesthetics and pharmaceuticals.[1] Furthermore, polymers based on fluorocarbons, such as Krytox™ and Teflon™, are exceptionally valuable as heat- and wear-resistant sealants, and non-stick coatings.[1] Synthetic routes to many important fluoropolymers employ radical initiators at either high temperatures or pressures, or environmentally problematic fluorosurfactants in aqueous emulsions.[2] One fluorinated reagent currently being employed for which there are growing concerns regarding toxicity is perfluorooctanoic acid (PFOA), which has been linked to low birth weight in humans and carcinogenicity in laboratory animals.[3] The 2010/15 PFOA Stewardship Program commenced in 2006 with the intent to reduce emissions of PFOA, precursor chemicals that can break down to PFOA, and related higher homologue chemicals, by 95% in the year 2010 and to achieve a complete phase-out of PFOA by 2015.[4] Although many organofluorine compounds are non-toxic, of concern is their persistence in the environment, resulting from the considerable stability of their carbon-fluorine bonds.

There has been wide-reaching interest in developing and understanding the processes involved in the 'green' synthesis of organofluorine compounds to replace energy-intensive and wasteful processes with more efficient alternatives and also to phase-out environmentally hazardous feedstocks and products.[5] New chemical technologies are required to provide cleaner and greener synthetic routes to partially fluorinated materials, notably hydrofluorocarbons, as these products would retain many of the useful properties of perfluorocarbons yet will undergo more rapid environmental degradation due to the reactive carbon-hydrogen bonds.[1]

1.2. Organofluorometallic Chemistry

One potential route to the production of FCs and FCDs by less environmentally damaging methods is by developing catalytic or metal-mediated routes. A large number of fundamental studies have previously been undertaken, examining the interactions of fluorinated substrates with metal complexes and select examples will be highlighted herein.

Pioneering work by Stone has provided insights into the interactions of metal centers with organofluorine compounds, notably metallacycle formation from fluoroalkenes.[6] The reactivity of perfluoroalkyl groups can be described as having pseudohalide characteristics due to their high group electronegativity. In 1961, Stone explored the reactivity of perfluoroalkyl iodides with low-valent transition metal complexes.[7] It was discovered that perfluoroalkyl iodides oxidatively add to $[Fe(CO)_5]$ to afford $[FeI(R_F)(CO)_4]$, with the I and R_F groups occupying *cis* positions in the product complex.[7] This transformation can be formally compared to the reaction of the carbonyl complex with I_2 to give $[FeI_2(CO)_4]$ due to the similarities between R_FI and I_2 (Scheme 1). Furthermore, $[Co(\eta^5\text{-}C_5H_5)(CO)_2]$ was found to undergo an analogous oxidative addition with perfluoroalkyl iodides to give $[CoI(R_F)(\eta^5\text{-}C_5H_5)(CO)]$, where Co^I (d^8) is oxidized to Co^{III} (d^6).[8]

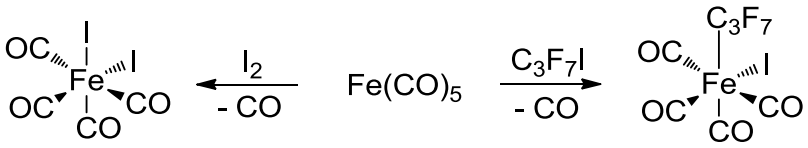

Scheme 1. Oxidative additions of I_2 and C_3F_7I to $[Fe(CO)_5]$.

The reactivity of late transition metal(0) complexes with tetrafluoroethylene (TFE) has been shown to yield a number of complexes through oxidative addition to the metal center (Figure 1). Formation of $[Pt(CF_2CF_2)(PPh_3)_2]$ (**1**) was achieved *via* treatment of $[Pt(PPh_3)_4]$ with TFE.[9] It is clear from in-depth ^{19}F NMR analysis that **1** is most accurately described as a metallacyclopropane with σ-bonds between the platinum and carbon atoms. At ambient temperatures, no rotation about the axis through the metal atom and midpoint of the carbon-carbon bond was apparent for **1**, in contrast to that observed for the hydrocarbon analogue, $[Pt(CH_2CH_2)(PPh_3)_2]$. Furthermore, the geminal fluorine-fluorine coupling constants for the CF_2 group were much higher then would be expected for fluorine atoms bonded to an sp^2 hybridized carbon atom. This is indicative of a metallacyclopropane complex containing sp^3-hybridized carbon atoms. Another common bonding mode for TFE involves the bridging of metal atoms. It has been demonstrated that TFE can insert into metal-metal bonds, as in the case of $[(CO)_4Co\text{-}Co(CO)_4]$ to form the bridged species $[(CO)_4Co\text{-}CF_2CF_2\text{-}Co(CO)_4]$.[10] In a further example, reaction of $[Pt(cod)_2]$ with excess TFE yielded $[Pt(\mu\text{-}C_4F_8)(cod)]_2$ (**2**) where the two metal centers were doubly bridged by CF_2CF_2 units.[11] The coupling of two TFE molecules at a metal center to form MC_4F_8 rings has been observed in a number of cases, yielding complexes classified as metallacycles. A metallacycle is widely defined as a carbocyclic system where at least one atom has been replaced with a transition metal.[12] Stone first isolated the metallacycle complexes $[Fe(C_4F_8)(CO)_4]$ (**3**),[13] and $[Co(C_4F_8)(\eta^5\text{-}C_5H_5)(CO)]$ (**4**),[14] by treatment of $[Fe(CO)_5]$ or $[Co(\eta^5\text{-}C_5H_5)(CO)_2]$ with TFE.

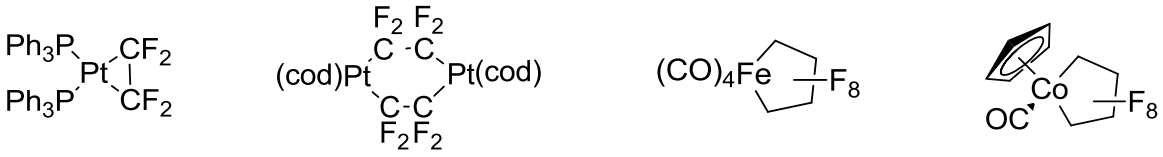

1 **2** **3** **4**

Figure 1. Selected complexes resulting from the oxidative addition of TFE to group VIII metal(0) centers.

1.3. Formation of Perfluorometallacycles

Metallacycles have been identified as key intermediates in a number of syntheses involving transition metals in either catalytic or stoichiometric transformations.[12] One commonly employed synthetic method for metallacycle formation is oxidative homocoupling of activated alkenes or alkynes.[12] In 1970, Stone reported a detailed study outlining the synthesis of a number of perfluorometallacycle complexes resulting from reactions of low valent nickel complexes with unsaturated fluorocarbons.[15] While metallacyclopropane complexes, such as **1**, were observed for platinum, reactions of TFE with a number of nickel(0) complexes resulted in the formation of stable metallacyclopentane complexes, **6**-**10** (Scheme 2).[16] In contrast, the treatment of the *t,t,t*-cyclododeca-1,5,9-triene nickel complex, [Ni(cdt)] with TFE afforded the metallacyclopropane complex [Ni(CF_2CF_2)(cdt)] (**11**).

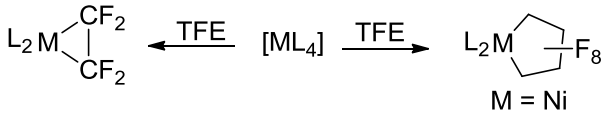

1 L = PPh_3 (M = Pt)
11 L = cdt (M = Ni)

6 L = PPh_3
7 L = $PMePh_2$
8 L = PEt_3
9 L= $P(^nBu)_3$
10 L = $P(OMe)_3$

Scheme 2. Metallacyclopropane versus metallacyclopentane formation in reactions of group 10 transition metal(0) complexes with TFE.

Treatment of [Ni(CF_2CF_2)(cdt)] (**11**) with triphenylphosphine yielded [Ni(CF_2CF_2)(PPh_3)$_2$], which in the presence of TFE rapidly afforded the metallacycle [Ni(C_4F_8)(PPh_3)$_2$] (**6**).[17] This study suggests that metallacyclopropane is an intermediate in the formation of the metallacyclopentane complex (Scheme 3). The inability of **11** to access the metallacyclopentane complex in the presence of TFE is likely due to steric hindrance of the bulky cdt ligand, which inhibits the coordination of a second fluoroalkene molecule. Interestingly, metallacycles comprised of more than five atoms have not been accessed *via* reaction of TFE with any group 10 transition metal complex.[6] Formation of metallacyclopropane versus metallacyclopentane complexes is controlled by a number of variables, including the group 10 metal involved, the relative σ-donor and π-acceptor properties of the ligands, and the nature of the fluorocarbon substrate molecules.

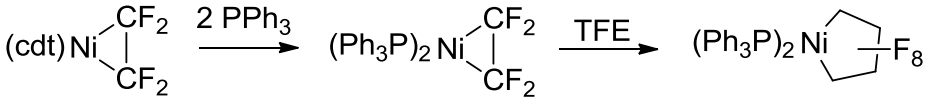

Scheme 3. Formation of [Ni(C_4F_8)(PPh_3)$_2$] (**6**) *via* a metallacyclopropane intermediate.

Polyfluorometallacycles can also be generated *via* the oxidative heterocoupling of alkenes and alkynes. Treatment of [Ni(η^2-$C_{10}H_6$)L_2] (L = PEt_3) with TFE resulted in the metallacycle **12**.[18] Furthermore, reaction of the C_2F_4 insertion product, **12**, with dimethyl acetylenedicarboxylate (dmad, RCCR [R = CO_2Me]) gave the seven-membered nickelacycle **13** (Scheme 4).

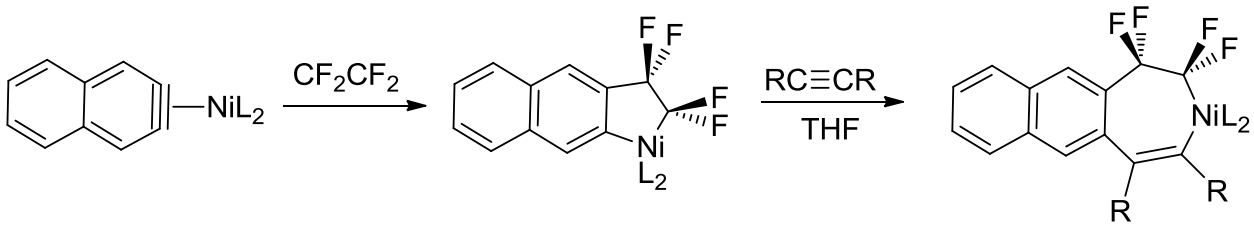

12 **13**

Scheme 4. Expansion of mixed metallacycle system. R = CO_2Me, L = PEt_3.

The analogous benzyne complex [Ni(η^2-C_6H_4)L_2] (L = PEt_3) was treated with TFE to afford **14** (Scheme 5) and subsequent treatment with CO (1 atmosphere) induced a reversible insertion into the Ni-Ar (aryl) bond generating complex **15** (Scheme 5).[19] Further reaction with CO, afforded [Ni$(CO)_2L_2$] and the cyclic organofluorine species **16** as highlighted in Scheme 5. Notably, insertions of both CO and dmad occurred exclusively into the Ni-Ar bond as opposed to the Ni-R_F (perfluoroalkyl) bond.

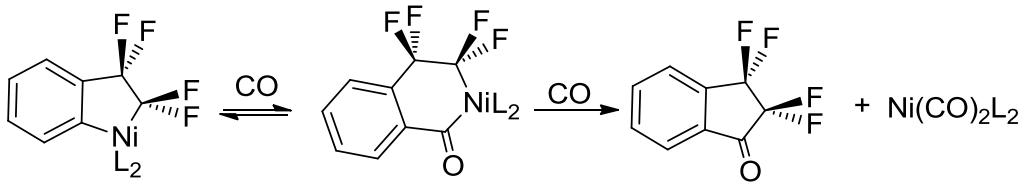

14 **15** **16**

Scheme 5. Insertion of CO into mixed metallacycle system and subsequent elimination of an organofluorine species. R = CO_2Me, L = PEt_3.

1.4. Insertion into the M-R_F Bond

The reactivity of M-R_F (perfluoroalkyl) bonds differs greatly from that of related M-R (alkyl) bonds, due to the inherent electronegativity of fluorine atoms and subsequent electropositive nature of the α-carbon of the R_F moiety. Thus, the increased ionic nature of the M-R_F bond results in a stronger interaction and, consequently, the multitude of different insertions observed for M-R bonds has not been achieved in related fluorinated derivatives.[20]

In contrast, CO insertion into the M-Ar_F (perfluoroaryl) bond has been observed *via* electrochemical and chemical oxidation.[21] The complex [Mo(C_6F_5)(η^7-C_7H_7)$(CO)_2$] (**17**) was demonstrated to undergo oxidatively induced CO insertion upon chemical oxidation, with $NOBF_4$ or ceric ammonium nitrate (CAN, $(NH_4)_2Ce(NO_3)_6$), in methanol to form methyl pentafluorobenzoate. It was proposed that this transformation involves a reversible electron transfer and subsequent competing reactions (Scheme 6). Pentafluorobenzene was suggested to result from direct reaction of the generated 17-electron cationic species **18** with methanol, prior to CO insertion, followed by further oxidation (Scheme 6). Conversely, the formation of methyl pentafluorobenzoate was proposed to result from insertion of CO into the Mo-C_6F_5 bond of the 17-electron cationic species **18** to afford **19**, followed by reaction with methanol and further

oxidation (Scheme 6). These findings suggest that similar insertions may be possible for M-R_F bonds of high-valent metal complexes.

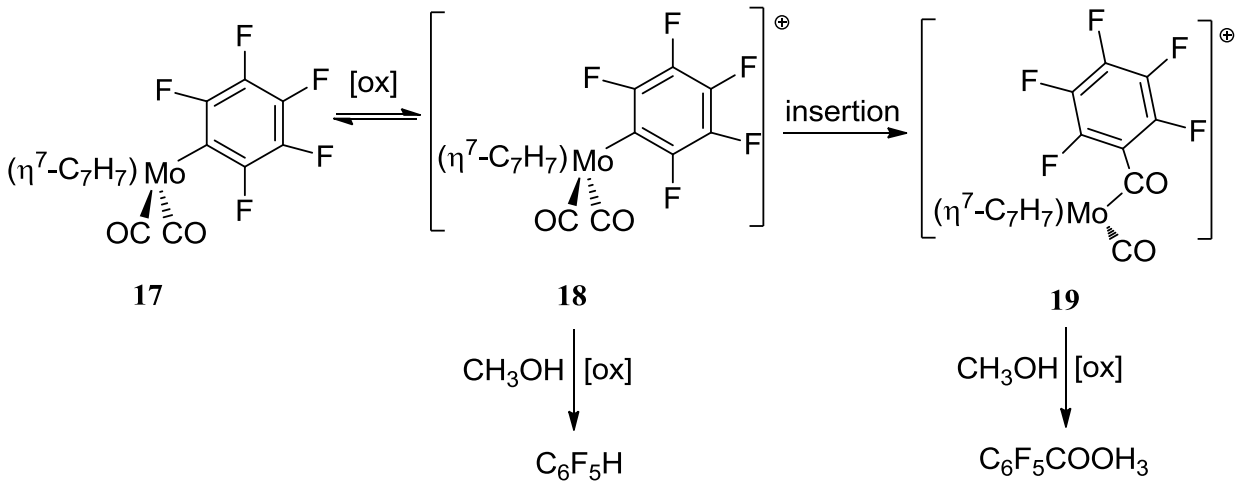

Scheme 6. CO insertion into the Mo-C_6F_5 bond by chemical or electrochemical oxidation [ox].

Although CO insertion into a Mo-Ar_F bond was achieved, attempts to induce insertion of CO into the Fe-R_F bond of $[Fe(C_4F_8)(CO)_4]$ (**3**) were unsuccessful, even with utilization of a moderate pressure of CO or under Lewis-acidic conditions.[22] Further studies examining $[Fe(COCF_2CF_2CO)(CO)_4]$ (**20**) and $[Fe(COCF_2CF_2CF_2CO)(CO)_4]$ (**21**) established that the perfluorodiacyl species were unstable at elevated temperatures and extruded CO cleanly to form the corresponding $[Fe(CF_2)_n(CO)_4]$ metallacycle (Scheme 7). The perfluorodiacyl species **20** and **21** were prepared *via* an alternative route, in which $[Fe(CO)_4]^{2-}$ was treated with the respective perfluorodiacyl chloride. The seven-membered metallacyclic complex, $[Fe(COC_4F_8CO)(CO)_4]$, was observed spectroscopically by ^{19}F NMR, but could not be isolated.[22]

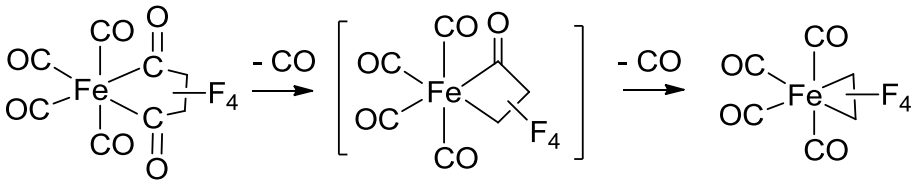

20 **22**

Scheme 7. Extrusion of CO from perfluorodiacyl species to afford a metallacyclopropane.

1.5. Hydrogenolysis of the M-R_F Bond

It has been established previously by researchers at DuPont that zero-valent nickel tertiary phosphite complexes, [NiL_4] (L = $P(OR)_3$), have the ability to efficiently catalyze the hydrodimerization of perfluoroalkenes. This transformation is achieved *via* formation of the metallacycle [$Ni(C_4F_8)L_2$], which readily undergoes hydrogenolysis of the Ni-R_F bonds (Scheme 8).[23]

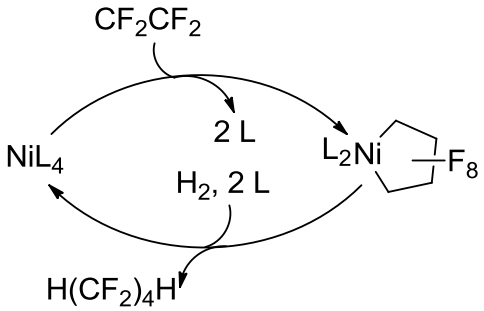

Scheme 8. Catalytic metallacycle formation and subsequent hydrogenolysis. L = $P(OR)_3$.

The related triphenylphosphine complex [$Ni(C_4F_8)(PPh_3)_2$] was found to be inert to hydrogenolysis.[24] When in the presence of a highly active hydrogenation catalyst (2 % palladium on Al_2O_3) it was found that hydrogenation of the triphenylphosphine ligands would occur at ca.

100 °C, in preference to hydrogenolysis of the Ni(C_4F_8) metallacycle group. The different reactivity of analogous phosphite and phosphine complexes (Ni(C_4F_8)L_2 (L = PPh_3 or $P(OR)_3$) indicate that introduction of π-acidic ligands can have a dramatic influence on the reactivity of the M-R_F bond. Alternatively, an increase in oxidation state of the central metal atom could also have a dramatic impact on the reactivity of the metal-carbon bond.[25] More specifically, the increase in oxidation state of nickel could weaken the Ni-C_F bond due to the increased partial positive charge on Ni and C_F, which could ultimately induce nucleophilic insertion into the bond with substrates such as acetonitrile.

1.6. High-Valent Organonickel Complexes

Higher oxidation states of nickel are less accessible than those of platinum and palladium as complexes of these metals are less prone to undergo reductive elimination reactions.[26] In spite of this, considerable interest in high-valent nickel complexes results from their potential relevance to catalytic reactions as intermediates.[26] Furthermore, the feasibility of Ni(IV) as a reaction intermediate is often proposed for mechanisms consisting of addition/elimination sequences, in which neither spontaneous reduction to Ni(0) or radical species are implicated.[27]

However, considerable growth in the number of Ni(III) and, to a lesser extent, Ni(IV) organometallic complexes has been observed in recent years.[28] This is in part due to the significant role nickel in the +3 oxidation state has in some metalloprotein systems.[29] Furthermore, the chemistry of organonickel(III) complexes has evolved greatly over the years.[30-35] The +4 oxidation state is considerably atypical for nickel, which often accounts for the high reactivity of Ni(IV) complexes.[36] To the best of my knowledge, the only reported organometallic Ni(IV) complexes have been outlined herein.

The first example of an octahedral diorganonickel(IV) complex, **24**, without oxidation-state ambiguity was synthesized by Klein in 1994 through an oxidative substitution reaction of the 18-electron acylnickel phenolate species **23** (Scheme 9) with iodomethane under mild conditions.[36] The iodide and methyl ligands are oxidatively added and the two coordinated PMe_3 ligands are *trans* to one another. A low spin d^6 nickel is accommodated by the resulting ligand field. The stability of **24** is attributed to the favorable balance of *trans* influences generated by the oxidative addition of methyl halide.

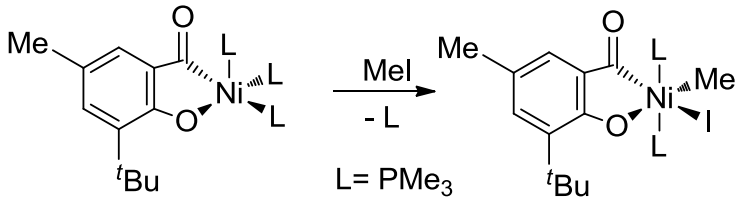

23 **24**

Scheme 9. The oxidative addition of methyl iodide to afford an octahedral diorganonickel(IV).

The synthesis of precursor complex **23**, was achieved *via* modification of **25** (Scheme 10), through a cyclometallation reaction, in which a nickel(IV)-hydride intermediate, **26** has been implicated.[27] Formation of the Ni hydride enables the reductive elimination of methane to afford **27**, a complex that is in equilibrium with **23** (Scheme 10).

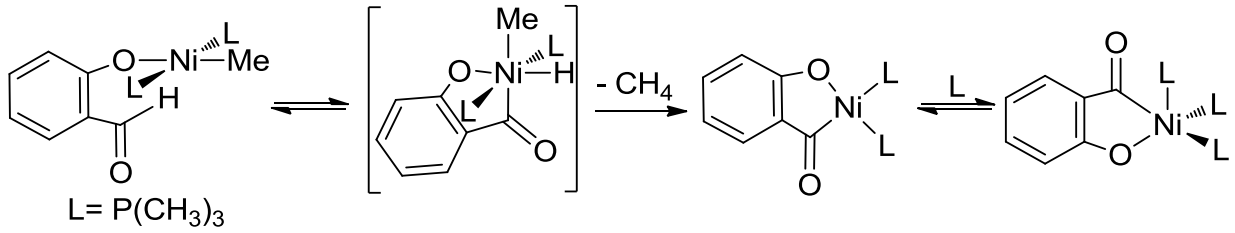

25 **26** **27** **23**

Scheme 10. Proposed mechanism for the formation of the acylnickel phenolate species.

Isolation and characterization of a coordinatively and electronically unsaturated four-coordinate triorganonickel(IV) complex has been achieved by Dimitrov *et al.* in 2003.[37] The bromotris(1-norbornyl)nickel(IV) complex, **28** (Figure 2), is the first example of a low-spin pseudotetrahedral organonickel 14-electron complex with a d^6 configuration. Complex **28** was synthesized *via* treatment of a tris(1-norbornyl)nickelate(II) complex, $[^nBu_4N]_2[NiBr(1\text{-nor})_3]$, with oxygen gas. Unusually, **28** is stable in air for several days in the solid state. Characterization of **28** by ^{13}C NMR spectroscopy demonstrates that the resonances of the norbornyl α-C atoms are shifted significantly downfield in comparison to the precursor Ni(II) complex, a consequence of the change in metal oxidation state. The strong σ-donating capability of the 1-norbornyl substituent provides the necessary electron density to stabilize the formal +4 oxidation state of nickel, conferring stability to this complex. More recently, Carnes synthesized the first stable tetraorganonickel(IV) complex (**29**) (Figure 2), which was found to spontaneously form at a slow rate *via* oxidative homocoupling of alkenes to a Ni(0) precursor.[38] Complex **29** was isolated from treatment of $[Ni(P^tBu_3)(cod)]$ with an excess of the strained, chiral alkene (5*Z*,11*E*)-dibenzo[*a*,*e*]cyclooctatetraene. The stability and lack of reactivity of the tetraorganonickel(IV) species **29** can be attributed to steric protection by the bulky ligands. Nonetheless, there is speculation as to the mode by which **29** is formed.[38]

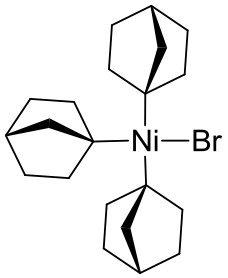

28

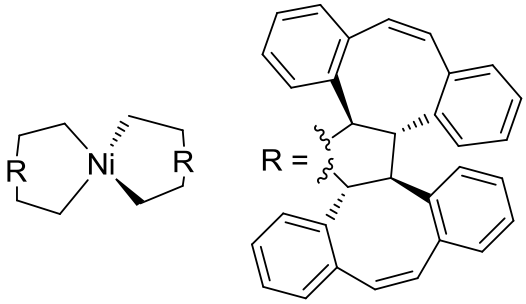

29

Figure 2. Tetracoordinate organonickel(IV) complexes.

1.7. Scope of this Thesis

This thesis outlines protocols for the synthesis and characterization of unprecedented Ni(IV) metallacycles, *via* a range of methodologies, including chemical oxidation and cyclic voltammetry. This work has been undertaken with the wider aim of developing reactive, high oxidation state nickel intermediates, which could allow for insertion into Ni-R_F bonds as a general method for the generation of organofluorine species. Furthermore, variation of the ligands on the perfluoronickelacycles has been explored with the aim of decreasing the formal oxidation potential of the Ni complex in order to fine tune the reactivity of the Ni-R_F bond. Full experimental details are outlined in Chapter 2 and further supporting information, including representative spectra are displayed in Appendices **A**-**D**. Chapter 3 describes the optimized synthesis of the trivalent [Ni(C_4F_8)(OAc)(N-N)] complexes, (N-N = bipy (**34**), phen (**35**), and tmeda (**36**)), as well as attempts to access the tetravalent $[Ni(C_4F_8)(OAc)(N\text{-}N)]^+$ cations. Chapter 4 describes the synthesis and characterization of the dimer $[Ni(C_4F_8)(bipy)(\mu\text{-}Cl)]_2$ (**37**). The stability of this dimer has been examined through a combination of experimental and

theoretical investigations, also outlined in Chapter 4, alongside further examination of a mixed valent [Ni(III)/Ni(IV)] radical cation. Chapter 5 describes the synthesis and characterization of [Ni(C_4F_8)Cl(bipy)(L)], (L = $NCCH_3$ (**39**)), and subsequent experimental and theoretical investigations outlining routes to Ni(IV) complexes. Lastly, Chapter 6 describes potential further investigations that could enable efficient access to the Ni(IV) oxidation state, and subsequent exploitation of its reactivity in the synthesis of fluorocarbon derivatives.

1. Experimental Methods

2.1. General Considerations

2.1.1. Reaction Conditions

Unless otherwise stated, all reactions and manipulations were performed under an atmosphere of dinitrogen utilizing standard Schlenk line techniques or an MBraun Labmaster glovebox. All glassware and Teflon^{TM}-coated magnetic stir bars were oven dried (115 °C) and cooled under vacuum prior to use.

2.1.2. Solvents

Dry, oxygen-free hexanes and toluene were obtained using an MBraun solvent purification system and stored over activated 4 Å molecular sieves, while acetonitrile was purchased from Aldrich (anhydrous 99.8%, reagent grade) and dried over activated 3 Å molecular sieves prior to use. Reagent grade dichloromethane and nitromethane were both dried over CaH_2, before being distilled under reduced pressure, degassed, and finally stored over activated molecular sieves (4 Å). Tetrahydrofuran, 1,2-dimethoxyethane, and diethyl ether were distilled under nitrogen from sodium/benzophenone and stored over activated 4 Å molecular sieves. The deuterated solvents d_3-acetonitrile, d_3-nitromethane, and d_2-dichloromethane, were all bought from Cambridge Isotope Laboratories and were all dried and degassed prior to use utilizing CaH_2 and freeze/pump/thaw cycles. All deuterated solvents were routinely stored over activated molecular sieves.

2.1.3. Reagents

Tetrafluoroethylene (TFE) was purchased from SynQuest Labs Ltd., while all other commercial reagents were purchased from Aldrich and were utilized without further purification.

Solid reagents were placed under dynamic vacuum at r.t. for 12 h to ensure dryness prior to use. Triisopropyl phosphite was distilled from sodium under reduced pressure. Similarly, pyridine was dried over sodium, distilled under vacuum and stored over activated 4 Å molecular sieves. The known complex $Ni[P(O^iPr)_3]_4$ was prepared by modifying an established literature procedure for the synthesis of $[Ni(PEt_3)_4]$.[39] The complexes $Ni(C_4F_8)[P(O^iPr)_3]_2$ (**30**),[40] $[Ni(C_4F_8)(bipy)]$ (**31**),[24] $[Ni(C_4F_8)(L)]$ (L = phen (**32**) or, tmeda (**33**)),[41] were prepared utilizing procedures outlined in the literature.

2.2. Spectroscopic Methods

2.2.1. IR Spectroscopy

Infrared spectra of solids were recorded using a Varian 640-IR spectrometer coupled to an attenuated total reflectance (ATR) accessory. The range for acquisition of IR spectra was 4000 to 550 cm^{-1}. IR spectra can be found in Appendix A.

2.2.2. Electronic Absorption Spectroscopy

Solution electronic absorption spectra were collected on a Varian Cary 100 UV/Vis spectrophotometer. Samples were prepared by dissolving the compounds in acetonitrile, dichloromethane, or nitromethane at ca. 2 mM. All spectra were collected at r.t. in a 10 mm path length quartz cell with a standard threaded top equipped with a septum seal cap (Starna Cells Inc.). The wavelength range used for acquisition of UV/Vis spectra was 350 to 800 nm. Solid state electronic absorption spectra were collected on a Varian Cary 300 UV/Vis spectrophotometer. Solid samples, prepared in an inert atmosphere, were pressed between two quartz disks enabling acquisition under air-free conditions. The wavelength range used for

acquisition of UV/Vis spectra was 250 to 700 nm. All spectra were collected at r.t. Corrected absorption spectra were calculated by subtracting solvent spectra from sample spectra.

2.2.3. NMR Spectroscopy

In this investigation NMR tubes fitted with J. Young's Teflon screw valves were utilized exclusively, with all samples being prepared under an inert atmosphere. Routine NMR spectra were recorded on Bruker 300 or 500 MHz instruments, with ^{1}H chemical shifts being referenced against residual protio impurities in the deuterated solvent. Solvent proton shifts (ppm): CD_3CN, 1.94; CD_2Cl_2, 5.30; CD_3NO_2, 4.33. The chemical shifts of ^{19}F spectra were referenced against TFA (-76.55 ppm) or $NOBF_4$ (-151.86 ppm).

2.2.4. Electron Paramagnetic Resonance (EPR) Spectroscopy

EPR spectra were obtained in collaboration with Mohammed Alsawafta and Dr. Sushil Misra at Concordia University. Spectra were recorded at X-band frequency (9.72 GHz) using a Bruker spectrometer at r.t. (293 K) and to a minimum temperature of 160 K, with temperature control enabled by a liquid nitrogen flow cryostat. Low-temperature EPR measurements at 10 K were measured at X-band or at Q-band (ca. 35 GHz) frequencies by Anna Nalepa and Dr. Sushil Misra at Max-Planck Institute fur Bioanorganische Chemie, Mulheim an der Ruhr, Germany. Samples for low-temperature EPR measurements used either acetonitrile or nitromethane as a glassing solvent, and the temperature was controlled using a liquid helium flow cryostat.

2.3. Analytical Methods

2.3.1. Elemental Analysis

Elemental analysis was carried out at Guelph Chemical Laboratories Ltd, under an inert atmosphere and in duplicate. Herein, average values are reported based on duplicate analysis.

2.3.2. High-Pressure Liquid Chromatography/ Mass Spectrometry

HPLC/MS analyses were performed on a Dionex Ultimate 3000 Liquid Chromatograph and an Applied Biosystem API2000 triple quadrupole mass spectrometer (LC/MS delay 0.27 min), using a reversed-phase gradient column (RSLC PA2 2.2 μm 120 Å, 2.1 x 150 mm) and a gradient mobile phase with an initial combination of 95 % A (90 % CH_3CN and 10 % H_2O) and 5 % B (90 % MeOH and 10 % H_2O) and a final combination of 50 % A and 50 % B and a flow rate of 0.1 mL min^{-1}. The analysis employed a DAD UV/Vis detector or mass spectrometer (Q1MS) with electrospray ionization (ESI-MS) in positive mode (ion spray voltage: 5000.0 V, TEM: 400.0 °C, declustering potential: 11.00 V and focusing potential: 300.0 V.)

2.3.3. Electrochemistry

Electrochemical experiments were carried out in ca. 0.1 M $[(^nBu)_4N][PF_6]/CH_3CN$ or ca. 0.1 M $[(^nBu)_4N][PF_6]/CH_3NO_2$ solutions in an inert atmosphere glovebox (MBraun) using a PAR Micro-Cell with a borosilicate glass bottom, a Pt wire working electrode, Pt wire counter electrode and an Ag wire quasi-reference electrode. Potentials are reported versus $[(C_5H_5)_2Fe]^{+/0}$ and were determined by addition of the ferrocene directly to the analyte solution following the voltammetric studies. The supporting electrolyte, $[(^nBu)_4N][PF_6]$ was dried prior to use by heating to 100 °C under dynamic vacuum for 10 h.[42]

2.4. Computational Details

All DFT calculations were performed by Tony St-Jacques and Dr. Serge Gorelsky with Gaussian 09 at the UB3LYP/TZVP level of theory.[43-45] Spin-unrestricted treatment was used for all open-shell species. Harmonic frequency calculations were used to determine free energies. Calculations of solvation energies of species in acetonitrile were performed using the polarizable continuum model (PCM) model with optimized gas-phase structures. Atomic charges and spin densities were calculated by natural population analysis (NPA),[46] as implemented by Gaussian 09. The symmetry of the open-shelled singlet states were broken by mixing the HOMO and the LUMO of the triplet states. Coordinates of DFT-optimized structures have been tabulated in Appendix C.

2.5. Synthesis

2.5.1. Improved synthesis of [Ni(C_4F_8)(OAc)(bipy)] (**34**)

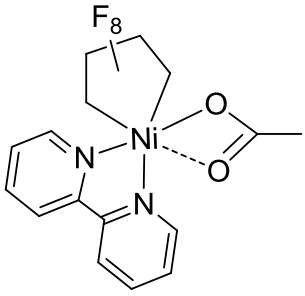

To a suspension of 800 mg (1.93 mmol) of [Ni(C_4F_8)(bipy)] (**31**) in 20 mL dry acetonitrile, 929 mg (2.88 mmol) of solid iodobenzene diacetate was slowly added and the mixture was heated to 80 °C for 2.5 h resulting in a purple solution. Following filtration of any residual **31**, the solvent was removed *in vacuo* and the resulting purple residue was dissolved in 15 mL of hot toluene (80 °C) and refiltered. The solution was then allowed to stand at r.t. for 12 h to afford crystalline **34**, which was filtered, washed with two aliquots of 5 mL hexane, and dried *in vacuo*. Yield: 830 mg (91 %). The IR spectrum of a sample of **34** prepared using this methodology was comparable with that previously reported by Baker *et al.*[41]

2.5.2. Improved synthesis of [Ni(C_4F_8)(OAc)(phen)] (**35**)

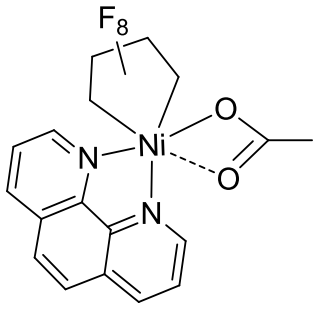

To a suspension of 21 mg (0.048 mmol) of [Ni(C_4F_8)(phen)] (**32**) in 4 mL dry acetonitrile, 16 mg (0.048 mmol) of solid iodobenzene diacetate was slowly added and the mixture was heated to 80 °C for 2 h to give a purple solution. Upon cooling, the solvent was removed *in vacuo*, and the resulting purple residue was dissolved in 5 mL of hot toluene (80 °C) and was filtered. The solution was then allowed to stand at r.t. for 12 h and the resulting crystalline **35** was collected, washed with two aliquots of 5 mL hexane and dried *in vacuo*. Yield: 23 mg (96%). IR (cm^{-1}): 1584 (w), 1582 (w), 1542 (m, OCO), 1516 (m, OCO), 1507 (w), 1496 (w), 1447 (s), 1427 (s, OCO), 1414 (m), 1339 (m), 1321 (w), 1308 (w), 1258 (m), 1237 (w), 1226 (w), 1212 (w), 1199 (w), 1169 (s, CF), 1163 (vs, CF), 1145 (s, CF), 1102 (s, CF), 1095 (m), 1076 (m), 1072 (m), 1063 (m), 1057 (m), 1037 (w), 1034 (w), 1004 (w), 990 (w), 963 (vs), 957 (vs), 943 (m), 924 (w), 902 (vs), 871 (w), 851 (vs), 828 (m), 809 (w), 781 (w), 734 (m), 725 (vs), 719 (m), 702 (w), 699 (w), 693 (m), 688 (m), 872 (s), 675 (m), 669 (w), 663 (w), 655 (w), 649 (w), 646 (m), 644 (w), 635 (w), 626 (w), 625 (w), 620 (m), 615 (w), 606 (w), 603 (w), 591 (m), 585 (w), 580 (w), 570 (w), 562 (m), 559 (m), 553 (w).

2.5.3. Improved synthesis of [Ni(C_4F_8)(OAc)(tmeda)] (**36**)

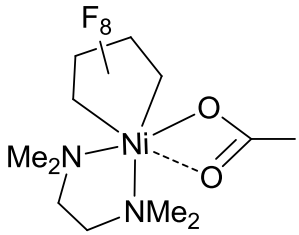

To a suspension of 100 mg (0.27 mmol) of [Ni(C_4F_8)(tmeda)] (**33**) in 5 mL of dry acetonitrile was slowly added 129 mg (0.27 mmol) of solid iodobenzene diacetate and the mixture was heated to 80 °C for 2 h to give a red-purple solution. The solvent was removed *in vacuo* and the resulting red-purple oil was washed with three 5 mL aliquots of DME to afford a red-purple semi-solid **36**. Yield: 107 mg (91%). The IR spectrum was comparable with that previously reported by Baker *et al*.[41]

2.5.4. Synthesis of [Ni(C_4F_8)(bipy)(μ-Cl)]$_2$ (**37**)

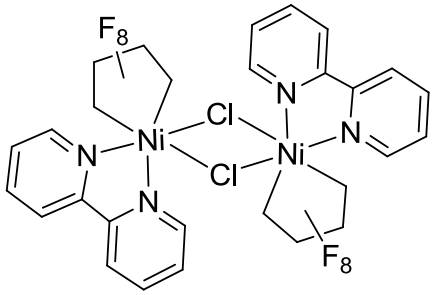

To a solution of 830 mg (1.75 mmol) [Ni(C_4F_8)(OAc)(bipy)] (**34**) in 20 mL dry DME was added 200 mg (1.85 mmol) trimethylsilyl chloride (TMS-Cl). The reaction mixture was stirred at r.t. for 12 h to give a dark solution. Upon cooling the reaction mixture to -35 °C a dark grey microcrystalline precipitate formed. This material was collected *via* filtration and washed with cold DME (3 mL) to afford 350 mg of **37**. The filtrate was then concentrated to 10 mL and cooled at -35 °C for 12 h to afford a second crop **(**265 mg) of microcrystalline **37**. Needle-like crystals suitable for X-ray diffraction (XRD) were produced by dissolving 6 mg of **37** in a minimal amount of THF. Yield: 615 mg (78 %). Anal. calc'd (found) for $C_{28}H_{19}Cl_2F_{16}N_4Ni_2$ (897.92 g mol^{-1}): C 37.34 (36.58), H 1.79 (1.40), N 6.22 (6.19). IR (cm^{-1}): 1605 (vw), 1602 (w), 1568 (vw), 1569 (vw), 1497 (w), 1443 (s), 1424 (w), 1341 (m). 1319 (w), 1279 (w), 1256 (s, CF), 1166 (vs, CF), 1147 (m), 1105

(s, CF), 1063 (s, CF), 1046 (m), 1029 (m), 1025 (s, CF), 1011 (w), 959 (vs), 960 (vs), 887 (vs), 812 (m), 766 (vs), 743 (m), 735 (s), 707 (w), 655 (m), 633 (w), 623 (w), 593 (m), 587 (m). UV/Vis and EPR spectra of **37** were obtained in solid state and in solution state using CH_2Cl_2 or nitromethane (Chapter 4, Section 4). The complex **37** was further analyzed by cyclic voltammetry (CV) (Chapter 4, Section 5) and ^{19}F NMR spectroscopy in nitromethane. ^{19}F NMR (CD_3NO_2, δ): -109.71 (br, α-CF_2 of **37**), -139.62 (br, β-CF_2 of **37**).

2.5.5. Alternative Synthesis of $[Ni(C_4F_8)(bipy)(\mu\text{-}Cl)]_2$ (**37**)

To a solution of 100 mg (0.24 mmol) of $[Ni(C_4F_8)(bipy)]$ (**31**) in 10 mL of dry C_6H_5Cl was added 1.5 mL (0.15 mmol) of 0.1 M SO_2Cl_2 solution in dichloromethane. The reaction mixture was stirred at r.t. for 1.5 h resulting in the formation of a brick red precipitate. The precipitate was collected *via* filtration and washed with cold (-20 °C) C_6H_5Cl before being dried *in vacuo* to yield 91 mg of a dark orange-red intermediate complex (**38**) (82%). The complex **38** was analyzed by solid state IR and UV/Vis (Chapter 4, Section 3). To isolate **37**, ca. 5 mg of **38** was dissolved in ca. 0.5 mL of THF upon warming. This solution was allowed to cool to r.t. and then layered with ca. 0.3 mL of Et_2O and left at r.t. After 2 d one large dark grey needle of **37** had formed. The solution was then left at -30 °C which produced more of the needle-like crystals. The solid state EPR and IR spectra of a sample of **37** prepared using this methodology was in good comparison with that reported above (2.5.4.).

2.5.6. Synthesis of [Ni(C_4F_8)Cl(bipy)(NCCH_3)] (**39**)

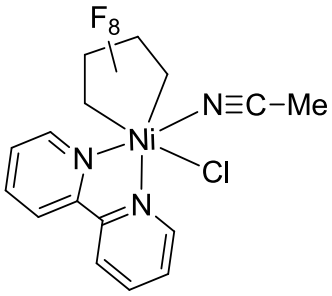

Dark crystals of **39** suitable for single crystal X-ray diffraction analysis were obtained by dissolving **37** in the minimum amount of CH_3CN and allowing this solution to sit at −35 °C for 12 h. The resulting solid was dried *in vacuo* and analyzed in CH_3CN using UV/Vis, EPR (Chapter 5, Section 3), NMR spectroscopy, and CV (Chapter 5, Section 4). ^{19}F NMR (CD_3CN, δ): -110.26 (br, α-CF_2 of **39**), -140.28 (br, β-CF_2 of **39**).

2.5.7. Synthesis of [Ni(C_4F_8)Cl(bipy)(py)] (**40**)

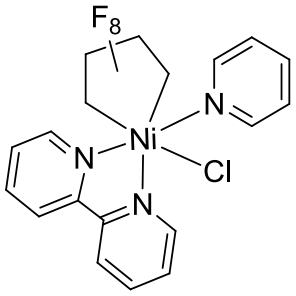

To a solution of 13 mg (0.029 mmol) of [Ni(C_4F_8)(bipy)(μ-Cl)]$_2$ (**37**) in 1.5 mL nitromethane was added 5 μL (0.064 mmol) of pyridine. The green mixture was stirred at r.t. for 12 h and was analyzed by CV (Chapter 5, Section 4) and ^{19}F NMR spectroscopy. This procedure was repeated but with substitution of the solvent, nitromethane, for pyridine to afford a blue solution that was analyzed *in situ* by UV/Vis (Chapter 5, Section 3) and ^{19}F NMR spectroscopy. ^{19}F NMR (CD_3NO_2, δ): -111.73 (br, α-CF_2 of **40**), -138.95 (br, β-CF_2 of **40**). EA and XRD of **40** were not obtained as only trace amounts of decomposition product, [Ni(C_4F_8)(bipy)] (**31**), were isolated.

2.5.8. Reaction of [Ni(C_4F_8)(bipy)(μ-Cl)]$_2$ (**37**) with 4-Dimethylaminopyridine (dmap)

To a solution of 12 mg (0.027 mmol) of [Ni(C_4F_8)(bipy)(μ-Cl)]$_2$ (**37**) in 1.5 mL nitromethane was added 4 mg (0.033 mmol) of dimethylaminopyridine (dmap). The solution

turned dark blue instantly and was stirred 12 h. After this reaction time, the solution appeared orange-brown in color and upon standing yielded ca. 8 mg of orange crystalline material confirmed to be [Ni(C_4F_8)(bipy)] (**31**) by single crystal X-ray diffraction analysis.

This reaction was repeated but with substitution of the solvent, nitromethane, for CH_2Cl_2. The formation of a green precipitate was observed upon addition of dmap. Collection of this material *via* filtration and subsequent analysis of a CH_2Cl_2 solution using UV/Vis spectroscopy (Chapter 5, Section 3) confirmed the presence of **37**.

2.6. Attempts to Generate Ni(IV) Complexes from [Ni(C_4F_8)(OAc)(N-N)] Precursors

2.6.1. Attempted reaction of [Ni(C_4F_8)(OAc)(N-N)] with $NOBF_4$

To a solution of 18 mg (0.036 mmol) [Ni(C_4F_8)(OAc)(bipy)] (**34**) in 1 mL d_3-acetonitrile was added 5 mg (0.043 mmol) $NOBF_4$ and the subsequent mixture was allowed to stir for 12 h. No new resonances where observed in the ^{19}F NMR spectrum of this solution. Additionally, no change in the ^{19}F NMR spectrum was observed after heating the mixture to 80 °C for 12 h.

This procedure was repeated but with substitution of [Ni(C_4F_8)(OAc)(N-N)] (N-N = bipy (**34**)) for N-N = phen (**35**) or N-N = tmeda (**36**). In both instances, no new resonances were observed in the ^{19}F NMR spectra of these solutions.

2.6.2. Reaction of [Ni(C_4F_8)(OAc)(bipy)] (**34**) with $(NH_4)_2Ce(NO_3)_6$

Dropwise addition of 45 mg (0.095 mmol) [Ni(C_4F_8)(OAc)(bipy)] (**34**) dissolved in 1 mL of dry acetonitrile to a stirring solution of 52 mg (0.095 mmol) $(NH_4)_2Ce(NO_3)_6$ (CAN) resulted in an immediate exothermic reaction. The reaction mixture was then analyzed using ^{19}F NMR spectroscopy, but no new resonances were observed. The reaction mixture was allowed to stir for

7 days after which time several new species were observed by ^{19}F NMR spectroscopy. ^{19}F (CD_3CN, δ): -109.67 (t, 6 Hz, α-CF_2 of **B**), -121.81 (s, α-CF_2 of **A**), -121.94 (t, 6 Hz, β-CF_2 of **B**), -128.92 (s), -129.32 (s, β-CF_2 of **A**), -129.77 (s), -133.97 (s, C_4F_8). The reaction mixture was diluted by a factor of 1/100 and was analyzed by LC/MS (Chapter 3, Section 2).

2.7. Attempts to Generate a Stable [Ni(III)/Ni(IV)] Radical Cation or Ni(IV) Complex from $[Ni(C_4F_8)(bipy)(\mu\text{-}Cl)]_2$ Precursor

Reactions involving the oxidation of **37** were conducted on a small scale, due to the low solubility of **37** in organic solvents.

2.7.1. Reaction of $[Ni(C_4F_8)(bipy)(\mu\text{-}Cl)]_2$ (**37**) with $NOBF_4$

To a solution of 3 mg (0.007 mmol) $[Ni(C_4F_8)(bipy)(\mu\text{-}Cl)]_2$ (**37**) in 1.5 mL nitromethane was added 1 mg (0.009 mmol) $NOBF_4$. The solution was stirred at r.t. for 1 h and the reaction was monitored by EPR.

Additionally, the reaction was repeated by substituting the solvent, nitromethane, for CH_2Cl_2 and was monitored after 4 d by UV/Vis and NMR spectroscopy. ^{19}F NMR (CD_2Cl_2, δ): -62.84 (s, α-CF_2 of **C**), -68.61 (t, 11 Hz, α-CF_2 of **D**), -96.56 (br d, 160 Hz, α-CF_2 of **E**), -101.01 (br d, 160 Hz, α-CF_2 of **E**), -117.76 (s), -119.74 (t, 11 Hz, β-CF_2 of **D**), -121.27 (s), -127.67 (s, α-CF_2 of **C**), -130.96 (s), -131.11 (s), -134.12 (s), -135.16 (br d, 90 Hz, β-CF_2 of **E**).

4.7.2. Reaction of $[Ni(C_4F_8)(bipy)(\mu\text{-}Cl)]_2$ (**37**) with $[Fe(C_5H_5)_2][BF_4]$

To a solution of 2 mg (0.004 mmol) $[Ni(C_4F_8)(bipy)(\mu\text{-}Cl)]_2$ (**37**) in 0.5 mL d_3-nitromethane was added 2 mg (0.007 mmol) of $[Fe(C_5H_5)_2][BF_4]$; the solution turned green

instantly. The mixture was stirred at r.t. for 2 d and analyzed by ^{19}F NMR spectroscopy. ^{19}F NMR (CD_3NO_2, δ): -106.21 (br, *α*-CF_2 of **F**), -139.36 (br, *β*-CF_2 of **F**).

2.8. Attempts to Generate Ni(IV) Complexes from [Ni(C_4F_8)(bipy)($NCCH_3$)] Precursor

Reactions involving the oxidation of Ni(III) complexes were conducted on a small scale, due to the low solubility of the Ni(III) complexes in organic solvents. When possible, these procedures were repeated on a larger scale to enable the identification of perfluorinated organic products.

2.8.1. Reaction of [Ni(C_4F_8)Cl(bipy)($NCCH_3$)] (**39**) with $NOBF_4$

A sample of 10 mg (0.024 mmol) [Ni(C_4F_8)(bipy)(μ-Cl)]$_2$ (**37**) was mixed with 2 mL acetonitrile (to generate **39** *in situ*). To this solution was added 6 mg (0.05 mmol) of $NOBF_4$ turning the solution purple instantly with visible gas evolution. The solution was stirred at r.t. for 1 h and the reaction followed by NMR spectroscopy. ^{19}F NMR (CD_3CN, δ): major products: -95.16 (br d, 165 Hz, *α*-CF_2 of **G**), -104.54 (br d, 165 Hz, *α*-CF_2 of **G**), -135.39 (br d, 150 Hz, *β*-CF_2 of **G**), -149.33 (br s), -149.91 (s), -150.58 (br s), minor products: -86.77 (br d, 153 Hz, *α*-CF_2 of **H**), -95.61 (d, 153 Hz *α*-CF_2 of **H**), -134.03 (d, 153 Hz *β*-CF_2 of **H**).

The mixture was stirred at r.t. for 7 d and the reaction followed by UV/Vis and NMR spectroscopy. The new resonances presented by the NMR spectra are as follow: ^{1}H NMR (CD_3CN, δ): 8.82 (m, bipy), 8.48 (m, bipy), 8.42 (m, bipy), 7.88 (m, bipy). ^{19}F NMR (CD_3CN, δ): major products: -69.44 (t, 11 Hz, *α*-CF_2 of **D**), -105.97 (s), -120.27 (t, 11 Hz, *β*-CF_2 of **D**), -129.33 (s), minor products: -115.36 (t, 11 Hz), -121.16 (m), -122.39 (s), -123.95 (m), -131.50

(septet, 6 Hz), -132.40 (septet, 6 Hz). Resonances in the $^{19}F\{^{1}H\}$ NMR spectrum that differ from the ^{19}F NMR spectrum are as follow: $^{19}F\{^{1}H\}$ (CD_3CN, δ): -131.45 (s), -132.36 (s).

The volatile components of this reaction mixture were separated by distillation and were analyzed by LC/MS and ^{19}F NMR spectroscopy. ^{19}F NMR (CD_3CN, δ): -105.97 (s), -129.33 (s), -149.91 (s). Additionally, the ^{19}F NMR spectra of the reaction mixture after heating to 60 °C for 12 h showed decomposition of the generated metallacycles.

2.8.2. Reaction of $[Ni(C_4F_8)Cl(bipy)(NCCH_3)]$ (**39**) with $[Fe(C_5H_5)_2][BF_4]$

To a solution of 2 mg (0.004 mmol) $[Ni(C_4F_8)(bipy)(\mu\text{-}Cl)]_2$ (**37**) in 0.5 mL d_3-acetonitrile (to generated **39** *in situ*). Upon treatment with 2 mg (0.007 mmol) of $[Fe(C_5H_5)_2][BF_4]$, the solution turned green instantly, and the mixture was stirred at r.t. for 1 d. ^{19}F (CD_3CN, δ): -106.89 (s, α-CF_2 of **I**), -110.30 (s, α-CF_2 of **31**), -139.64 (s, β-CF_2 of **I**), -140.41 (s, β-CF_2 of **31**). The mixture was stirred at r.t. for 4 d and the only resonances presented by the ^{19}F NMR spectra were: ^{19}F NMR (CD_3CN, δ): -110.30 (s, α-CF_2 of **31**), -140.41 (s, β-CF_2 of **31**).

2.9. Single Crystal X-Ray Diffraction

Single crystal X-ray diffraction (XRD) analysis of **31**, **37**, and **39** was performed by Dr. Ilia Korobkov at the University of Ottawa. A single crystal of **31**, **37**, or **39** was mounted on a glass fibre using Paratone-N oil. Indexing and intensity data collection at 200 K was performed on a Bruker Kappa X8 APEX CCD single-crystal diffractometer equipped with a sealed Mo tube and graphite monochromator (λ = 0.71073 Å). The SHELX Bruker software package was used to solve and refine the structure.[47] An empirical absorption correction was applied using the SADABS, Bruker 2003 program.[48] The structure was solved by direct methods and refined by

the full-matrix least-squares method minimization of $(\Sigma w(F_o - F_c)^2)$. The crystallographic data for **31**, **37**, and **39** are summarized in Appendix B.

3. Investigations of [Ni(C_4F_8)(OAc)(N-N)] Complexes

3.1. Synthesis of [Ni(C_4F_8)(OAc)(N-N)] Complexes

As outlined in Chapter 1, Section 7, an increase in the oxidation state of nickel from Ni(III) to Ni(IV) is of particular interest, as this could dramatically modify the reactivity of the Ni-R_F bond.[41] With this in mind, previous investigations conducted by Baker *et al*. have outlined the synthesis and characterization of trivalent nickel precursors (Scheme 11), from which high-valent Ni(IV) complexes were observed by cyclic voltammetry.[41] The synthetic procedures developed by Baker and co-workers are outlined in Scheme 10. Treatment of [Ni(C_4F_8)L_2] (L = P(O^iPr)$_3$ (**30**)), with the chelating bidentate nitrogen ligands (N-N), 1,1'-bipyridine (bipy), 1,10-phenanthroline (phen), *N,N,N'N'*-tetramethylethylenediamine (tmeda), afforded the respective [Ni(C_4F_8)(N-N)] metallacycles (N-N = bipy (**31**), phen (**32**), tmeda (**33**)). One-electron oxidation of **31**-**33** with iodobenzene diacetate [PhI($OAc)_2$] yielded the trivalent [Ni(C_4F_8)(OAc)(N-N)] complexes (N-N = bipy (**34**), phen (**35**), tmeda (**36**)).

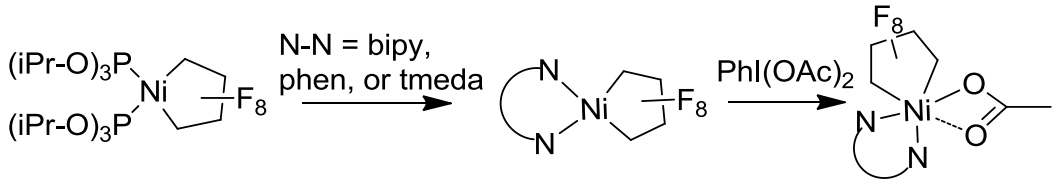

30

31 N-N = bipy
32 N-N = phen
33 N-N = tmeda

34 N-N = bipy
35 N-N = phen
36 N-N = tmeda

Scheme 11. Synthetic route to Ni(III) acetate complexes.

In work conducted for this thesis, initial investigations involved optimization of the syntheses of acetate complexes **34**-**36**. Previously, the syntheses of the complexes had involved

treatment of the divalent nickel complexes **31**-**33** with two equivalents of iodobenzene diacetate ($PhI(OAc)_2$). Theoretically only half an equivalent of $PhI(OAc)_2$ is required to oxidize **31**-**33** to the respective [Ni(C_4F_8)(OAc)(N-N)] complexes **34**-**36**. However, when **32** was initially treated with half an equivalent of $PhI(OAc)_2$ in acetonitrile the reaction did not go to completion; it required the addition of a further portion of $PhI(OAc)_2$ (1 equiv. total) to afford **35** in high yield (96 %) upon heating (80 °C, 2 h). The analogous reaction of **33** also required one equivalent of $PhI(OAc)_2$ to afford **36** in high yield (91 %). For the synthesis of **36**, acetonitrile was used instead of toluene to avoid the formation of an oily residue. Following the removal of acetonitrile *in vacuo* it was found that washing with DME was the most effective means of purifying **36**. The bipy analogue **31** required 1.5 equivalents of $PhI(OAc)_2$ to afford **34** in high yield (91 %). The reaction of **31**-**33** with $PhI(OAc)_2$ was followed by a color change of the initial yellow slurry to a deep purple solution on completion. Formation of the [Ni(C_4F_8)(OAc)(N-N)] complexes was confirmed by IR spectroscopy with the presence of medium to strong bands due to vibrational modes of the η^2-acetate (OCO) in the range of 1600-1400 cm^{-1}.[41,49]

3.2. Investigations into the Generation of Ni(IV) Complexes from [Ni(C_4F_8)(OAc)(N-N)] Precursors

The Ni(III) complexes **34** and **36** were previously analyzed by cyclic voltammetry in acetonitrile by Baker and co-workers and demonstrated a reversible oxidation to the respective Ni(IV), low-spin $[Ni(C_4F_8)(OAc)(N\text{-}N)]^+$ (bipy (**34**) and tmeda (**36**)) cations.[41] The reversible oxidation wave for the (Ni(III)/Ni(IV)) transition was observed at 0.89 V for **34**, with the corresponding reversible oxidation wave of the tmeda analogue **36** presenting at the more positive potential of 0.70 V, versus $[(C_5H_5)_2Fe]^{+/0}$.[41] With the aim of building upon this initial

investigation, in this thesis work, $NOBF_4$ was selected as an oxidant, due to its high formal potential of 0.87 V versus $[(C_5H_5)_2Fe]^{+/0}$ in acetonitrile,[50] which was anticipated to enable access to tetravalent $[Ni(C_4F_8)(OAc)(N\text{-}N)]^+$ cations. Furthermore, the entropically favorable loss of NO gas to afford cationic **34**-**36** complexes with a $[BF_4]^-$ counter ion was predicted to proceed as a clean reaction. However, despite repeated attempts, treatment of **34**, **35**, or **36** with $NOBF_4$ at r.t. or with heating to 80 °C (Scheme 12) did not result in the formation of diamagnetic Ni(IV) complexes as observed by ^{19}F NMR spectroscopy.

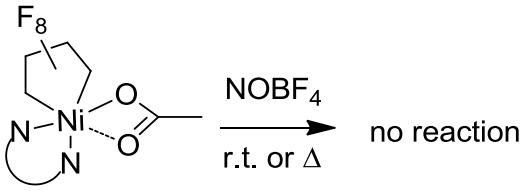

34 N-N = bipy

35 N-N = phen

36 N-N = tmeda

Scheme 12. Attempted Reactions of $[Ni(C_4F_8)(OAc)(N\text{-}N)]$ with $NOBF_4$.

One explanation for the lack of reaction could be the tendency of the nitrosonium cation, $[NO]^+$, to undergo an inner-sphere electron transfer (ET) mechanism, which results from coordination of NO to the metal center.[51] As **34**-**36** are coordinatively saturated, the nitrosonium cation cannot coordinate and, thus, this reaction pathway is inhibited. Significantly, reaction of $NOBF_4$ *via* an outer-sphere ET mechanism is known to be disfavored.[52]

When an excess of the strong oxidant ceric ammonium nitrate (CAN, $(NH_4)_2Ce(NO_3)_6$) was added to **34** in acetonitrile an immediate exothermic reaction occurred. However, no new resonances were immediately apparent in the ^{19}F NMR spectrum of the reaction mixture. As

CAN is sparingly soluble in acetonitrile, the chemical redox reaction is heterogeneous, which results in slow reactions with significant mass transfer factors and commonly inhibited reaction rates.[51] With this in mind, a solution of **34** and CAN was continuously stirred at r.t. for 7 days and then analyzed by ^{19}F NMR (Figure 3). In addition to new resonances resulting from perfluorinated organic species, including perfluorocyclobutane, C_4F_8, at -133.97 ppm,[53] resonances that could be assigned to two metallacycle complexes were observed. Notably, sharp singlets at -129.45 and -134.17 ppm are in a 1:1 ratio as well as having a similar line width. Hence, these resonances can be assigned to the α-CF_2 and β-CF_2 of a new metallacycle complex (**A**) (Figure 3). Another metallacycle complex (**B**) gave rise to two triplets in a 1:1 ratio at -109.67 and -121.94 ppm due to the α-CF_2 and β-CF_2. An aliquot of the reaction solution was diluted and analyzed by HPLC/MS. A number of chromatographic methods were employed, including variable solvent gradients and elevated temperatures, yet this analysis consistently proved to be inconclusive. Evidently, this system generates multiple reaction products of similar polarity that cannot be easily separated by HPLC. Attempts to isolate metallacycle **A** from the reaction by concentrating and allowing the solution to stand at -35 °C were unsuccessful.

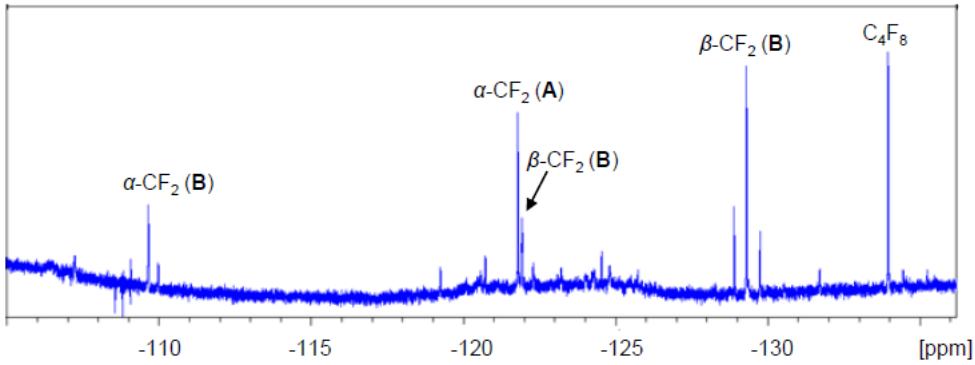

Figure 3. ^{19}F NMR spectrum of the reaction solution of [Ni(C_4F_8)(OAc)(bipy)] (**34**) with CAN in acetonitrile.

3.3. Conclusions

The synthetic procedure for [Ni(C_4F_8)(OAc)(N-N)] metallacycles (N-N = bipy (**34**), phen (**35**), tmeda (**36**)) has been optimized, based on prior syntheses involving treatment of [Ni(C_4F_8)(N-N)] (N-N = bipy (**31**) phen (**32**), tmeda (**33**)) with $PhI(OAc)_2$. In this investigation, it was found that excess $PhI(OAc)_2$ is required for efficient conversion of [Ni(C_4F_8)(N-N)] (N-N = bipy (**31**) phen (**32**), tmeda (**33**)) to the respective trivalent acetate complexes.

Multiple attempts to access Ni(IV) perfluorometallacycles *via* the treatment of **34**-**36** with $NOBF_4$ did not result in the formation of new diamagnetic metallacycles according to ^{19}F NMR. Conversely, treatment of **34** with CAN resulted in the formation of new metallacyclic complexes **A** and **B**, along with perfluorocyclobutane as determined using ^{19}F NMR spectroscopy. As treatment of [Ni(C_4F_8)(OAc)(N-N)] precursors with the chemical oxidants $NOBF_4$ and CAN cannot cleanly generate stable Ni(IV) complexes, alternative routes to Ni(IV) complexes have been explored. One means of facilitating Ni(IV) formation would be by lowering the formal redox potential of the Ni(III)/Ni(IV) couple. This could be achieved by further modifications of the ligand sphere. As such, Chapter 4 outlines the synthesis of a new nickel(III)-chloride dimer and subsequent attempts to access the Ni(IV) oxidation state.

4. Investigations into the Synthesis and Reactivity of [Ni(C_4F_8)(bipy)(μ-Cl)]$_2$

4.1. Synthesis of [Ni(C_4F_8)(bipy)(μ-Cl)]$_2$

As discussed in Chapter 3, Section 2 there was a 0.2 V decrease in the formal potential associated with the assigned redox couple (Ni(III)/Ni(IV)) of [Ni(C_4F_8)(OAc)(N-N)] corresponding to substitution of N-N = bipy (**34**) for N-N = tmeda (**36**).[41] With the aim of further investigating the impact of ligand variation upon oxidation potential, the acetate ligand of **34** was substituted with a chloride ligand. This is of particular interest, as this modification would feasibly open up a Ni coordination site allowing for more efficient coordination of substrates that may ultimately insert into the Ni-R_F bond. The acetate group of **34** was readily replaced by a chloride *via* treatment of **34** with trimethylsilyl chloride (TMS-Cl).[54] Evidently, this is a thermodynamically favored reaction, driven by Si-O bond formation and subsequent elimination of TMS-OAc (Scheme 13). The nickel(III) chloride complex was isolated as the dimer [Ni(C_4F_8)(bipy)(μ-Cl)]$_2$ (**37**) in good yield (78 %).

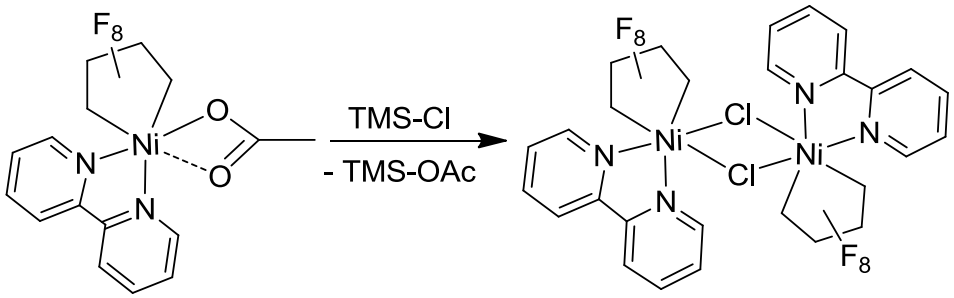

34 **37**

Scheme 13. Treatment of [Ni(C_4F_8)(OAc)(bipy)] (**34**) with TMS-Cl as chloride source.

4.2. Analysis of the Molecular Structure of [Ni(C_4F_8)(bipy)(μ-Cl)]$_2$

Dark grey needle-like single crystals of [Ni(C_4F_8)(bipy)(μ-Cl)]$_2$ (**37**) of sufficient quality for single crystal X-ray diffraction (XRD) analysis (Figure 4) were obtained *via* recrystallization of **37** from a saturated solution in THF. A disordered, non-coordinating THF molecule co-crystallized with **37** in the unit cell. Selected bond lengths and angles relating to the molecular structure of **37** have been reported in Table 1 and further crystallographic information can be found in Appendix B. The molecular structure demonstrates that, for [Ni(C_4F_8)(bipy)(μ-Cl)]$_2$ (**37**), the coordination sphere of each nickel atom has a pseudo-octahedral geometry, and the nickel atoms are bridged by two chloride ligands. The sum of the equatorial bond angles is equal to 360.21°, signifying that the C(14), N(1), C(11), Cl(1) atoms lie in within the same plane, as required for an octahedral geometry. There is a notable Jahn-Teller (JT) axis through the atoms N(2)-Ni(1)-Cl(1A), which has an axial bond angle of 164.90(6)°, a distortion from the idealized 180°. The Ni-C_F bond distances of the Ni(C_4F_8) metallacycle are 1.972(2) Å (Ni(1)-C(14), *trans* to Cl(1)) and 1.985(2) Å (Ni(1)-C(11), *trans* to N(1)) both being comparable to that found for a related trivalent [Ni(C_4F_8)(OAc)(phen)] complex previously characterized by Baker and coworkers.[41] Notably, no molecular structures relating to complexes containing Ni(C_4F_8), or analogous Ni(C_4H_8), metallacycles have previously been deposited at the Cambridge Crystallographic Data Center (CCDC) (March, 2010). A notable consequence of the JT distortion, is that the Ni(1)-Cl(1) bond distance of 2.3211(5) Å is significantly shorter than that found for the Ni(1)-Cl(1A) contact (2.5615(6) Å). The obtained molecular structure demonstrates that the 17-electron [Ni(C_4F_8)Cl(bipy)] complex dimerizes in the solid state to afford the 19-electron Ni(III) centered dimer **37**, in which each Cl atom bridges the two Ni centers through a two-centered, two-electron bond.

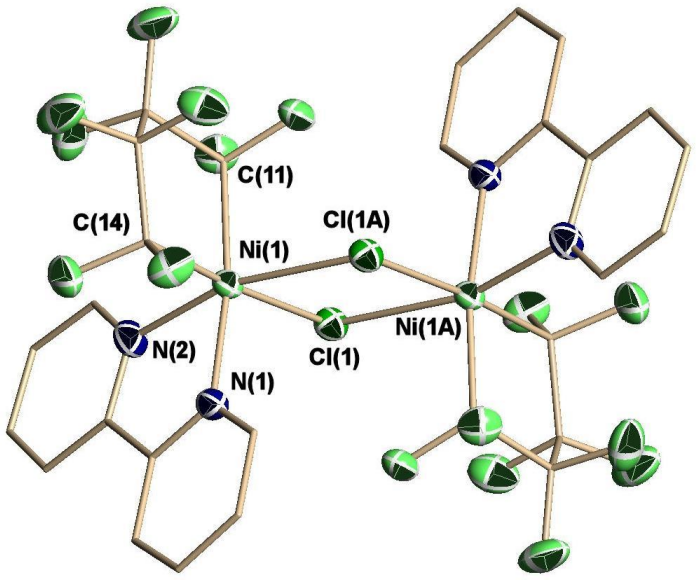

Figure 4. Thermal ellipsoid representation (50% probability ellipsoids) of the molecular structure of [Ni(C$_4$F$_8$)(bipy)(μ-Cl)]$_2$ (**37**).

Table 1. Selected bond lengths (Å) and angles (°) of [Ni(C$_4$F$_8$)(bipy)(μ-Cl)]$_2$ (**37**).

	Bond Length (Å)		**Bond Length (Å)**
Ni(1)-C(14)	1.972(2)	Ni(1)-N(2)	2.1309(19)
Ni(1)-C(11)	1.985(2)	Ni(1)-Cl(1)	2.3211(5)
Ni(1)-N(1)	2.0181(17)	Ni(1)-Cl(1A)	2.5615(6)
	Bond Angle (°)		**Bond Angle (°)**
C(14)-Ni(1)-C(11)	84.32(8)	N(1)-Ni(1)-Cl(1)	96.79(5)
C(14)-Ni(1)-N(1)	86.41(8)	N(2)-Ni(1)-Cl(1)	87.15(5)
C(11)-Ni(1)-N(1)	170.10(8)	C(14)-Ni(1)-Cl(1A)	94.30(6)
C(14)-Ni(1)-N(2)	96.99(8)	C(11)-Ni(1)-Cl(1A)	92.40(6)
C(11)-Ni(1)-N(2)	98.64(8)	N(1)-Ni(1)-Cl(1A)	91.73(5)
N(1)-Ni(1)-N(2)	79.05(8)	N(2)-Ni(1)-Cl(1A)	164.90(6)
C(14)-Ni(1)-Cl(1)	175.20(6)	Cl(1)-Ni(1)-Cl(1A)	82.052(18)
C(11)-Ni(1)-Cl(1)	92.69(6)	Ni(1)-Cl(1)-Ni(1A)	97.950(18)

For comparison, the molecular structure of **37** was calculated using density functional theory (DFT) at the UB3LYP/TZVP level of theory by Tony St-Jacques and Dr. Serge Gorelsky (Figure 5, Appendix C). The calculated Ni(1)-ligand bond distances of **37** in the triplet spin state (S = 1) and the open-shell single spin state (S = 0) are reported in Table 2. The simulated bond distances were found to be ca. 0.05 Å longer than that determined experimentally by XRD, as expected when using UB3LYP.[43-45] Furthermore, the direction of the JT axis was correctly reproduced through the atoms N(2)-Ni(1)-Cl(1A). The Ni-Ni distance in the dimer **37** for S = 1 and S = 0 were found to be comparable at 3.76 Å and 3.77 Å respectively.

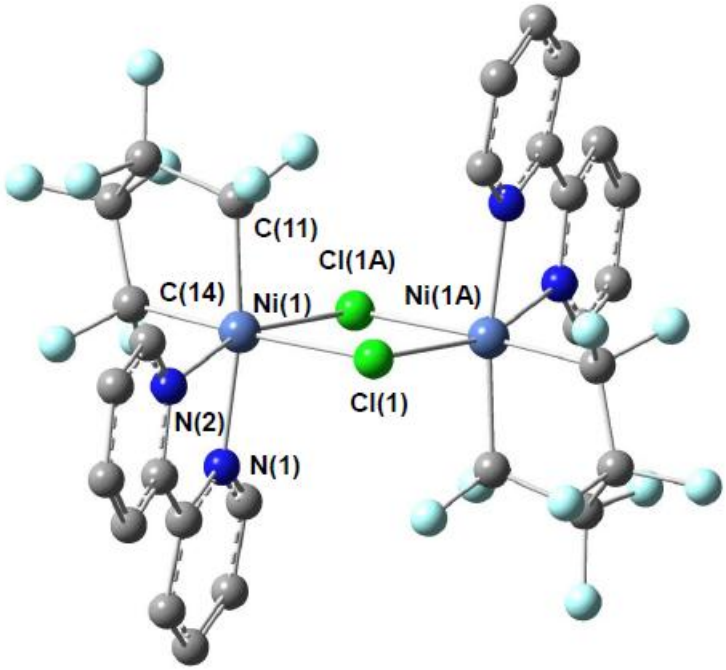

Figure 5. Optimized molecular structure of [Ni(C_4F_8)(bipy)(μ-Cl)]$_2$ (**37**) by DFT.

Table 2. Calculated bond lengths (Å) of [Ni(C_4F_8)(bipy)(μ-Cl)]$_2$ (**37**) in S = 1 (S = 0).

	Bond Length (Å)		**Bond Length (Å)**
Ni(1)-C(14)	2.00 (2.00)	Ni(1)-N(2)	2.21 (2.20)
Ni(1)-C(11)	2.01 (2.01)	Ni(1)-Cl(1)	2.37 (2.37)
Ni(1)-N(1)	2.07 (2.07)	Ni(1)-Cl(1A)	2.61 (2.62)

The Ni^{III} (d^7) dimer **37** has a distorted octahedral geometry resulting from a lowering of symmetry, arising from a first-order JT distortion of the $(t_{2g})^6(e_g)^1$ electron configuration at each Ni center. Natural population analysis (NPA) derived a spin density for the Ni(1) atom of 0.922 when the dimer **37** is in the triplet spin state (S = 1) and 0.921 in the singlet spin state (S = 0). The NPA derived spin density for the Ni(1A) is of equal value to Ni(1), but is of opposite sign in the case of S = 0. This indicates that an unpaired electron is largely localized on each of the Ni atoms. Furthermore, the calculated charge on the Ni atom was similar for **37** in the S = 1 and S = 0 at 0.386 and 0.387 respectively. The unpaired electron resides in the α-spin Highest Occupied Molecular Orbital (HOMO) of each [Ni(C_4F_8)Cl(bipy)] unit, which has been depicted using an isosurface value of 0.1 (Figure 6). The HOMO is made up of antisymmetric contributions of the Ni d_{z2} orbital and the p_z orbitals of the Cl and N_{bipy} atoms of the JT axis, as well as the sp^3 orbital of C_{C4F8} *trans* to the second N_{bipy} atom.

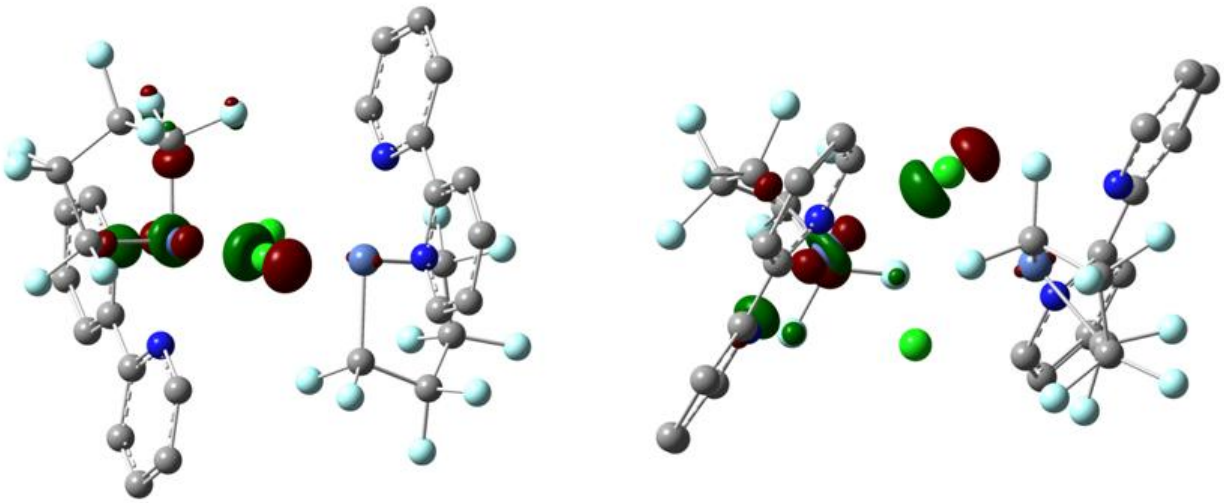

Figure 6. α-Spin HOMO of [Ni(C_4F_8)(bipy)(μ-Cl)]$_2$ (**37**) represented in two views.

In comparing the energies outlined in Table 3, the free energy in gas-phase for **37** with S = 1 is slightly lower at 5.51 kcal mol^{-1} than S = 0 at 6.11 kcal mol^{-1}. When solvation in CH_3CN is taken into account, the free energy of **37** with the S = 1 and S = 0 was found to increase to 15.00 and 15.55 kcal mol^{-1} respectively. The energy of formation of the dimer **37** refers to the bridging of two monomeric [Ni(C_4F_8)Cl(bipy)] units and is comparable for S = 1 and S = 0 where the triplet spin state is larger by 0.02 kcal mol^{-1}. The very minor differences in energies for the triplet and singlet spin states suggests that there is weak coupling of the Ni centers in **37**. Furthermore, the large increase in free energy in acetonitrile, compared to the gas-phase, suggests that the dimeric structure of **37** is not favorable in solution.

Table 3. Energies (kcal mol^{-1}) calculated for [Ni(C$_4$F$_8$)(bipy)(μ-Cl)]$_2$ (**37**) in the singlet (S = 0) and triplet (S = 1) spin states.

	Gas-phase free energy	**Free energy in solution (CH_3CN)**	**Energy of formation**
S = 0	6.11	15.55	-10.37
S = 1	5.51	15.00	-10.35

4.3. Alternative Synthesis of [Ni(C$_4$F$_8$)(bipy)(μ-Cl)]$_2$

The treatment of [Ni(C$_4$F$_8$)(bipy)] (**31**) with SO_2Cl_2 was carried out in anticipation of a direct route to the Ni(IV) complex [Ni(C$_4$F$_8$)Cl$_2$(bipy)]. However, even with excess SO_2Cl_2, the formation of the Ni(IV) complex was not observed. Addition of SO_2Cl_2 to a chlorobenzene solution of **31**, resulted in the formation of an orange-red precipitate that was found to be an intermediate complex (**38**). Significantly, dissolution of **38** in either THF or DME, affords complex [Ni(C$_4$F$_8$)(bipy)(μ-Cl)]$_2$ (**37**) (Scheme 14). Isolation of **37** from THF was confirmed by XRD and by comparison with the previously recorded IR spectrum of **37** as reported in Chapter 2, Section 5.4.

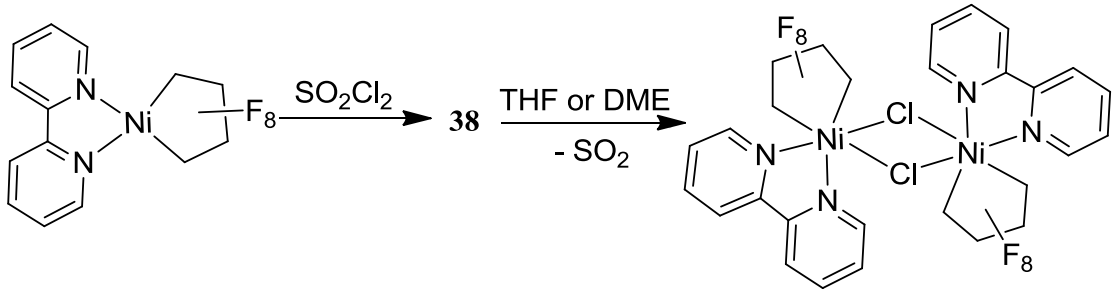

31 **37**

Scheme 14. Synthesis of [Ni(C$_4$F$_8$)(bipy)(μ-Cl)]$_2$ (**37**) with SO_2Cl_2 as chloride source.

The intermediate complex (**38**) was characterized in the solid state by UV/Vis and IR spectroscopy. Frequencies at 1232, 1182, 1142, 903 and 866 cm^{-1} of the IR of **38** (Appendix A) could be assigned to vibrational modes associated with a coordinated SO_2Cl_2 moiety,[55] suggesting that **38** could have either the molecular formula of [Ni(C_4F_8)(Cl_2SO_2)(bipy)] or [Ni(C_4F_8)(bipy)(μ-Cl_2SO_2)]$_2$. Repeated attempts to isolate a sample of **38** suitable for XRD analysis have consistently afforded **37** due to the instability of **38** in solution. The solid state UV/Vis electronic absorption spectrum of **38** illustrated in Figure 7 (a) differs from that of **37**, which is depicted in Figure 7 (b).

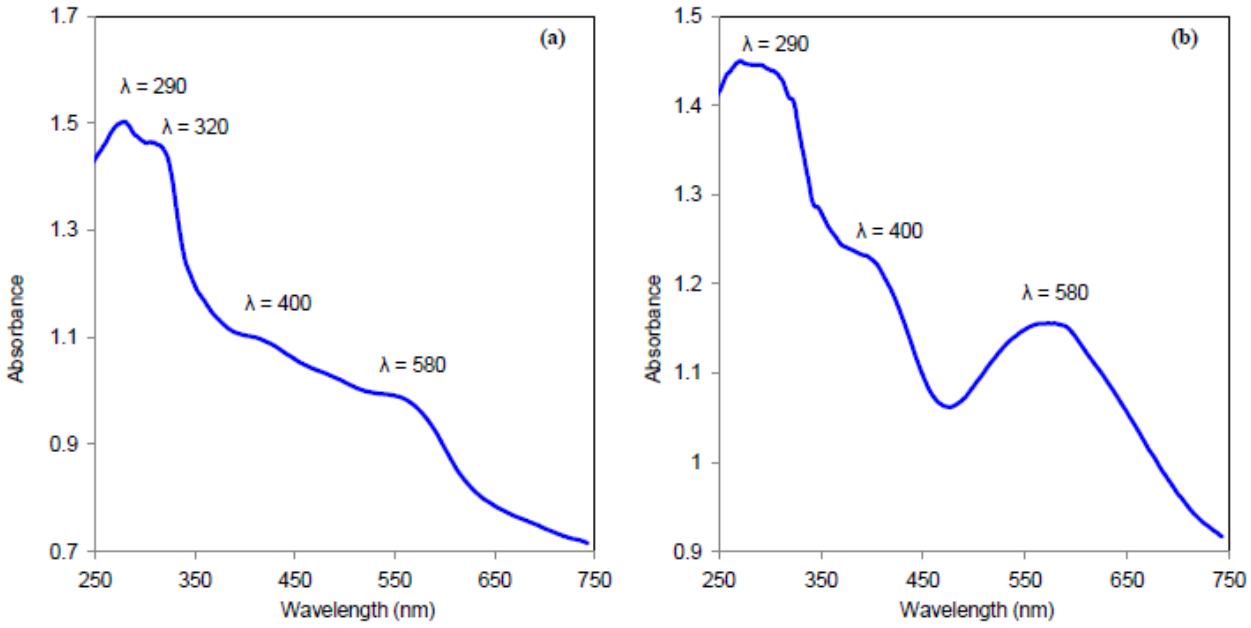

Figure 7. Solid state UV/Vis absorption spectrum of (a) intermediate complex **38**. (b) [Ni(C_4F_8)(bipy)(μ-Cl)]$_2$ (**37**).

4.4. Further Spectroscopic Characterization of [Ni(C_4F_8)(bipy)(μ-Cl)]$_2$

Further investigations into the solution state electronic absorption spectra of **37** demonstrate differences in the coordination sphere of complex **37** upon dissolution. The UV/Vis absorption spectrum of **37** in nitromethane (Figure 8 (a)) was found to differ significantly from that of solid **37** (see above Figure 7 (b)) with bands at 436 nm and 390 nm. Although nitromethane is known to be weakly coordinating, polar solvent, with a low Gutmann donor number of 2.7 kcal mol^{-1},[56] the difference in absorption spectra suggests that there is an interaction between **37** and nitromethane.[57] Further comparison was made with the UV/Vis absorption spectrum of **37** in another weakly coordinating solvent, CH_2Cl_2,[58] in which a band was observed at 432 nm (Figure 8 (b)). Comparing this spectrum with that of solid **37** (Figure 7(b)) further suggests that the dimeric structure does not persist in solution.

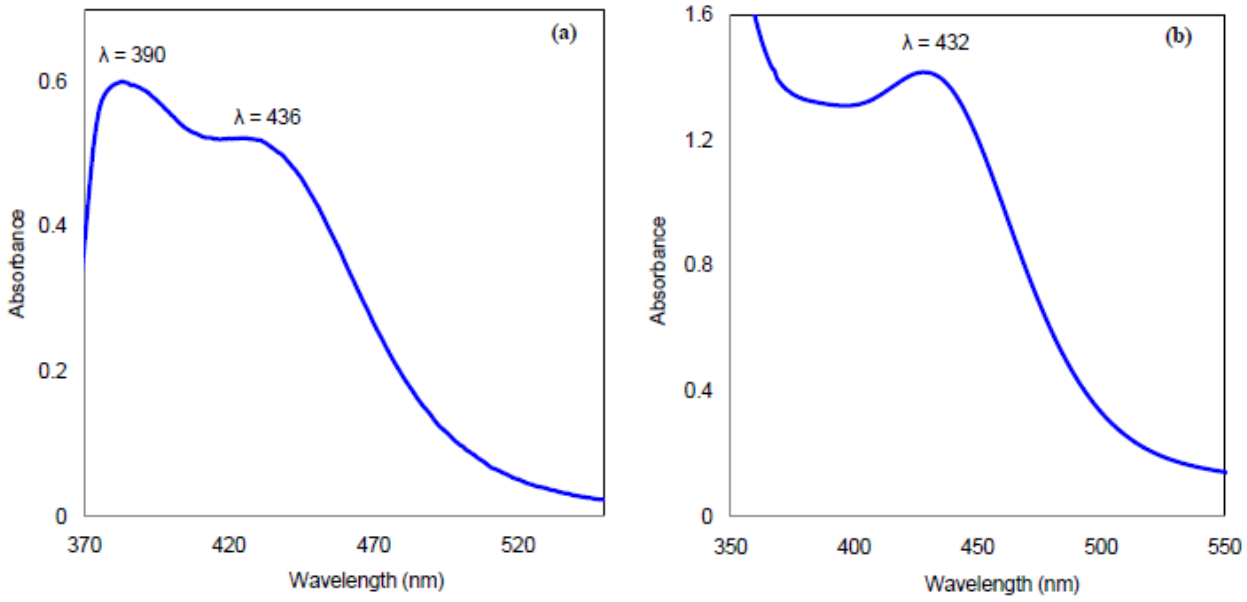

Figure 8. UV/Vis absorption spectra obtained by dissolving [Ni(C_4F_8)(bipy)(μ-Cl)]$_2$ (**37**) in (a) nitromethane. (b) dichloromethane.

The X-band EPR spectrum of **37** in the solid state showed a single broad resonance with a g-value of 2.155 at 171 K (Figure 9 (a)). By lowering the temperature to 10 K, the amplitude of the spectral line was found to increase (Figure 9 (b)). Interestingly, no hyperfine coupling to the N_{bipy} is observed at 10 K as found for the [Ni(C_4F_8)(OAC)(N-N)] complexes, with (N-N) = bipy (**34**), phen (**35**), tmeda (**36**).[41] The fact that the EPR spectral line is observed (Figure 9), infers that the complex **37** favors a triplet spin state (S = 1), as suggested by the computational studies discussed in Chapter 4 Section 2.

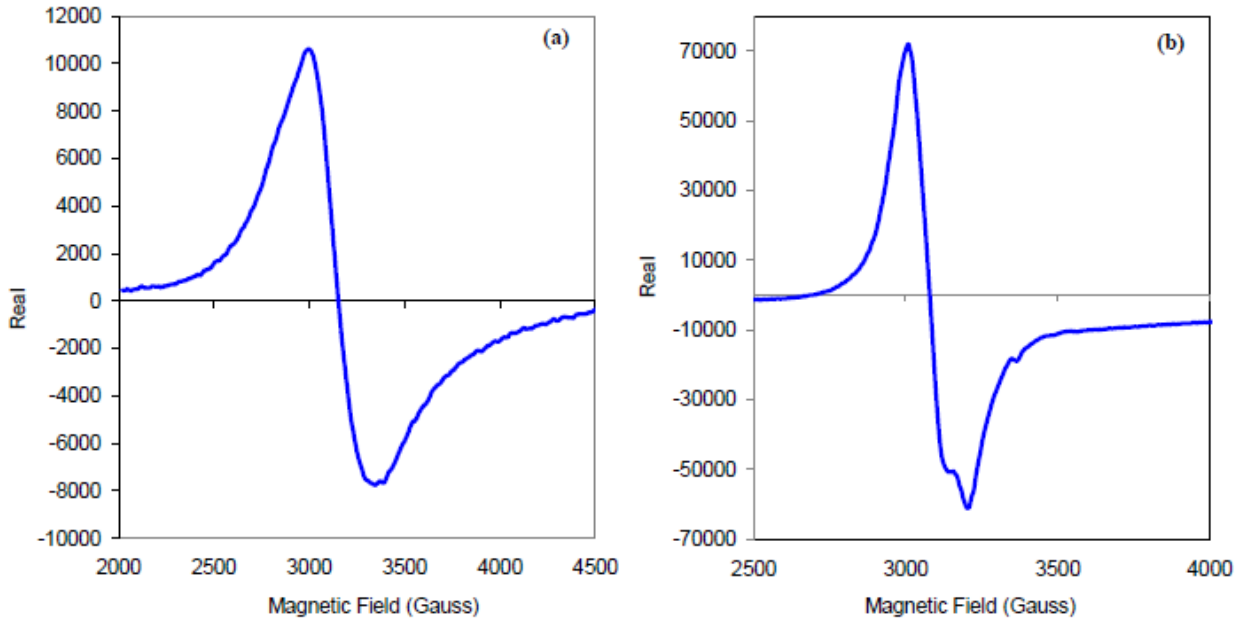

Figure 9. EPR spectrum of [Ni(C_4F_8)(bipy)(μ-Cl)]$_2$ (**37**) in the solid state measured at (a) 171 K. (b) 10 K.

The X-band EPR spectrum of **37** in a nitromethane glass at 160 K showed a weak, broad resonance with a g-value of 2.553 which sharpened somewhat in the Q-band spectrum with

overlapped g_1 and g_2 of ca. 2.223 and g_3 of 2.174 at 10 K (Figure 10). This further demonstrates differences of **37** in the solid state versus nitromethane solution.

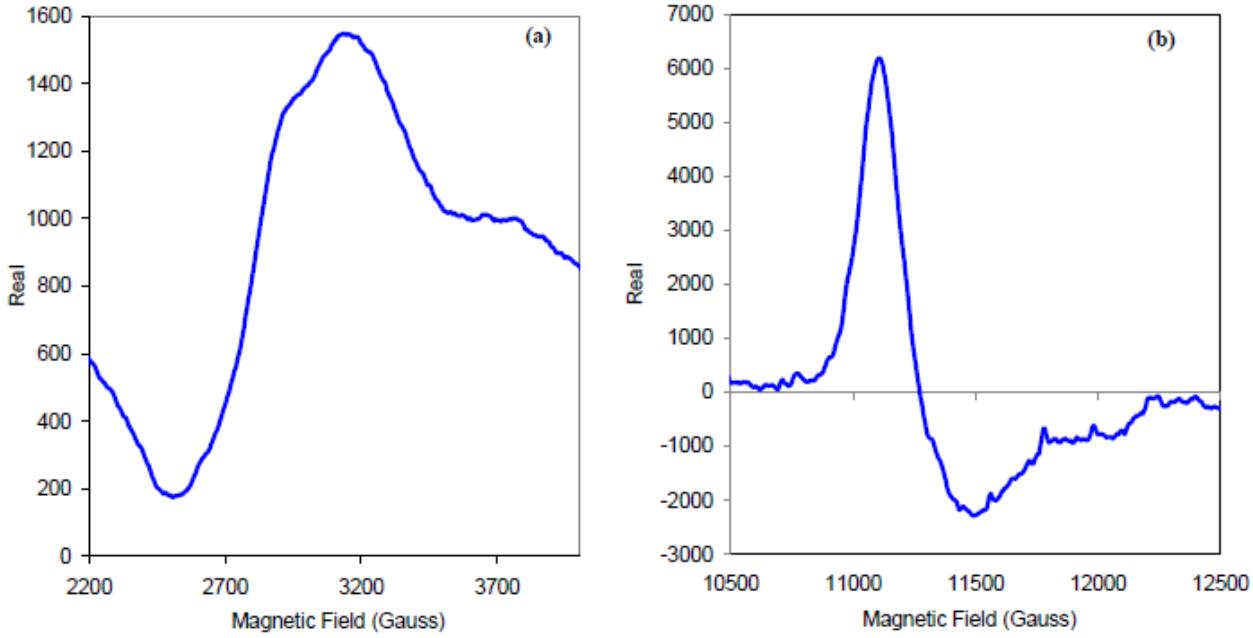

Figure 10. EPR spectrum of [Ni(C$_4$F$_8$)(bipy)(μ-Cl)]$_2$ (**37**) in nitromethane measured at (a) X-band, 160 K (b) Q-band, 10 K.

4.5. Electrochemistry of [Ni(C$_4$F$_8$)(bipy)(μ-Cl)]$_2$

The accessibility of Ni(IV) complexes from [Ni(C$_4$F$_8$)(bipy)(μ-Cl)]$_2$ (**37**) in nitromethane was investigated by cyclic voltammetry (CV). This approach is particularly advantageous as information can be obtained on the reversibility and formal potential of an electrochemical transformation.[59] Furthermore, CV can be used to examine transient complexes, without requiring their isolation.

The cyclic voltammogram (CV) of [Ni(C$_4$F$_8$)(bipy)(μ-Cl)]$_2$ (**37**) was obtained in nitromethane in the presence of the supporting electrolyte [(^{n}Bu)$_4$N][PF$_6$] at a Pt working

electrode. Prior to CV analysis, **37** was recrystallized twice to ensure that any potential couples observed were indeed due to the complex of interest. Furthermore, a blank scan of a 0.1 M [(^{n}Bu)$_4$N][PF_6] in nitromethane indicated the system was free of impurities. A 3 mM solution of **37**, was scanned at a sweep rate (v) of 0.1 V s^{-1} in the potential range of 1.8 to -0.6 V (corrected versus [$(C_5H_5)_2Fe]^{+/0}$) and ran initially from 0 V versus open circuit (OC) with the forward scan in the positive direction to obtain the CV in Figure 11. It is apparent that no reversible redox processes were detected. The reversible couple for the coordinated bipy could not be observed as it would be present at a more negative potential of -1.5 V which is not accommodated by the potential range of nitromethane. The first wave consists of an anodic peak at the potential (E_{pa}) 0.35 V with a shoulder at 0.52 V and a cathodic peak at the potential (E_{pc}) -0.27 V. The large separation of the E_{pa} and E_{pc} couples (ΔE_p of 0.62 V) is indicative of an irreversible process. The second wave has an E_{pa} at 1.20 V where the coupled E_{pc} has a shoulder at 1.07 V and a peak at 0.74 V.

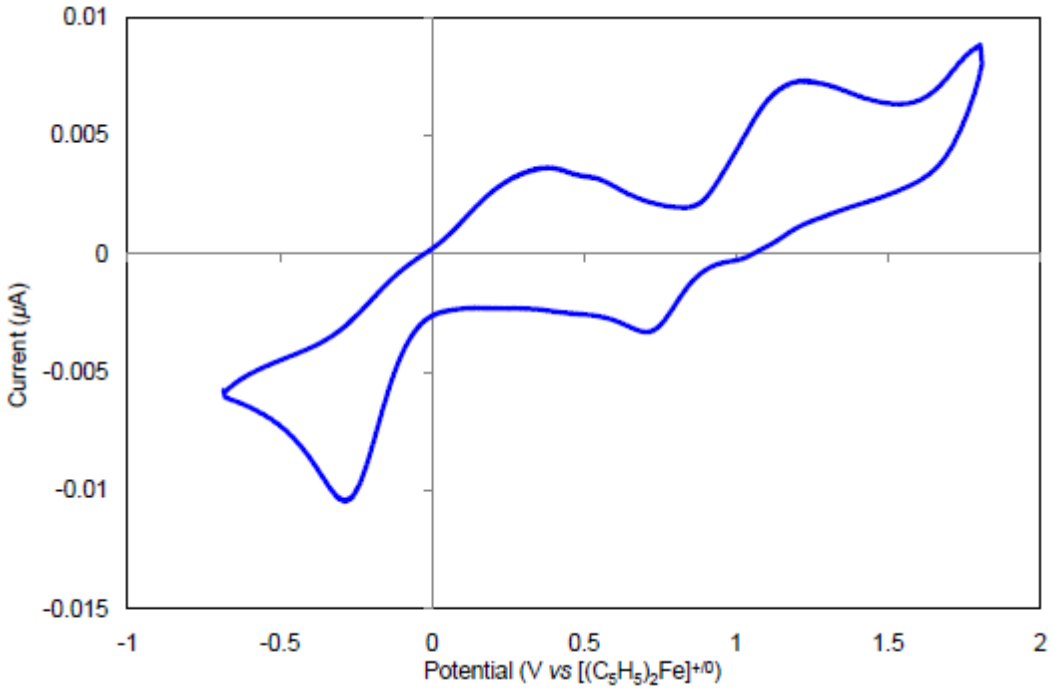

Figure 11. Cyclic voltammogram of [Ni(C$_4$F$_8$)(bipy)(μ-Cl)]$_2$ (**37**) in 0.1 M [(^{n}Bu)$_4$N][PF$_6$]/NO$_2$Me (v = 0.1 V s^{-1}).

The second wave was examined in closer detail from the range of 0.3 V to 1.5 V. The E_{pa} and E_{pc} were confirmed to be coupled due to the decrease in the amplitude of the E_{pc} observed with the narrowing of the potential range by 0.1 V increments on the more positive side. Furthermore, the sweep rate dependence for the second wave was investigated by varying the scan rate from 0.05 V/s to 0.2 V/s, which demonstrated a decrease in amplitude of the E_{pa} and E_{pc} with the decrease in sweep rate (Figure 12). This further signifies that this wave is of an irreversible coupled chemical reaction, with related oxidation and reduction processes. In addition, even at the higher sweep rate of 0.2 V/s, the CV did not show any quasireversibility (Figure 12).[60]

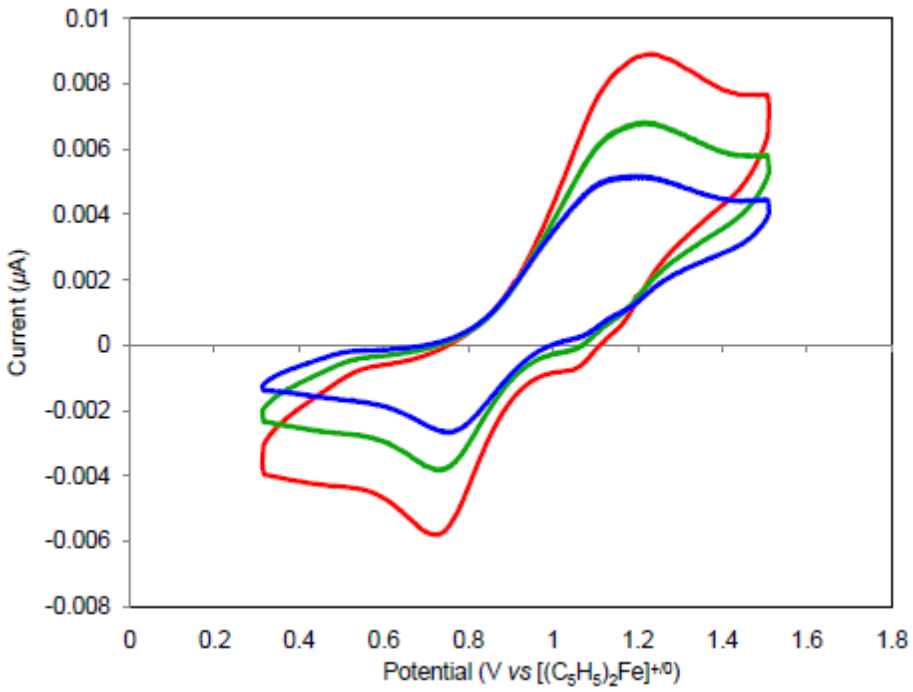

Figure 12. Cyclic voltammogram of [Ni(C$_4$F$_8$)(bipy)(μ-Cl)]$_2$ (**37**) in 0.1 M [(^{n}Bu)$_4$N][PF$_6$]/NO$_2$Me with sweep rates of 0.05 V s^{-1} (blue), 0.1 V s^{-1} (green) and 0.2 V s^{-1} (red).

4.6. Investigations to Generate [Ni(III)/Ni(IV)] Mixed-Valent Complexes or Ni(IV) Complexes from [Ni(C$_4$F$_8$)(bipy)(μ-Cl)]$_2$ Precursor

A stable mixed-valent [Ni(III)/Ni(IV)] radical cation could feasibly result from a one electron oxidation of **37**. The one-electron oxidant NOBF$_4$ was employed due to its high formal potential versus [(C$_5$H$_5$)$_2$Fe]$^{+/0}$ in nitromethane (0.98 V).[52] The treatment of [Ni(C$_4$F$_8$)(bipy)(μ-Cl)]$_2$ (**37**) with NOBF$_4$ in nitromethane was analyzed by X-band EPR at 160 K. Upon addition of excess NOBF$_4$ the solution became orange-brown in color and a new, distinct spectral line was observed with overlapped g_1 and g_2 of ca. 2.47 and g_3 of 2.27 (Figure 13 (a)). Moreover, the EPR spectral line at X-band sharpened with the temperature lowered to 10 K (Figure 13 (b)).

Additionally, EPR measurements at Q-band (10 K) demonstrated the resonance ($g_1 = g_2 = 2.223$ and $g_3 = 2.174$) previously observed for **37** in nitromethane (Chapter 4, Section 4) was greatly weakened following treatment with excess $NOBF_4$. These EPR spectra suggest a new metallacycle complex has been generated upon treatment of **37** with $NOBF_4$ in nitromethane, which may be a mixed valent [Ni(III)/Ni(IV)] radical cation, a complex that could feasibly form *via* a 1-electron oxidation. This proposal is currently being explored through appropriate simulations and DFT calculations.

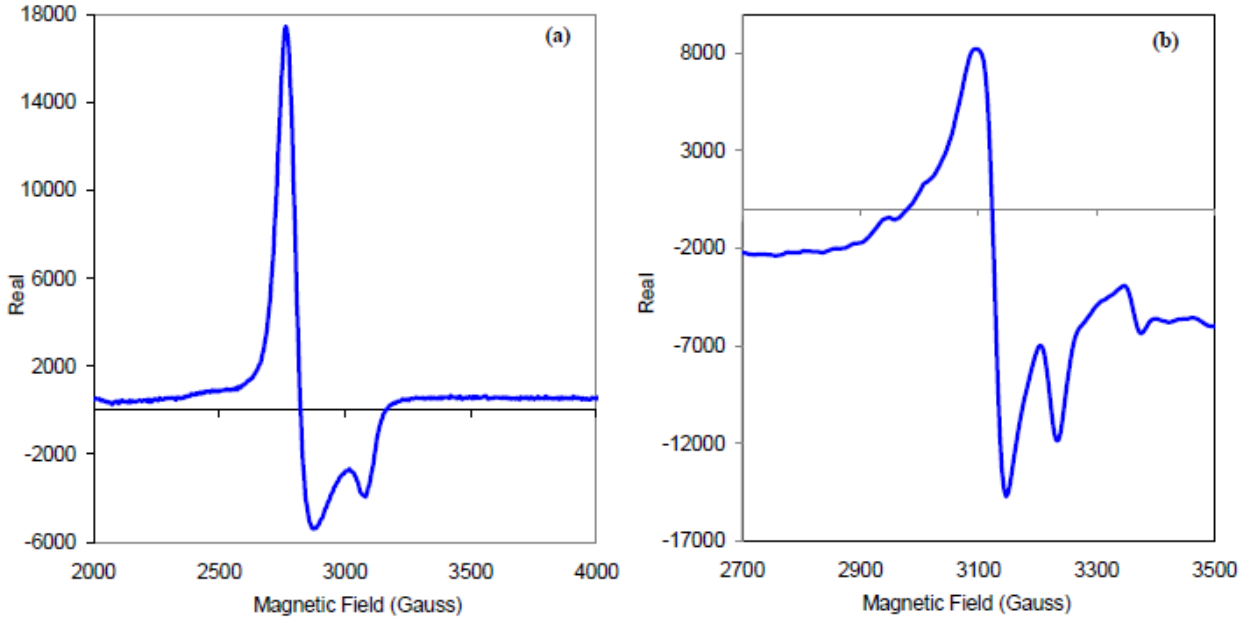

Figure 13. EPR spectrum of [Ni(C_4F_8)(bipy)(μ-Cl)]$_2$ (**37**) with $NOBF_4$ in nitromethane measured at (a) X-band, 160 K. (b) X-band, 10 K.

The ^{19}F NMR spectrum correlating to the treatment of **37** with $NOBF_4$ in nitromethane indicated that no diamagnetic, Ni(IV) metallacycle complexes were derived from **37**. As the solvent can have a dramatic impact on the relative formal potentials in redox reactions, this

procedure was repeated using dichloromethane. Addition of $NOBF_4$ to a CH_2Cl_2 solution of **37** followed by stirring for 4 days at r.t., resulted in the formation of new products, which were observed using ^{19}F NMR spectroscopy (Figure 14). Notably, broad resonances due to a new metallacycle complex (**E**) were observed, which represent two sets of inequivalent geminal fluorine atoms attributed to the α-carbons (α-CF_2) and β-carbons (β-CF_2) of the metallacycle moiety. The broad doublets due to the α-CF_2 groups (-96.56 and -101.1 ppm) exhibit $^2J_{FF\text{-}gem}$ of 160 Hz. The β-CF_2 moieties of **E** apparently have similar chemical shifts, which gives rise to a broad apparent doublet resonance at -135.16 ppm. Integration of these peaks is consistent with the 1:1:2 ratio required for a metallacycle with a mirror plane that bisects the C-Ni-C angle but no mirror plane relating the "up" and "down" F atoms of the CF_2 groups. Several sharp ^{19}F NMR resonances were also observed from this reaction solution, including those due to two diamagnetic metallacycle complexes **C** and **D** with higher symmetry than **E** (Figure 14).

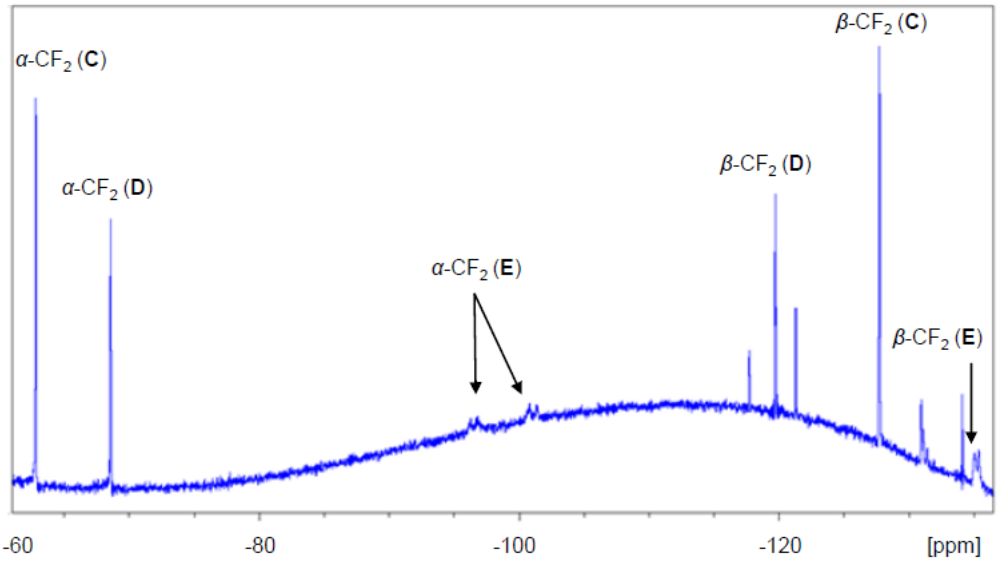

Figure 14. ^{19}F NMR spectrum of the reaction solution of [Ni(C$_4$F$_8$)(bipy)(μ-Cl)]$_2$ (**37**) and NOBF$_4$ in dichloromethane.

Treatment of [Ni(C$_4$F$_8$)(bipy)(μ-Cl)]$_2$ (**37**) with [Fe(C$_5$H$_5$)$_2$][BF$_4$] in nitromethane turned the solution green instantly. The ^{19}F NMR spectrum of the reaction solution following 2 d at r.t. showed two weak, broad resonances at -106.21 (α-CF$_2$) and -139.36 (β-CF$_2$) that have been assigned to metallacycle **F** (Figure 15). The paramagnetic complex **F** differs from **E** generated in the oxidation of NOBF$_4$ in that it would be a highly symmetric metallacycle with similar chemical shifts. The ^{19}F NMR resonances of **E** and **F** could be compared directly as solvent effects do not have a large impact on chemical shifts observed in ^{19}F NMR.[61]

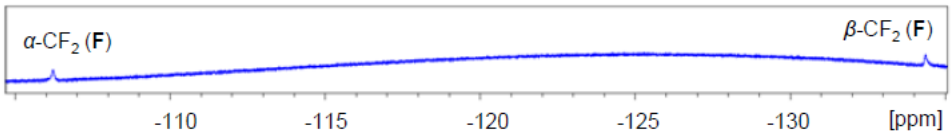

Figure 15. ^{19}F NMR spectrum of the reaction solution of [Ni(C$_4$F$_8$)(bipy)(μ-Cl)]$_2$ (**37**) and [Fe(C$_5$H$_5$)$_2$][BF$_4$] in nitromethane.

The feasibility of accessing a stable mixed-valent [Ni(III)/Ni(IV)] radical cation of **37** *via* a one-electron oxidation was investigated computationally, by Tony St-Jacques and Dr. Serge Gorelsky. There are two competing factors that influence the stability of the mixed-valent [Ni(III)/Ni(IV)] radical cation of **37**. The oxidation of an 19-electron nickel center would be stabilizing, but this is counteracted by a destabilizing affect attributed to the increased Coulomb repulsion between the Ni centers of the mixed-valent [Ni(III)/Ni(IV)] radical cation. The probability of removing an electron from the Ni d_{z2} contribution of the α-spin HOMO (discussed in Chapter 4, Section 2) was found to occur 20 % of the time, whereas removal from the Cl p_z contribution had a probability of 30 %. The molecular structure of the dimer **37** (S = 1) was optimized with a +1 charge, in order to model the [Ni(III)/Ni(IV)] radical cation complex. The calculated Ni-ligand bond distances of the mixed-valent [Ni(III)/Ni(IV)] radical cation (Figure 16, Appendix C) are listed in Table 4. The Ni-Ni distance in the mixed-valent [Ni(III)/Ni(IV)] radical cation was calculated to be 3.66 Å; significantly decreased from that calculated in the Ni(III) dimer (3.76 Å), as the Ni-Cl bond distances become shorter, increasing the Coulomb repulsion between the Ni centers and ultimately destabilizing the mixed-valent [Ni(III)/Ni(IV)] radical cation.

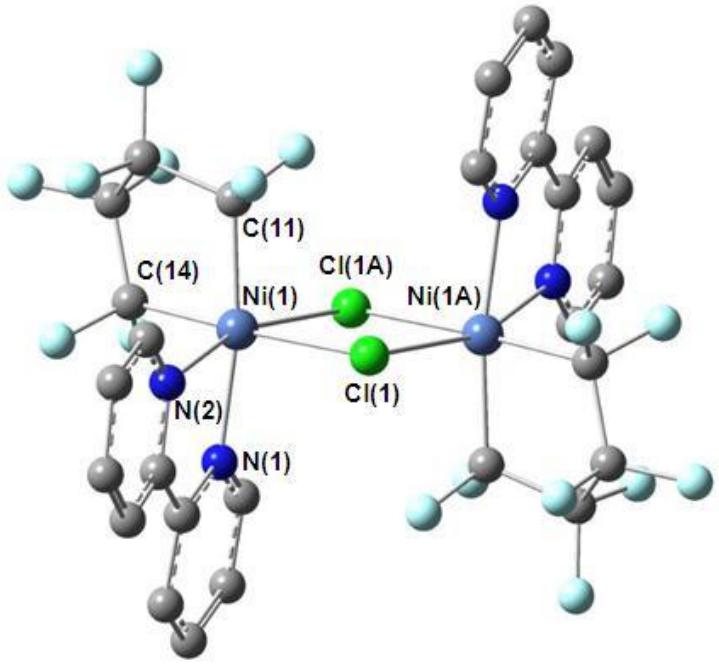

Figure 16. Optimized molecular structure of mixed-valent [Ni(III)/Ni(IV)] radical cation derived from [Ni(C$_4$F$_8$)(bipy)(μ-Cl)]$_2$ (**37**) by DFT.

Table 4. Calculated bond lengths (Å) of mixed-valent [Ni(III)/Ni(IV)] radical cation derived from [Ni(C$_4$F$_8$)(bipy)(μ-Cl)]$_2$ (**37**).

	Bond Length (Å)		**Bond Length (Å)**
Ni(1)-C(14)	2.02	Ni(1)-N(2)	2.09
Ni(1)-C(11)	2.04	Ni(1)-Cl(1)	2.44
Ni(1)-N(1)	2.06	Ni(1)-Cl(1A)	2.40

4.7. Conclusions

Modification of the Ni ligand sphere was achieved by treatment of [Ni(C$_4$F$_8$)(OAc)(bipy)] (**34**) with TMS-Cl to afford [Ni(C$_4$F$_8$)(bipy)(μ-Cl)]$_2$ (**37**). Alternatively, **37** can be formed *via* treatment of [Ni(C$_4$F$_8$)(bipy)] with SO_2Cl_2. The molecular structure of

[Ni(C_4F_8)(bipy)(μ-Cl)]$_2$ (**37**) was obtained *via* XRD. It is evident from the molecular structure of **37** that this complex contains a Jahn-Teller distortion, which has been rationalized using DFT.

Further characterization of **37** by UV/Vis and EPR spectroscopy indicates that complex **37** dissociates in solution, generating a complex that interacts with a range of organic solvents. The weak EPR spectral line observed for **37** in nitromethane indicated that some of the dimeric complex was present in solution, suggesting that the monomeric and dimeric complexes are in equilibrium. Minimal coupling of the Ni centers in the dimer **37** was also indicated by computational work. The cyclic voltammogram of **37** in nitromethane did not indicate the presence of a reversible oxidation wave which could be unambiguously assigned to a Ni(III)/Ni(IV) couple.

Treatment of **37** with $NOBF_4$ or [Fe(C_5H_5)$_2$][BF_4] in weakly coordinating solvents,[57,58] CH_2Cl_2 or nitromethane, resulted in the formation of new paramagnetic and diamagnetic metallacycles, as indicated by EPR and ^{19}F NMR spectroscopy. While the structures of the resulting complexes are not known, DFT calculations indicate the formation of the mixed-valent [Ni(III)/Ni(IV)] radical cation would not be favorable.

In work outlined in this chapter, reaction of [Ni(C_4F_8)(bipy)(μ-Cl)]$_2$ (**37**) has not unambiguously allowed access to Ni(IV) either by electrochemical or chemical oxidation. In Chapter 5 derivatives of **37** have been synthesized *via* addition of monodentate nitrogen ligands. These new complexes have been used as precursors to access the Ni(IV) oxidation state.

5. Investigations in the Synthesis and Reactivity of [Ni(C_4F_8)Cl(bipy)(L)]

5.1. Synthesis of [Ni(C_4F_8)Cl(bipy)($NCCH_3$)]

As described in Chapter 3, EPR and UV/Vis spectroscopy both indicate that [Ni(C_4F_8)(bipy)(μ-Cl)]$_2$ (**37**) is only stable in the solid state and upon dissolution favors dissociation to monomeric [Ni(C_4F_8)Cl(bipy)] units. Interestingly, the monomeric nickel(III) chloride was isolated as an acetonitrile adduct [Ni(C_4F_8)Cl(bipy)($NCCH_3$)] (**39**) even though in previous instances the dimeric complex **37** has been isolated *via* recrystallization from both THF and acetonitrile solutions (Scheme 15).

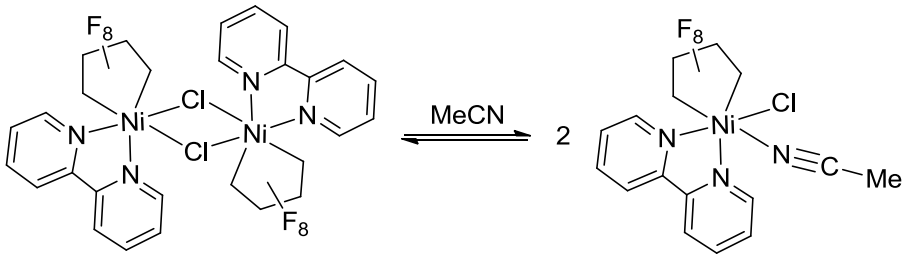

37 **39**

Scheme 15. Formation of monomeric acetonitrile adduct [Ni(C_4F_8)Cl(bipy)($NCCH_3$)] (**39**).

5.2. Analysis of the Molecular Structure of [Ni(C_4F_8)Cl(bipy)($NCCH_3$)]

Single crystals of **39** were isolated by Amani Farhat from a saturated solution of acetonitrile and analyzed by XRD.[54] The thermal ellipsoid representation of the molecular structure of **39** is represented in Figure 17. Selected bond lengths and angles are listed in Table 5 and further crystallographic information can be found in Appendix B. The molecular structure of complex **39** has a pseudo-octahedral geometry around the Ni atom. The sum of the equatorial bond angles equals 360.0° demonstrating that the C(11), N(1) , N(2) and N(3) atoms lie within the same plane. Furthermore, the axial bond angle, C(14)-Ni(1)-Cl(1), at 175.4(2)° is close to the

idealized 180° angle. The Ni-C_F bond distances of the Ni(C_4F_8) metallacycle in **39** at 1.962(7) Å (Ni(1)-C(14)) and 1.996(8) Å (Ni(1)-C(11)) are comparable to those found for the [Ni(C_4F_8)(bipy)(μ-Cl)]$_2$ dimer (**37**). Conversely, the two Ni-N bonds distances of the chelating bipy ligand of **39** are relatively long at 2.196(6) Å and 2.021(6) Å for the Ni(1)-N(1) and Ni(1)-N(2) bonds respectively, which are longer in comparison to the related contacts associated with dimer **37**. The Cl atom preferentially lies *trans* to C(14) of the metallacycle and the Ni(1)-Cl(1) bond distance is 2.281(2) Å. The acetonitrile ligand coordinated *trans* to the N(1) of the bipy ligand has a Ni(1)-N(3) bond distance of 2.180(7) Å. A search of the relevant molecular structures, currently deposited in the CCDC (March, 2010) indicates that the average Ni-N bond distance associated with a coordinating $NCCH_3$ is 2.061 Å. This suggests that for **39**, the $NCCH_3$ ligand is relatively weakly associated. Comparable to **37**, complex **39** also has a 19-electron Ni^{III} (d^7) center, owing to its tendency to adopt a pseudo-octahedral geometry.

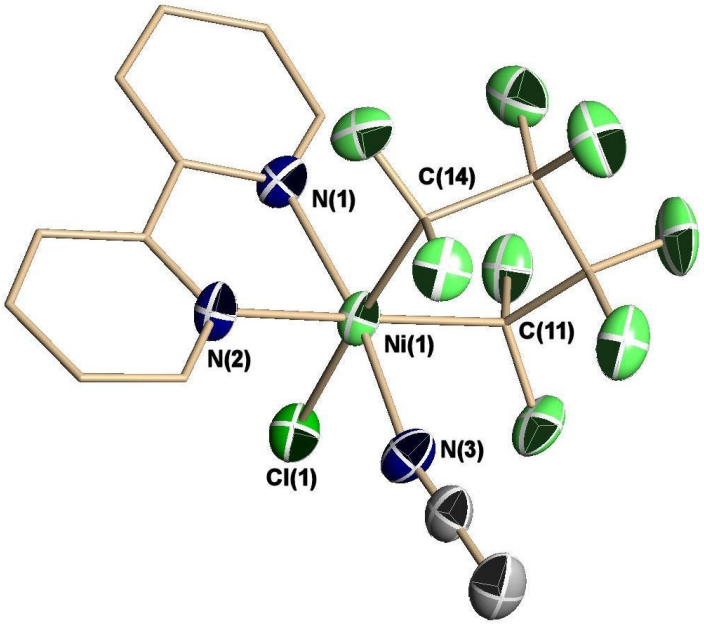

Figure 17. Thermal ellipsoid representation (50% probability ellipsoids) of the molecular structure of [Ni(C_4F_8)Cl(bipy)($NCCH_3$)] (**39**).

Table 5. Selected bond lengths (Å) and angles (°) of [Ni(C_4F_8)Cl(bipy)($NCCH_3$)] (**39**).

	Bond Length (Å)		**Bond Length (Å)**
Ni(1)- C(14)	1.962(7)	Ni(1)-N(3)	2.180(7)
Ni(1)-C(11)	1.996(8)	Ni(1)-N(1)	2.196(6)
Ni(1)-N(2)	2.021(6)	Ni(1)-Cl(1)	2.281(2)
	Bond Angle (°)		**Bond Angle (°)**
C(14)-Ni(1)-C(11)	84.8(3)	N(2)-Ni(1)-N(1)	78.7(2)
C(14)-Ni(1)-N(2)	91.8(3)	N(3)-Ni(1)-N(1)	169.8(2)
C(11)-Ni(1)-N(2)	176.3(3)	C(14)-Ni(1)-Cl(1)	175.4(2)
C(14)-Ni(1)-N(3)	90.6(3)	C(11)-Ni(1)-Cl(1)	90.6(2)
C(11)-Ni(1)-N(3)	87.4(3)	N(2)-Ni(1)-Cl(1)	92.7(2)
N(2)-Ni(1)-N(3)	91.1(3)	N(3)-Ni(1)-Cl(1)	89.8(2)
C(14)-Ni(1)-N(1)	90.1(3)	N(1)-Ni(1)-Cl(1)	90.32(18)
C(11)-Ni(1)-N(1)	102.8(3)		

Isolation of [Ni(C_4F_8)Cl(bipy)($NCCH_3$)] (**39**) further indicates that the related dimeric complex [Ni(C_4F_8)(bipy)(μ-Cl)]$_2$ (**37**) in dissociates in organic solvents. As was previously discussed in Chapter 4, Section 2, the free energy associated with **37** was found to increase upon solvation. To further investigate the instability of **37** in solution, DFT calculations examining the molecular structure of the monomeric [Ni(C_4F_8)Cl(bipy)] unit have been performed by Tony St-Jacques and Dr. Serge Gorelsky. The calculated Ni(1)-ligand bond distances of the monomeric [Ni(C_4F_8)Cl(bipy)] unit (Figure 18 and Appendix C) are reported in Table 6. Notably, all bond distances were found to be comparable with those obtained from the molecular structure of related [Ni(C_4F_8)Cl(bipy)($NCCH_3$)] (**39**) by XRD. Optimization of the monomeric unit [Ni(C_4F_8)Cl(bipy)], demonstrates its relative stability and further supports that **37** favors a triplet spin state. In addition, this further indicates a dynamic interaction can readily occur between coordinating solvents and dimer **37**.

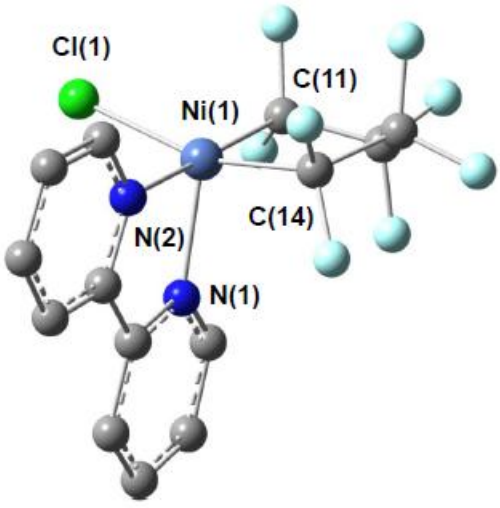

Figure 18. Optimized molecular structure of monomeric [Ni(C_4F_8)Cl(bipy)] unit by DFT.

Table 6. Calculated bond lengths (Å) of monomeric [Ni(C_4F_8)Cl(bipy)] unit.

	Bond Length (Å)		**Bond Length (Å)**
Ni(1)-C(14)	2.00	Ni(1)-N(2)	2.03
Ni(1)-C(11)	1.97	Ni(1)-Cl(1)	2.24
Ni(1)-N(1)	2.10		

5.3. Spectroscopic Characterization of [Ni(C_4F_8)(N-N)Cl(L)] Complexes

The X-band EPR spectrum of [Ni(C_4F_8)Cl(bipy)($NCCH_3$)] (**39**) in acetonitrile showed a spectral line with a g-value of 2.177, which could not be further resolved at 171 K (Figure 19 (a)). By lowering the temperature to 10 K and examining the sample at the higher frequency of Q-band, a well resolved spectrum was obtained, demonstrating the weak anisotropic character of **39** (Figure 19 (b)). The EPR spectral line was observed at Q-band (10 K) had overlapping g_1 and g_2 of ca. 2.233 and g_3 of 2.084. Similar to [Ni(C_4F_8)(bipy)(μ-Cl)]$_2$ (**37**), no hyperfine coupling was observed to N_{bipy}, even at Q-band at 10 K. Based on this EPR analysis, simulations are currently being conducted, with the aim of examining the solution state structure of **39**.

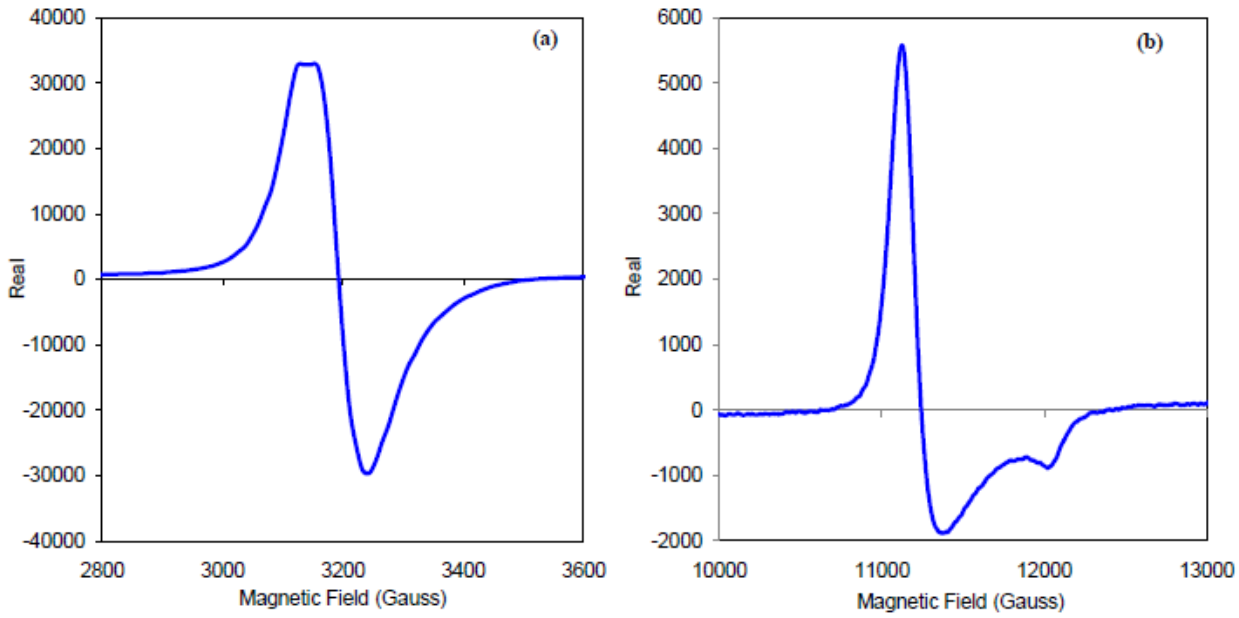

Figure 19. EPR spectrum of [Ni(C_4F_8)Cl(bipy)($NCCH_3$)] (**39**) in acetonitrile measured at (a) X-band, 171 K. (b) Q-band, 10 K.

The adduct [Ni(C_4F_8)Cl(bipy)($NCCH_3$)] **39** in acetonitrile presents an absorption band at 536 nm in the UV/Vis spectrum (Figure 20 (a)). The derivative [Ni(C_4F_8)Cl(bipy)(L)], L = pyridine (py) (**40**) was pursued for comparison to L = $NCCH_3$ (**39**) as py is often more coordinating and the resulting [Ni(C_4F_8)Cl(bipy)(py)] complex may have a more favorable formal oxidation potential. The pyridine adduct [Ni(C_4F_8)Cl(bipy)(py)] (**40**) was synthesized by dissolving [Ni(C_4F_8)(bipy)(μ-Cl)]$_2$ (**37**) in pyridine. Complex **40** was characterized by UV/Vis with an absorption band at 592 nm (Figure 20 (b)). Although attempts to isolate single crystals of **40** for XRD analysis were unsuccessful, it is clear by UV/Vis that the complex was formed *in situ* (Figure 20).

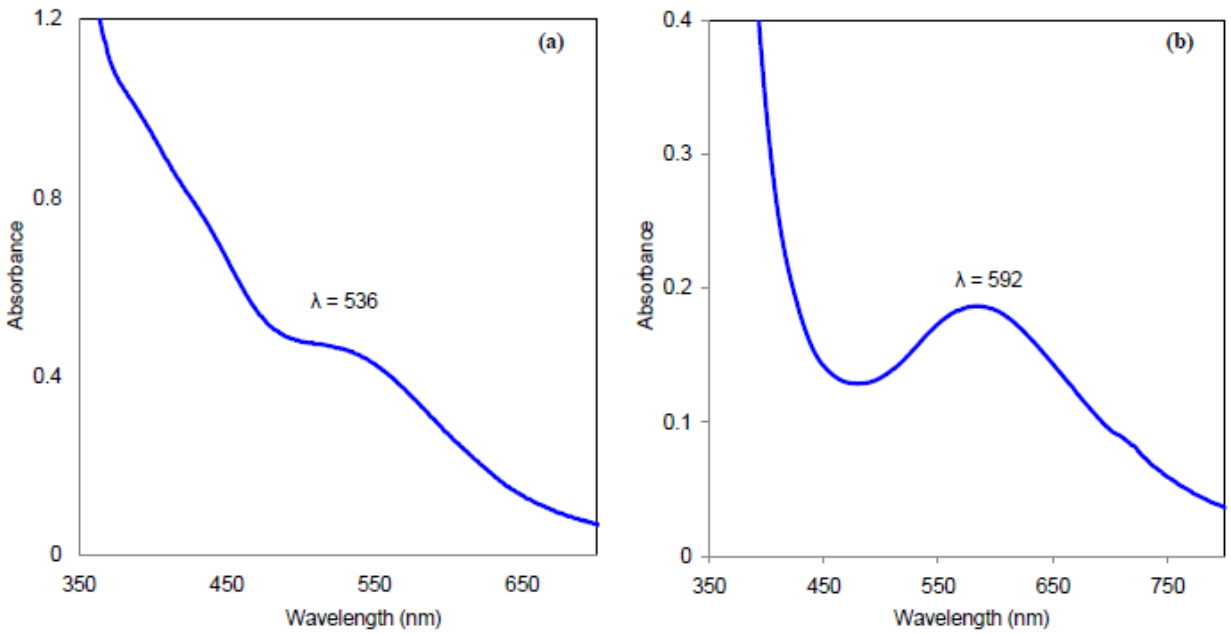

Figure 20. UV/Vis absorption spectra of (a) [Ni(C_4F_8)Cl(bipy)($NCCH_3$)] (**39**) in acetonitrile. (b) [Ni(C_4F_8)Cl(bipy)(py)] (**40**) in pyridine.

It is feasible that by employing 4-dimethylaminopyridine (dmap) as the coordinating ligand (L) of [Ni(C_4F_8)Cl(bipy)(L)], the resulting complex may be oxidized more readily than when L = CH_3CN or py. The resonance structures of free dmap are highlighted in Figure 21, and the capacity to delocalize charge in this π-conjugated system could feasibly stabilize a Ni(IV) complex.

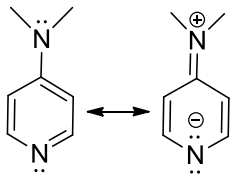

Figure 21. Resonance structures of 4-dimethylaminopyridine (dmap).

Treatment of a nitromethane solution of **37** with dmap instantly resulted in a dark blue solution which over time turned orange-brown. Upon sitting, a near stoichiometric amount of orange rectangular crystals formed. A single crystal was analyzed by XRD and was determined to be [Ni(C_4F_8)(bipy)] (**31**) (Figure 22 and Table 7). While **31** is a known complex, its molecular structure has not been published in the CCDC. The thermal ellipsoid representation of the molecular structure of **31** is displayed in Figure 22. Selected bond lengths and angles of **31** have also been reported in Table **7** and further crystallographic information can be found in Appendix B. Complex [Ni(C_4F_8)(bipy)] (**31**) has a square planar geometry, where the sum of the bond angles is equal to 360.0° signifying that the N(1), N(2), C(11) and C(14) atoms are contained within the same plane. The Ni-N bond distances for the chelating bipy ligand are 1.966(3) Å (Ni(1)-N(1)) and 1.956(3) Å (Ni(1)-N(2)) and are shorter in comparison to the Ni-N_{bipy} bond distances in [Ni(C_4F_8)(bipy)(μ-Cl)]$_2$ (**37**) and [Ni(C_4F_8)Cl(bipy)($NCCH_3$)] (**39**). Notably, the Ni-C_F bond distances in **31** at 1.906(4) Å and 1.911(5) Å, for Ni(1)-C(14) and Ni(1)-C(11) respectively, are also shorter in comparison to the Ni-C_F bond distances in [Ni(C_4F_8)(bipy)(μ-Cl)]$_2$ (**37**) (Chapter 4, Section 2) and [Ni(C_4F_8)Cl(bipy)($NCCH_3$)] (**39**) (Chapter 5, Section 2). This supports the hypothesis that an increase in oxidation state of nickel can activate the Ni-R_F bond.

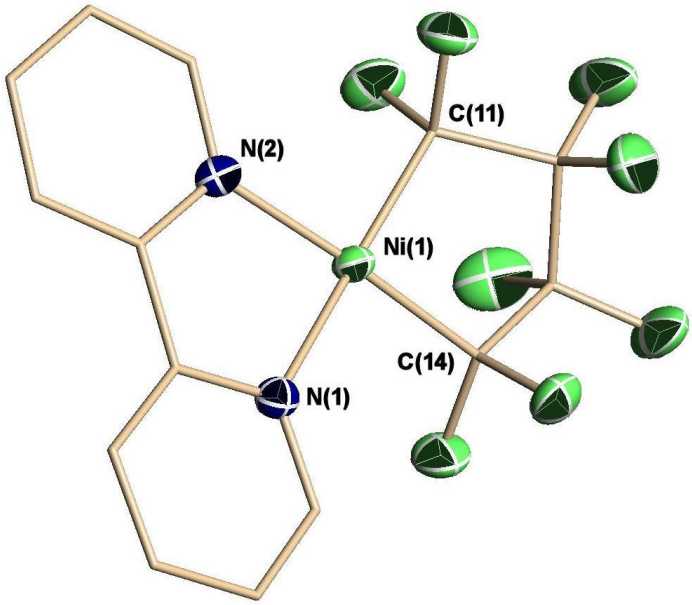

Figure 22. Thermal ellipsoid representation (50% probability ellipsoids) of the molecular structure of [Ni(C_4F_8)(bipy)] **31**.

Table 7. Selected bond lengths (Å) and angles (°) of [Ni(C_4F_8)(bipy)] (**31**).

	Bond Length (Å)		**Bond Length (Å)**
Ni(1)-C(14)	1.906(4)	Ni(1)-N(1)	1.966(3)
Ni(1)-C(11)	1.911(5)	Ni(1)-N(2)	1.956(3)
	Bond Angle (°)		**Bond Angle (°)**
C(14)-Ni(1)-C(11)	85.22(8)	C(14)-Ni(1)-N(1)	95.64(7)
C(14)-Ni(1)-N(1)	175.70(8)	C(11)-Ni(1)-N(1)	175.78(8)
C(11)-Ni(1)-N(2)	96.51(7)	N(1)-Ni(1)-N(2)	82.92(6)

Treatment of **37** with dmap was repeated in CH_2Cl_2, and after 12 h a pale green solid had precipitated from solution. The UV/Vis spectrum of this material in CH_2Cl_2 contains a strong absorbance band at 432 nm, the same absorbance found for a discrete sample of **37**. Evidently, in

CH_2Cl_2, interaction between **37** and dmap is relatively disfavored, suggesting that the mildly acidic nature of nitromethane is required for conversion of **37** to **31**.[62]

5.3. Electrochemistry of [Ni(C_4F_8)(N-N)Cl(L)] Complexes

Cyclic voltammetric data was collected for [Ni(C_4F_8)Cl(bipy)] (**39**) in ~ 0.1 M [(^{n}Bu)$_4$N][PF_6] in acetonitrile at a Pt wire working electrode. The acetonitrile adduct **39** was generated and characterized *in situ* by dissolving recrystallized [Ni(C_4F_8)(bipy)(μ-Cl)]$_2$ (**37**) in acetonitrile to afford a 3 mM solution of **39**. The solution was scanned at a sweep rate of 0.1V/s in the potential range of 1.4 to -1.6 V (corrected versus $[(C_5H_5)_2Fe]^{+/0}$) and ran initially from 0 V versus open circuit (OC) in the positive to negative direction to obtain the CV in Figure 23 (a). The first wave is reversible at -1.37 V, and can be attributed to the coordinated bipy ligand.[63] The second wave at 0.23 V, consisting of an anodic peak at the potential (E_{pa}) 0.31 V and a cathodic peak at the potential (E_{pc}) 0.15 V, results from a quasireversible process. Based on previous investigations made by Baldwin *et al.*, this wave can be attributed to a Ni(III) to Ni(IV) couple.[64] The third wave is due to an as yet unknown irreversible process, potentially involving a bipy radical species with an E_{pa} at 1.00 V.[59] The potential range was narrowed to 0.7 to -1.6 V at a sweep rate of 0.1 V/s in order to focus in on the significant transformations. The reversible oxidation wave was again observed for the coordinated bipy ligand at -1.4 V alongside the Ni(III) to Ni(IV) couple at 0.23 V, which now displays a higher degree of reversibility (Figure 23 (b)).

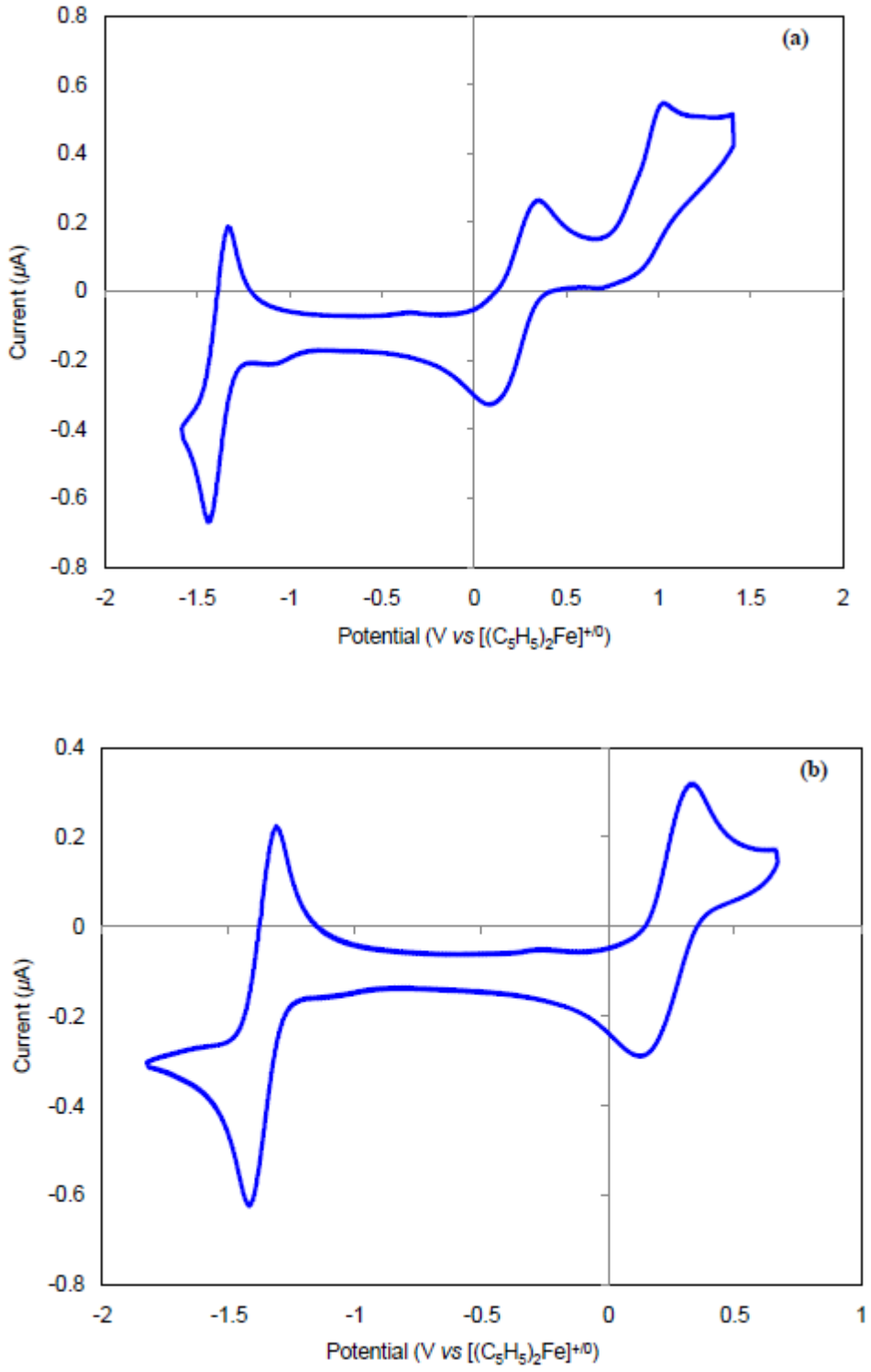

Figure 23. Cyclic voltammogram of [Ni(C_4F_8)Cl(bipy)($NCCH_3$)] (**39**) in 0.1 M [(^{n}Bu)$_4$N][PF_6]/CH_3CN (v = 0.1 V s^{-1}).

Cyclic voltammetric data were also collected for [Ni(C_4F_8)Cl(bipy)(py)] (**40**) in nitromethane with the supporting electrolyte [(^{n}Bu)$_4$N][PF_6] at a Pt wire working electrode. The adduct **40** was made and characterized *in situ* by treating [Ni(C_4F_8)(bipy)(μ-Cl)]$_2$ (**37**) with an equivalent of pyridine (py) in nitromethane to afford a ca. 3 mM solution of **40**. The solution was initially scanned at a sweep rate of 0.1V/s in the potential range of 1.5 to -0.7 V (corrected versus [(C_5H_5)$_2$Fe]$^{+/0}$) and ran initially from 0 V versus open circuit (OC) in the positive to negative direction to obtain the CV depicted in Figure 24. The first wave results from an as yet unknown irreversible transformation with an anodic peak at the potential (E_{pa}) 0.38 V and a cathodic peak at the potential (E_{pc}) -0.02 V. A second quasireversible wave is observed at 0.88 V, consisting of an E_{pa} at 0.92 V and a E_{pc} at 0.84 V with a shoulder at 0.62 V. Although the electrochemistry in nitromethane is still not entirely understood, it is clear that the second wave at 0.88 V becomes quasireversible due to the addition of pyridine.

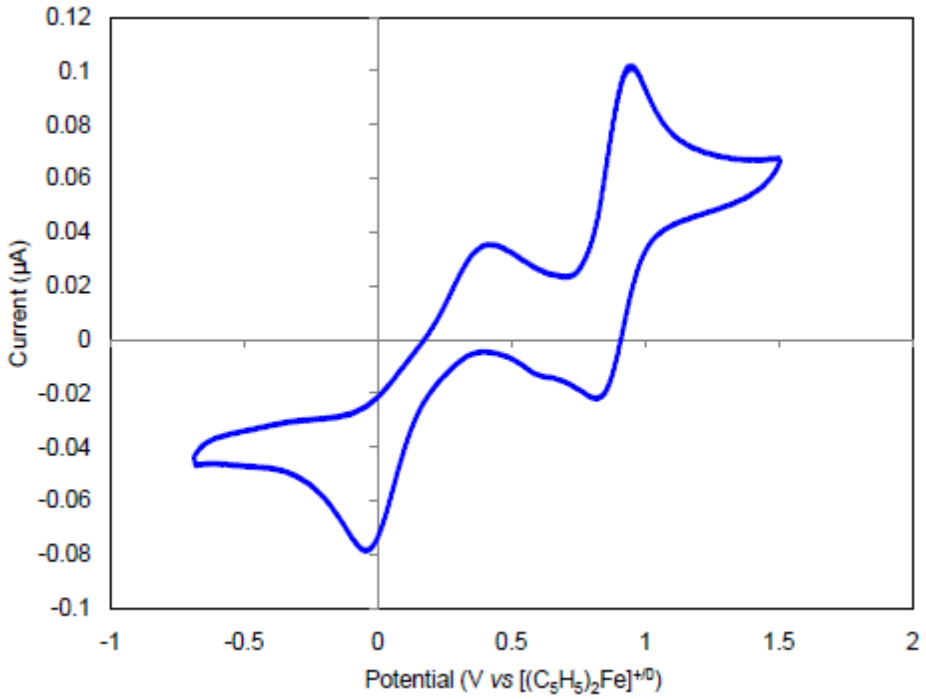

Figure 24. Cyclic voltammogram of [Ni(C_4F_8)Cl(bipy)(py)] (**40**) in 0.1 M [(^{n}Bu)$_4$N][PF_6]/CH_3NO_2 (v = 0.1 V s^{-1}).

Additionally, the sweep rate dependence for the second wave was observed by varying the scan rate from 0.3 V/s to 1.2 V/s (corrected versus $[(C_5H_5)_2Fe]^{+/0}$) (Figure 25). A noticeable change in the relative peak amplitude was observed with the increase in scan rate, as would be expected for a coupled transformation. Furthermore, the E_{pa} at 0.6 V became much more pronounced at the higher sweep rate.

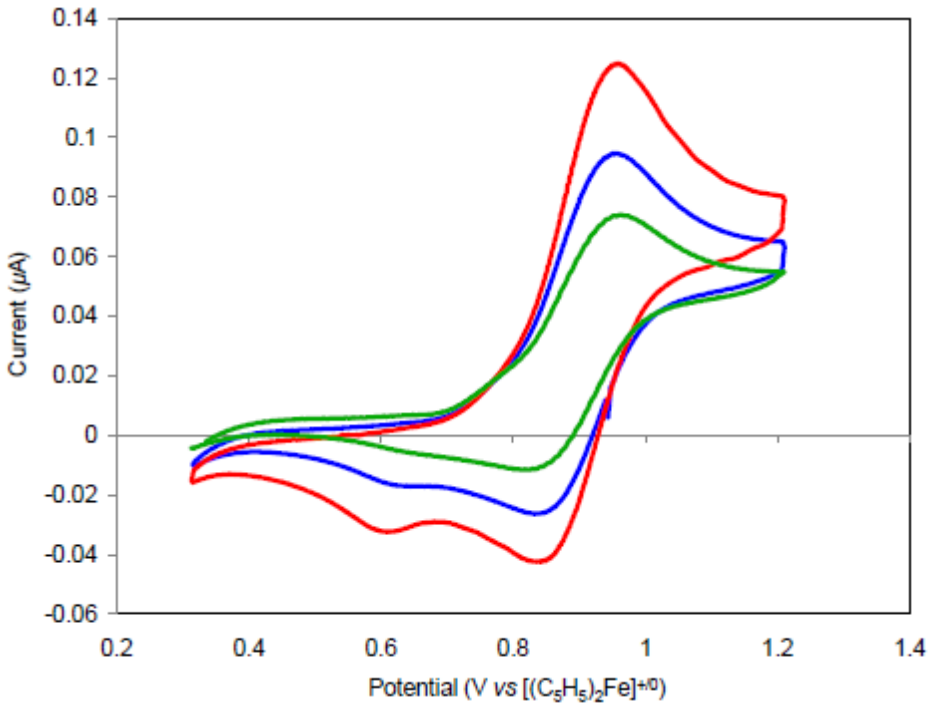

Figure 25. Cyclic voltammogram of [Ni(C_4F_8)Cl(bipy)(py)] (**40**) in 0.1 M [(^{n}Bu)$_4$N][PF_6]/CH_3NO_2 (v = 0.05 V s^{-1} (green), 0.1 V s^{-1} (blue) and 0.2 V s^{-1} (red)).

5.4. Investigations to Generate Ni(IV) Complexes from [Ni(C_4F_8)Cl(bipy)($NCCH_3$)] Precursor

One electron oxidation of the 19-electron complex, [Ni(C_4F_8)Cl(bipy)($NCCH_3$)] (**39**), would afford an 18-electron Ni(IV) complex, which could allow for increased reactivity of the Ni-R_F bond and ultimately afford fluorocarbon derivatives. Investigations were performed in acetonitrile due to the possibility of subsequent insertion of $NCCH_3$ into the Ni-R_F bond following the oxidation.[65] Initial studies to generate Ni(IV) complexes from **39** in acetonitrile involved the oxidant $NOBF_4$. A red-brown solution of **39** in acetonitrile instantly turned to bright purple and gas was evolved upon addition of $NOBF_4$. After 1 h the ^{19}F NMR spectrum (Figure

26) showed a new metallacycle species **G** with inequivalent α-CF_2 assigned to two broad doublets at -95.61 and -104.54 ppm with $^2J_{FF\text{-}gem}$ coupling of 165 Hz. The β-CF_2 moieties of **G** apparently have similar chemical shifts, which gives rise to a broad apparent doublet resonance at -135.39 ppm. Integration of these peaks is consistent with the 1:1:2 ratio required for a metallacycle with a mirror plane that bisects the C-Ni-C angle but no mirror plane relating the "up" and "down" F atoms of the CF_2 groups.

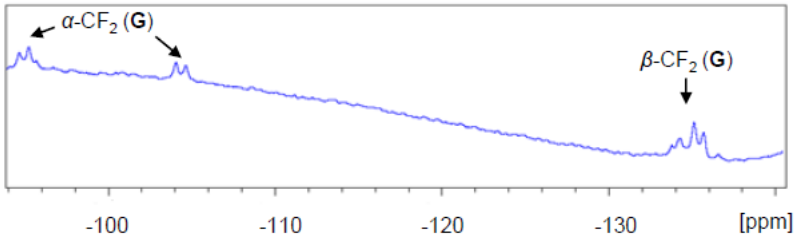

Figure 26. Selected range of ^{19}F NMR spectrum of the reaction solution of [Ni(C_4F_8)Cl(bipy)($NCCH_3$)] (**39**) with $NOBF_4$ in acetonitrile after 1 h.

In general, ^1H NMR analysis of reaction solutions of Ni(III) metallacycles with oxidants did not prove conclusive as resonances present for protio impurities were greater in ratio to resonances of the generated metallacycles. For instance, resonances assigned to the bipy ligand of a generated, diamagnetic metallacycle only became apparent when the reaction mixture was allowed to stir for 7 d. However, multiple new resonances in the ^{19}F NMR spectrum were observed at this time (Figure 27). Two sets of ^{19}F resonances were correlated by an ^{19}F-^{19}F COSY experiment. The first set consists of two triplets at -69.44 ppm and -120.27 ppm, which can be assigned to the α-CF_2 and β-CF_2 resonances of a new metallacycle complex **D**. The second set of resonances consists of two singlets at -105.83 and -129.31 ppm and can be assigned

to the product C_4F_6.[66] In addition to complex **G**, a second metallacycle (**H**) with inequivalent α-CF_2 (-86.77 and -95.61 ppm, $^2J_{FF\text{-}gem}$ = 153 Hz) and β-CF_2 (-134.03 ppm) moieties was generated. As Ni(IV) metallacycles would be isoelectronic to the related Fe(II) metallacycle complexes (d^6), it may be expected that the α-CF_2 and β-CF_2 resonances may have similar chemical shifts in the ^{19}F NMR spectra of the related complex. For instance, the ^{19}F NMR spectrum of the highly symmetric Fe(II) metallacycle [Fe(C_4F_8)($CO)_4$] has been previously reported to show two singlets at -83.6 (α-CF_2) and -123.9 ppm (β-CF_2).[22] A number of the described metallacycle complexes generated from oxidation reactions had comparable chemical shifts.

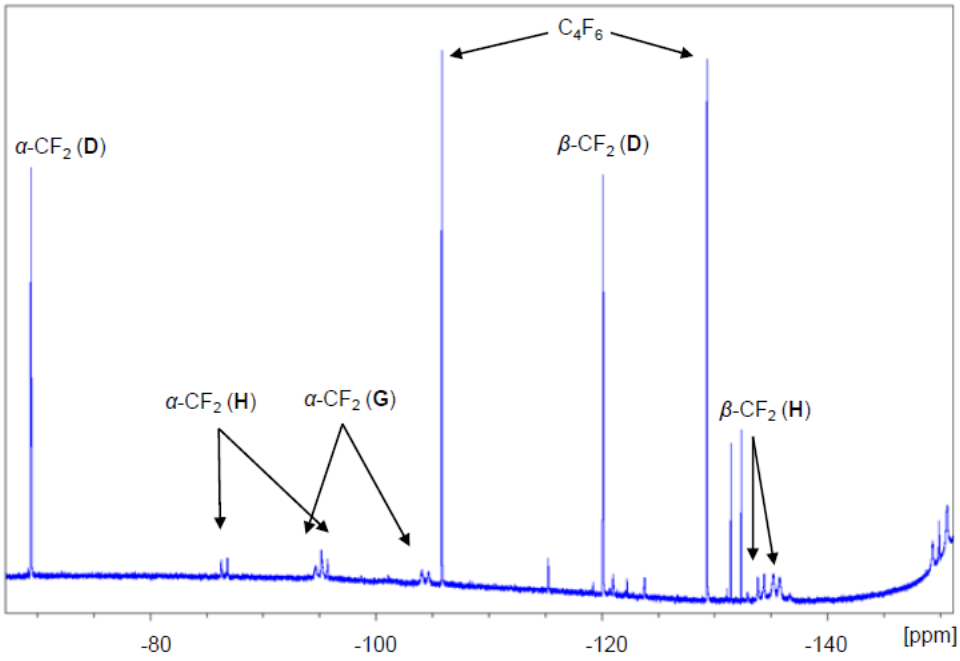

Figure 27. Selected range of $^{19}F\{^1H\}$ NMR spectrum of the reaction solution of [Ni(C_4F_8)Cl(bipy)($NCCH_3$)] (**39**) with $NOBF_4$ in acetonitrile stirred 7 d.

To confirm the formation of perfluorocarbon byproducts, the volatile components of the reaction were distilled and the resulting clear solution was analyzed by ^{19}F NMR and HPLC/MS. The ^{19}F NMR of the organic fraction, depicted in Figure 28, showed three singlets, of which the singlets at -105.83 and -129.31 ppm, correlated by a ^{19}F-^{19}F COSY experiment, were consistent with the presence of C_4F_6.[53]

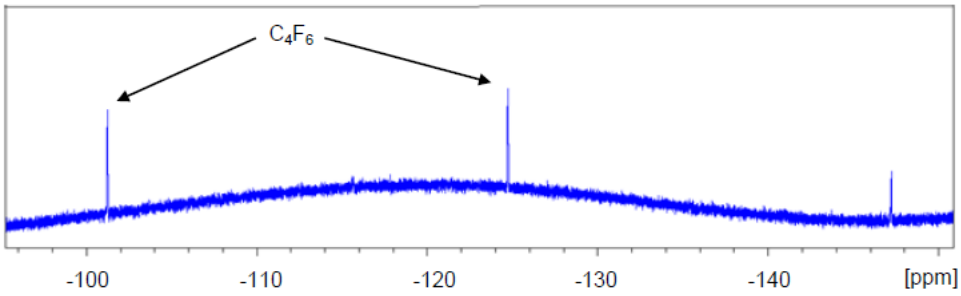

Figure 28. ^{19}F NMR of the organic fraction of the reaction solution of [Ni(C_4F_8)Cl(bipy)($NCCH_3$)] (**39**) with $NOBF_4$ in acetonitrile.

HPLC/MS was used as a second method of identifying generated fluorocarbon species. The optimal peak separation was observed with the UV/Vis detector (Appendix D) with a gradient mobile phase with A (90 % CH_3CN and 10 % H_2O) and B (90 % CH_3OH and 10 % H_2O) with a flow rate of 0.1 mL min^{-1}. The mass spectrogram (Appendix D) confirmed the presence of a species at 9.55 min, which corresponded to a broad UV absorption band at 8.11 min. Other absorption bands in the UV are due to species outside of the examined M_W range. This species was found to have mass to charge ratio (m/z) of 248.2, 217.0, 203.1, and 200.9 g mol^{-1} by Q1MS. The low-resolution MS suggested that the m/z of 203.1 is due to C_4F_6 $[M+Na{\cdot}H_2O]^+$ with the found M_W = 202.9 g mol^{-1}.

An alternative route attempted for the generation of Ni(IV) metallacycles involved treatment of [Ni(C_4F_8)Cl(bipy)($NCCH_3$)] (**39**) with the one-electron oxidant [Fe(C_5H_5)$_2$][BF_4] in acetonitrile. The ^{19}F NMR spectrum of the reaction solution after 1 d (Figure 29) showed sharp resonances at -110.30 ppm (α-CF_2) and -140.41 ppm (β-CF_2) that are assigned to previously characterized metallacycle **31** as well as a second new metallacycle complex **I** with α-CF_2 and β-CF_2 resonances at -106.89 and -139.64 ppm with a smaller line-width compared to **31**. Moreover, the generated metallacycles **I** would be expected to have high symmetry due to equivalent α-CF_2 and β-CF_2 F atoms. A possible structure for this type of Ni(IV) metallacycle could be [Ni(C_4F_8)(bipy)L_2]$^{2+}$ (L = $NCCH_3$) with L ligands occupying mutually *trans* positions and chloride and BF_4^- counter-ions.[67] Evidently, [Fe(C_5H_5)$_2$][BF_4] can oxidize **39** relatively cleanly, affording only two products at ca. 1:1 ratio according to ^{19}F NMR spectroscopy.

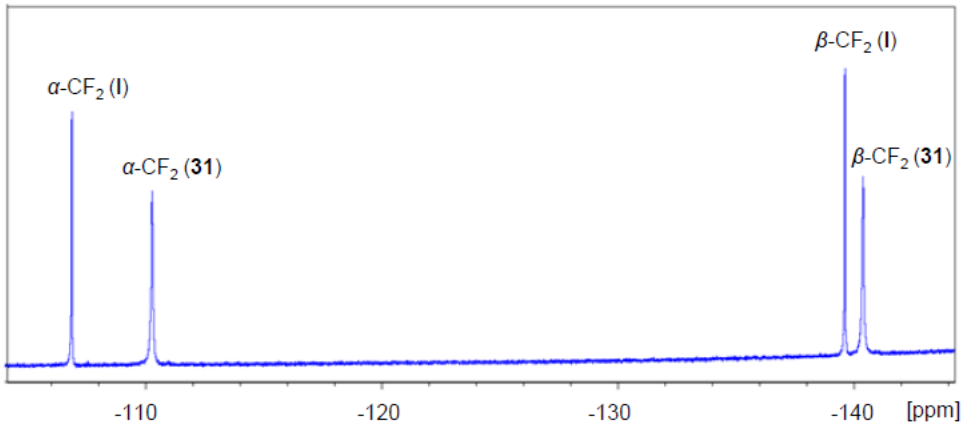

Figure 29. Selected range of ^{19}F NMR spectrum from the reaction of [Ni(C_4F_8)Cl(bipy)($NCCH_3$)] (**39**) with [Fe(C_5H_5)$_2$][BF_4] in acetonitrile.

5.5. Conclusions

Isolation of the adduct [Ni(C_4F_8)Cl(bipy)($NCCH_3$)] (**39**) was achieved following treatment of [Ni(C_4F_8)(bipy)(μ-Cl)]$_2$ (**37**) with acetonitrile. Complex **39** was characterized by a combination of EPR, UV/Vis spectroscopy, and CV. The latter demonstrated a quasireversible oxidation wave at 0.23 V, which is assignable to a Ni(III)/Ni(IV) couple. Furthermore, the molecular structure of complex **39** has been determined by single crystal XRD analysis. Relevant bond distances indicate that the $NCCH_3$ moiety of **39** is weakly bound, and this ligand can be displaced by donors such as py, giving a new adduct [Ni(C_4F_8)Cl(bipy)(py)] (**40**), which has been characterized using UV/Vis spectroscopy. Furthermore, CVs were obtained following the *in situ* formation of **40** in nitromethane by treating [Ni(C_4F_8)(bipy)(μ-Cl)]$_2$ (**37**) with py. Although the electrochemistry in nitromethane is not fully understood, it is clear that the addition of pyridine dramatically changes the CV relating to **37**. Upon addition of py, the oxidation wave at 0.88 V becomes quasireversible, this could result from the presence of **40.** Alternatively, deprotonation of nitromethane by py,[68] could yield [Ni(C_4F_8)(bipy)(X)] (X = $[NO_2CH_2]^-$).

Attempts to synthesize adducts employing stronger monodentate nitrogen ligands, such as dmap did not result in isolable [Ni(C_4F_8)Cl(bipy)(dmap)]. Instead, addition of dmap to **37** in nitromethane yielded [Ni(C_4F_8)(bipy)] (**31**), with the molecular structure of **31** being confirmed by single crystal XRD. The formation of **31** could have resulted from a disproportionation reaction of a reactive Ni(III) complex. Alternatively, **31** could have formed *via* reductive elimination of an unstable Ni(IV) intermediate. Inspection of the ^{1}H NMR did not indicate the formation of a postulated by-product 4-dimethylaminopyidinium chloride. Initial investigation has been made employing CH_2Cl_2 as the reaction solvent, in substitution for nitromethane. It was

found that **31** was not generated, indicating that an acidic solvent is required for this transformation.

The adduct [Ni(C_4F_8)Cl(bipy)($NCCH_3$)] (**39**) was treated with a range of one-electron oxidants in acetonitrile. Treatment of **39** with $NOBF_4$ resulted in both gas formation and a mixture of metallacycle products. It is evident that this system also generates volatile perfluorocarbon species, such as C_4F_6 and C_4F_8, which have been examined using ^{19}F NMR and HPLC/MS. Encouragingly, treatment of **39** with [Fe(C_5H_5)$_2$][BF_4] in acetonitrile proceeded relatively cleanly, generating two new metallacycles that have been observed using ^{19}F NMR. Further investigations of this reaction by direct injection into the MS may help in characterizing a resulting Ni(IV) cation of this reaction and is discussed further in Chapter 6 as a general approach to further characterization of the generated metallacyclic products.

6. Conclusions and Future Directions

The work described in this thesis has been focused on the generation of Ni(IV) metallacycle complexes *via* one-electron oxidations of various Ni(III) precursors. Synthesis and characterization (NMR, EPR, UV/Vis, IR spectroscopy and electrochemistry) of new Ni(III) precursors has also been described.

Another method that may prove valuable for the investigation of systems in which transient Ni(IV) cationic complexes are generated in trace amounts is mass spectrometry (MS). Direct injection of reaction solutions into the MS may allow for further characterization of generated cationic Ni(IV) complexes. Colton *et al*. have previously described employing electrospray mass spectrometry (ESMS) to study cationic products generated *via* the treatment of Ni(II) dithiocarbamate with $NOBF_4$.[69] The ES technique allows for the generated ions complexes in solution to be very gently transferred to the gas phase with minimal fragmentation.

Further investigations into the treatment of $[Ni(C_4F_8)(bipy)(\mu\text{-}Cl)]_2$ (**37**) with dmap in CH_2Cl_2 are necessary to determine the exact mode of $[Ni(C_4F_8)(bipy)]$ (**31**) formation. Although CV experiments of $[Ni(C_4F_8)(bipy)(\mu\text{-}Cl)]_2$ (**37**) with dmap performed in nitromethane were inconclusive, investigations into the electrochemistry of the analogous CH_2Cl_2 system could prove useful in characterizing the likely intermediate $[Ni(C_4F_8)Cl(bipy)(dmap)]$.

Another approach that may prove valuable in isolating a Ni(IV) complex and probing the reactivity of the Ni-R_F bond is by synthesizing the analogous cyano-bridged dimer $[Ni(C_4F_8)(bipy)(\mu\text{-}CN)]_2$. The formation of the paramagnetic cyano-bridged complex can be probed readily by IR spectroscopy, due to the strong $\upsilon(C{\equiv}N)$ stretching frequency. Furthermore, the mixed-valent [Ni(III)/Ni(IV)] radical cation may be stabilized by the strongly bridging-cyano moieties.

References

(1) Chambers, R. D., *Fluorine in Organic Chemistry*, Wiley-Blackwell, **2004**, p. 3-5.

(2) Kitazume, T., *J. Fluorine Chem.* **2000**, *105*, 265-278.

(3) Benskin, J. P., Yeung, L. W. Y., Yamashita, N. Taniyasu, S., Lam, P. K. S., Martin, J. W., *Environ. Sci. Technol.* ***2010,*** *44*, 9049 and references therein.

(4) Adams, D. E. C., Halden, R. U., *ACS Symposium Series: Contaminants of Emerging Concern in the Environment: Ecological and Human Health Considerations* **2010**, *1048*, 539-560.

(5) Tavener, S. J., Clark, J. H., *J. Fluorine Chem.* **2003**, *123*, 31-36.

(6) Stone, F. G., *J. Fluorine Chem.* **1999**, *100*, 227-234.

(7) King, R. B., Stafford, S. L., Treichel, P. M., Stone, G. A., *J. Am. Chem. Soc.* **1961**, *83*, 3604-3608.

(8) King, R. B., Treichel, P. M., Stone, F. G. A., *J. Am. Chem. Soc.* **1961**, *83*, 3593-3597.

(9) Green, M., Osborn, R. B. L., Rest, A. J., Stone, F. G. A., *J. Chem. Soc. (A)* **1968**, 2525-2530.

(10) Beveridge, A. D., Clark, H. C., *J. Organomet. Chem.* **1968**, *11*, 601-614.

(11) Green, M., Howard, J. A. K., Laguna, A., Murray, M., Spencer, J. L., Stone. F. G. A., *J. Chem. Soc. Chem. Commun.* **1975**, 451.

(12) Cámpora, J., Palma, P., Carmona, E., *Coord. Chem. Re*v. **1999**, *193*, 207-281.

(13) Manuel, T., Stafford, S. L., Stone, F. G. A., *J. Am. Chem. Soc.* **1961**, *83*, 249-250.

(14) Coyle, T. D., King, R. B., Pitcher, E., Stafford, S. L., Treichel, P. M., Stone, F. G. A., *J. Inorg. Nucl. Chem.* **1961**, *20*, 172-173.

(15) Cundy, C. S., Green, M., Stone, F. G. A., *J. Chem. Soc. (A)* **1970**, 1647-1653.

(16) Mukhedkar, A. J., Green, M., Stone, F. G. A., *J. Chem. Soc. (A)* **1969**, 3023-3026.

(17) Greco, A., Green, M., Shakshooki, S. K., Stone, F. G. A., *J. Chem. Soc., Chem. Commun.* **1970**, *20*, 1374-1375.

(18) Bennett, M. A., Hockless, D. C. R., Wenger, E., *Organometallics* **1995**, *14*, 2091-2101.

(19) Bennett, M. A., Glewis, M., Hockless, D. C. R., Wenger, E., *Dalton Trans*. **1997**, *18*, 3105-3114.

(20) Richmond, T. G., *Angew. Chem. Int. Ed.* **2000**, *39*, 3241-3244.

(21) Gipson, S. L., Kneten, K., *Inorg. Chim. Acta* **1989**, 157, 143-145.

(22) Karel, K. J., Tulip, T. H., Ittel, S. D., *Organometallics* **1990**, *9*, 1276-1282.

(23) Baker, R. T., Beatty, R. P., Sievert, A. C., Wallace, R. L., Jr., *PCT Int. Appl.* **1996**, U.S Patent 5,670,679, E. I. Du Pont de Nemours & Co., USA.

(24) Gasafi-Martin, W., Oberendfellner G., von Werner, K., *Can. J. Chem.* **1996**, *74*, 1922-1924.

(25) Schwiebert, K., Stryker, J. M., *J. Am. Chem. Soc.* **1994**, *116*, 11570-11571.

(26) Klein, H.-F., Kraikivskii, P., *Angew. Chem. Int. Ed.* **2009**, *48*, 260-261.

(27) Klein, H.-F., Bickelhaupt, A., Jung, T., Cordier, G., *Organometallics* **1994**, *13*, 2557-2559.

(28) Crabtree, R. H., Mingos, D. M. P., *Comprehensive Organometallic Chemistry III* **2007**, *13*, p. 101-132.

(29) Jiang, H.-W., Chem, Q.-Y., Xiao, J.-C., Gu, Y.-C. *Chem. Commun.* **2009**, 3732-3734.

(30) Bhattacharya, S., Saha, B., Dutta, A., Banerjee, P., *Coord. Chem. Rev.* **1998**, *170*, 47-74.

(31) Haines, R. I., McAuley, A. *Coord. Chem. Rev.* **1981**, *39*, 77-119.

(32) Nag, K., Chakravorty, A. *Coord. Chem. Rev.* **1980**, *33*, 87-147.

(33) Alonso, P. J., Falvello, L. R., Forniés, J., Martin, A., Menjón, B., Rodríguez, G. *Chem. Commun.* **1997**, 503-504.

(34) Kleij, A. W., Gossage, R. A., Klein Gebbink, R. J. M., Brinkmann, N., Reijerse, E. J., Kragl, U., Lutz, M., Spek, A. L, van Koten, G. *J. Am. Chem. Soc.* **2000**, *122*, 12112-12124.

(35) van de Kuil, L. A., Veldhuizen, Y. S. J., Grove, D. M., Zwikker, J. W., Jenneskens, L. W., Drenth, W., Smeets, W. J. J., Spek, A. L., van Koten, G. *J. Organomet. Chem.* **1995**, *488*, 191-197.

(36) Klein, H.-F., Bickelhaupt, A., Hammerschmitt, B., Flörke, U., Haupt, H. J., *Organometallics* **1994**, *13*, 2944-2950.

(37) Dimitrov, V., Linden, A., *Angew. Chem. Int. Ed.* **2003**, *42*, 2631-2633.

(38) Carnes, M., Buccella, D., Chen, J. Y.-C., Ramirez, A. P., Turro, N. J., Nuckolls, C., Steigerwald, M., *Angew. Chem. Int. Ed.* **2009**, *48*, 290-294.

(39) Olechowski, J. R., McAlister, C. G., Clark, R. F., *Inorg. Chem.* **1964**, 246-247.

(40) Cundy, C. S., Green, M, Stone, F. G. A., *J. Chem. Soc. (A)* **1970**, 1647-1653.

(41) Harmjanz, M., Gorelsky, S. I., Morris, D. E., Scott, B. L., Baker, R. T., Knottenbelt, S. Z., Kirk, M. L., paper submitted for publication, **2011**.

(42) Izutsu, K., *Electrochemistry in Nonaqueous Solutions*, Wiley-VCH, **2009**, p. 329.

(43) Becke, A. D., *J. Chem. Phys.* **1993**, *98*, 5648-5652.

(44) Lee, C., Yang, W., Parr, R. G., *Phys. Rev.* **1988**, *37*, 785-789.

(45) Schafer, A., Huber, C., Ahlrichs, R., *J. Chem. Phys.* **1994**, *100*, 5829-5835.

(46) Reed, A. E.; Curtiss, L. A.; Weinhold, F. *Chem. Rev.* **1988**, *88*, 899-926.

(47) Sheldrick, G. M. *SHELXS-97*, University of Göttingen: Göttingen, Germany, **1997**.

(48) Sheldrick, G. M. - Bruker AXS Inc., Madison, Wisconsin, USA, **2003**.

(49) Curtis, N. F., *J. Chem. Soc. (A),* **1968**, 1579-1584.

(50) Kochi, J. K., *Acc. Chem. Res.***1992**, *25*, 39-47.

(51) Connelly, N. G., Davies, J. D., *J. Organomet. Chem.* **1972**, *38*, 385-390.

(52) Connelly, N. G., Geiger, W. E., *Chem. Rev.* **1996**, *96*, 877-910.

(53) Gash, V. W., Bauer, D. J., *J. Org. Chem.* **1966**, *31*, 3602-3607.

(54) Ahn, G., Baker, R. T., Harmjanz, M., Farhat, A., unpublished work.

(55) Gillespie, R. J., Robinson, E. A., *Can. J. Chem.* **1961**, *39*, 2171-2178.

(56) Gutmann, V., *Coord. Chem. Rev.*, **1976**, *18*, 225-255.

(57) Duffin, B., Wallwork, S. C., *Acta Cryst.* **1966**, *20*, 210-213.

(58) Butts, M. D., Scott, B. L., Kubas, G. J. *J. Am. Chem. Soc.* **1996**, *118*, 11831-11843.

(59) Compton, R. G., Banks, C. E., *Understanding Voltammetry*, World Scientific, **2007**, p. 107.

(60) Monk, P. M. S., *Fundamentals of Electroanalytical Chemistry*, John Wiley and Sons, **2001**, p. 158.

(61) Dolbier, W.R. Jr., *Guide to Fluorine NMR for Organic Chemists*, Wiley: New Jersey, **2009**, p. 13.

(62) Augustin-Nowacka, D., Chmurzyński, L., *J. Solution Chem.* **2000**, *29*, 837-846.

(63) Henne, B. J., Bartak, D. E. *Inorg. Chem.* **1984**, *23*, 369-373.

(64) Goldcamp, M. J., Robison, S. E., Krause Bauer, J. A., Baldwin, M. J., *Inorg. Chem.* **2002**, *41*, 2307-2309.

(65) Chlistunoff, J. B., Bard, A. J., *Inorg. Chem.* **1992**, *31*, 4582-4587.

(66) Ceder, R. M., Muller, G., Ordinas, M. Ordinas, J. I. *Dalton Trans.* **2007**, 83-90.

(67) Barefield, E. K., Busch, D. H., *Chem. Commun.* **1970**, 523-524.

(68) Steinfeld, G., Kersting, B., *Z. Anorg. Allg. Chem.* **2009**, *635*, 260-264.

(69) Bond, A. M., Colton, R., D'Agostino, A., Harvey, J., Traeger, J. C., *Inorg. Chem.* **1993**, *32*, 3952-3956.

Appendix A. IR Spectra.

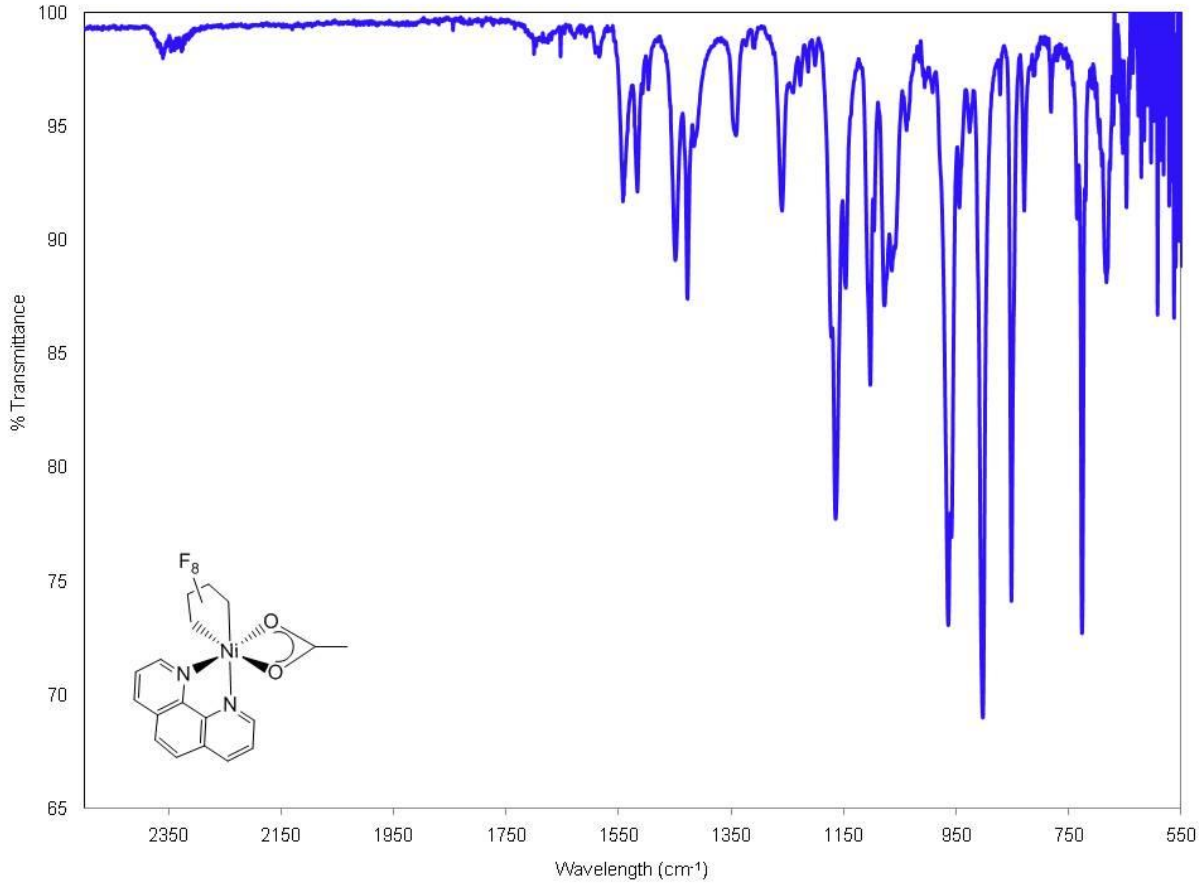

Figure A1. IR spectrum of [Ni(C_4F_8)(phen)(OAc)] (**35**).

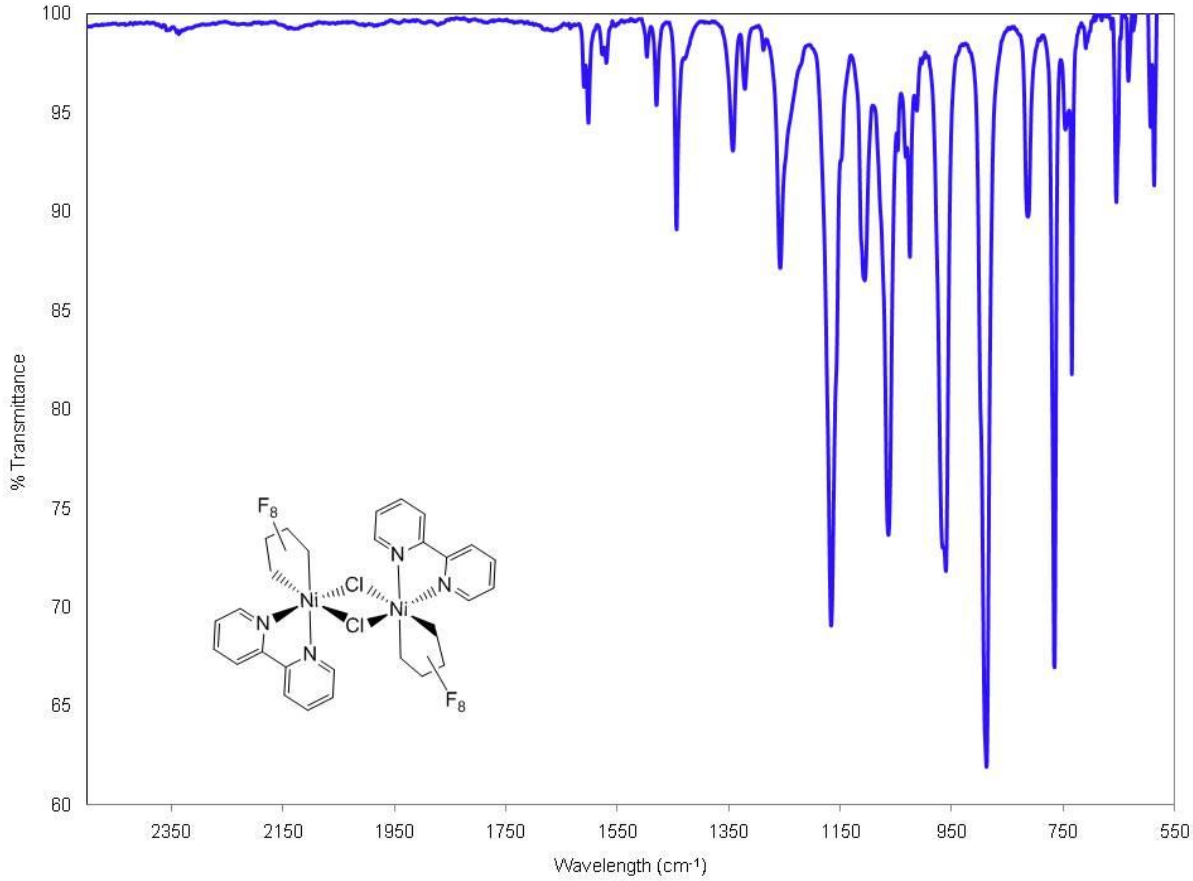

Figure A2. IR spectrum of $[Ni(C_4F_8)(bipy)(\mu\text{-}Cl)]_2$ (**37**).

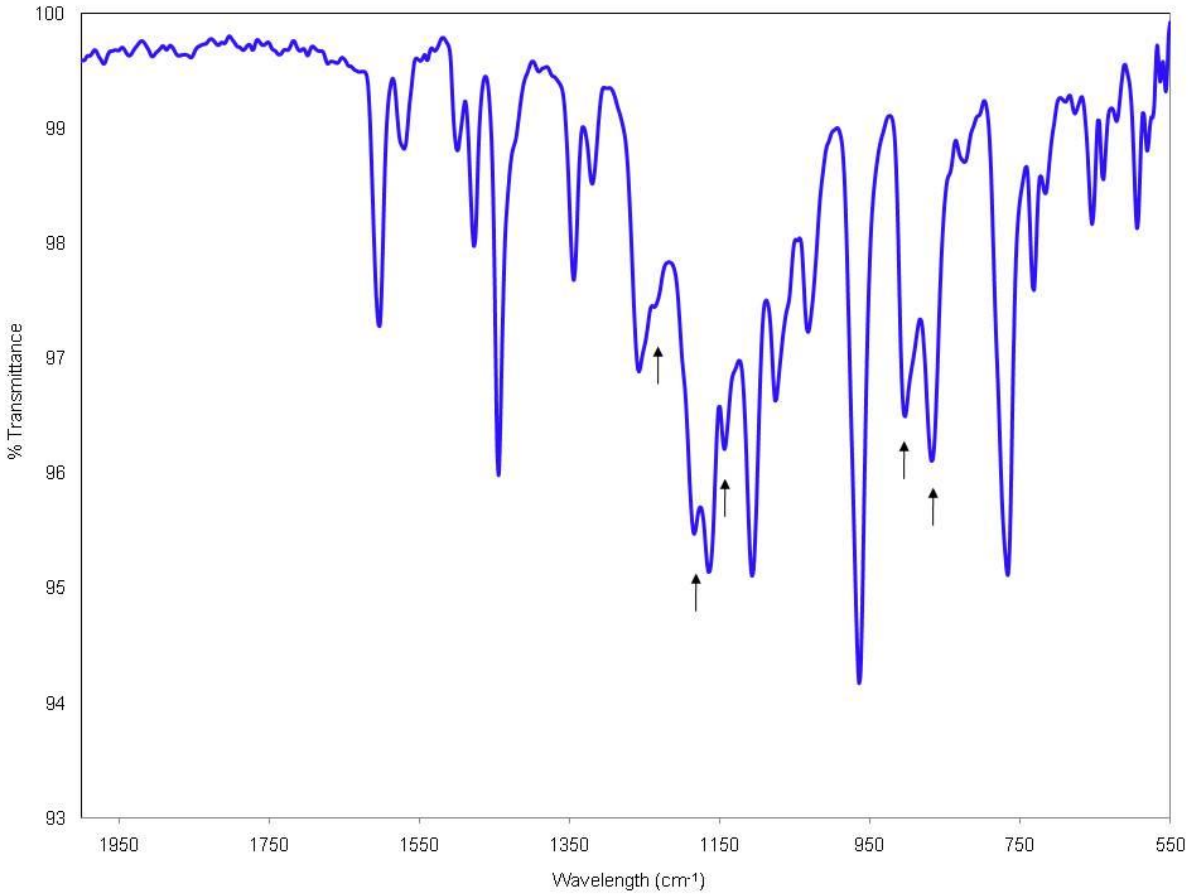

Figure A3. IR spectrum of intermediate complex **38**.

Appendix B. Single Crystal XRD Data.

Table B1. Crystallographic experimental parameters for **31**, **37**, and **39**.

	31	**37**	**39**
Empirical Formula	$C_{14}H_8F_8N_2Ni$	$C_{32}H_{24}C_{l2}F_{16}N_4Ni_2O$	$C_{16}H_{11}ClF_8N_3Ni$
Formula weight	414.91	972.87	491.44
Crystal system	monoclinic	monoclinic	monoclinic
Space group	P 21/c	P 21/c	P2(1)/c
a (Å)	10.3442(3)	10.0256(3)	9.1412(14)
b (Å)	6.7466(2)	20.1881(6)	12.956(2)
c (Å)	19.7628(7)	10.1123(3)	15.689(2)
α (deg)	90	90	90
β (deg)	93.550(2)	103.630(2)	97.788(3)
γ (deg)	90	90	90
V ($Å^3$)	1376.56(8)	1989.07(10)	1840.9(5)
Z	4	2	4
ρ_{calc} (Mg/m^3)	2.002	1.624	1.773
F (000)	824.0	972.0	980
Absorption coefficient (mm^{-1})	1.507	1.188	1.284
T (K)	200	200	200
λ (Å)	0.71073	0.71073	0.71073
Reflections collected / unique	9195 / 4089	28153 / 4911	12316 / 2987
R1[a]	0.0344	0.0378	0.0721
wR2[b]	0.0851	0.1162	0.1640
GOF (F^2)	1.014	1.040	1.050

[a] $R1 = [\Sigma||F_o| - |F_c||]/ \Sigma/|F_o|$ for $F_o^2 > 2\sigma(F_o^2)$. [b] $wR2 = \{[\Sigma w(F_o^2 - F_c^2)^2]/[\Sigma w(F_o^4)]\}^{1/2}$ for all data.

Table B2. Bond distances (Å) in [Ni(C_4F_8)(bipy)] (**31**).

Bond	**Distance (Å)**	**Bond**	**Distance (Å)**
Ni(1)-C(14)	1.9061(19)	C(7)-C(8)	1.380(3)
Ni(1)-C(11)	1.9113(19)	C(8)-C(9)	1.381(3)
Ni(1)-N(2)	1.9558(15)	C(9)-C(10)	1.381(3)
Ni(1)-N(1)	1.9660(15)	F(1)-C(11)	1.386(2)
N(1)-C(1)	1.344(2)	F(2)-C(11)	1.386(2)
N(1)-C(5)	1.354(2)	F(3)-C(12)	1.353(2)
N(2)-C(10)	1.345(2)	F(4)-C(12)	1.369(3)
N(2)-C(6)	1.357(2)	F(5)-C(13)	1.372(3)
C(1)-C(2)	1.392(3)	F(6)-C(13)	1.353(2)
C(2)-C(3)	1.372(3)	F(7)-C(14)	1.389(2)
C(3)-C(4)	1.378(3)	F(8)-C(14)	1.381(2)
C(4)-C(5)	1.394(2)	C(11)-C(12)	1.531(3)
C(5)-C(6)	1.470(3)	C(12)-C(13)	1.500(3)
C(6)-C(7)	1.385(3)	C(13)-C(14)	1.527(3)

Table B3. Bond angles (°) in [Ni(C_4F_8)(bipy)] (**31**).

Bond	**Angle (°)**	**Bond**	**Angle (°)**
C(14)-Ni(1)-C(11)	85.22(8)	C(7)-C(6)-C(5)	123.64(17)
C(14)-Ni(1)-N(2)	175.70(8)	C(6)-C(7)-C(8)	119.37(19)
C(14)-Ni(1)-N(2)	175.70(8)	C(9)-C(8)-C(7)	118.97(19)
C(11)-Ni(1)-N(2)	96.51(7)	C(8)-C(9)-C(10)	118.8(2)
C(14)-Ni(1)-N(1)	95.64(7)	N(2)-C(10)-C(9)	123.15(19)
C(11)-Ni(1)-N(1)	175.78(8)	F(1)-C(11)-F(2)	103.47(15)
N(2)-Ni(1)-N(1)	82.92(6)	F(1)-C(11)-C(12)	104.53(17)
C(1)-N(1)-C(5)	118.03(16)	F(2)-C(11)-C(12)	107.12(16)
C(1)-N(1)-Ni(1)	128.17(13)	F(1)-C(11)-Ni(1)	115.93(12)
C(5)-N(1)-Ni(1)	113.74(12)	F(2)-C(11)-Ni(1)	112.53(14)
C(10)-N(2)-C(6)	117.58(16)	C(12)-C(11)-Ni(1)	112.40(13)
C(10)-N(2)-Ni(1)	128.14(13)	F(3)-C(12)-F(4)	107.63(18)
C(6)-N(2)-Ni(1)	114.18(12)	F(3)-C(12)-C(13)	113.19(19)
N(1)-C(1)-C(2)	122.74(19)	F(4)-C(12)-C(13)	107.45(18)
C(3)-C(2)-C(1)	118.84(19)	F(3)-C(12)-C(11)	113.41(17)
C(2)-C(3)-C(4)	119.33(18)	F(4)-C(12)-C(11)	109.24(18)
C(3)-C(4)-C(5)	119.31(19)	C(13)-C(12)-C(11)	105.73(17)
N(1)-C(5)-C(4)	121.74(18)	F(6)-C(13)-F(5)	107.23(17)
N(1)-C(5)-C(6)	114.76(15)	F(6)-C(13)-C(12)	112.83(19)
C(4)-C(5)-C(6)	123.49(17)	F(5)-C(13)-C(12)	107.24(19)
N(2)-C(6)-C(7)	122.07(18)	F(6)-C(13)-C(14)	113.89(18)
N(2)-C(6)-C(5)	114.29(15)	F(5)-C(13)-C(14)	109.36(18)
C(12)-C(13)-C(14)	106.09(16)	F(8)-C(14)-F(7)	104.21(14)
F(8)-C(14)-C(13)	105.46(16)	F(7)-C(14)-C(13)	106.64(15)
F(8)-C(14)-Ni(1)	114.93(12)	F(7)-C(14)-Ni(1)	112.04(13)
C(13)-C(14)-Ni(1)	112.80(13)		

Table B4. Bond distances (Å) in [Ni(C_4F_8)(bipy)(μ-Cl)] (**37**).

Bond	**Distance (Å)**	**Bond**	**Distance (Å)**
Ni(1)-C(14)	1.972(2)	C(3)-C(4)	1.373(4)
Ni(1)-C(11)	1.985(2)	C(4)-C(5)	1.401(3)
Ni(1)-N(1)	2.0181(17)	C(5)-C(6)	1.472(4)
Ni(1)-N(2)	2.1309(19)	C(6)-C(7)	1.391(3)
Ni(1)-Cl(1)	2.3211(5)	C(7)-C(8)	1.364(5)
Ni(1)-Cl(1A)	2.5615(6)	C(8)-C(9)	1.369(5)
Cl(1)-Ni(1A)	2.5615(6)	C(9)-C(10)	1.387(4)
N(1)-C(1)	1.342(3)	C(11)-C(12)	1.532(3)
N(1)-C(5)	1.345(3)	C(12)-C(13)	1.510(3)
N(2)-C(10)	1.338(3)	C(13)-C(14)	1.534(3)
N(2)-C(6)	1.349(3)	O(1)-C(15)	1.55(5)
F(1)-C(11)	1.365(2)	O(1)-C(18)	1.40(2)
F(2)-C(11)	1.356(2)	C(15)-C(16)	1.578(15)
F(3)-C(12)	1.365(3)	C(16)-C(17)	1.657(16)
F(4)-C(12)	1.345(3)	C(17)-C(18)	1.378(16)
F(5)-C(13)	1.356(3)	O(1')-C(15')	1.54(5)
F(6)-C(13)	1.348(3)	O(1')-C(18')	1.405(19)
F(7)-C(14)	1.361(2)	C(15')-C(16')	1.664(18)
F(8)-C(14)	1.360(2)	C(16')-C(17')	1.627(18)
C(1)-C(2)	1.388(3)	C(17')-C(18')	1.364(19)
C(2)-C(3)	1.365(4)		

Table B5. Bond angles (°) in [Ni(C_4F_8)(bipy)(μ-Cl)] (**37**).

Bond	**Angle (°)**	**Bond**	**Angle (°)**
C(14)-Ni(1)-C(11)	84.32(8)	N(2)-C(10)-C(9)	122.6(3)
C(14)-Ni(1)-N(1)	86.41(8)	F(2)-C(11)-F(1)	104.99(16)
C(11)-Ni(1)-N(1)	170.10(8)	F(2)-C(11)-C(12)	106.56(17)
C(14)-Ni(1)-N(2)	96.99(8)	F(1)-C(11)-C(12)	107.61(17)
C(11)-Ni(1)-N(2)	98.64(8)	F(2)-C(11)-Ni(1)	112.64(13)
N(1)-Ni(1)-N(2)	79.05(8)	F(1)-C(11)-Ni(1)	113.53(14)
C(14)-Ni(1)-Cl(1)	175.20(6)	C(12)-C(11)-Ni(1)	111.04(14)
C(11)-Ni(1)-Cl(1)	92.69(6)	F(4)-C(12)-F(3)	107.08(19)
N(1)-Ni(1)-Cl(1)	96.79(5)	F(4)-C(12)-C(13)	111.8(2)
N(2)-Ni(1)-Cl(1)	87.15(5)	F(3)-C(12)-C(13)	108.08(19)
C(14)-Ni(1)-Cl(1A)	94.30(6)	F(4)-C(12)-C(11)	113.45(19)
C(11)-Ni(1)-Cl(1A)	92.40(6)	F(3)-C(12)-C(11)	109.09(19)
N(1)-Ni(1)-Cl(1A)	91.73(5)	C(13)-C(12)-C(11)	107.17(17)
N(2)-Ni(1)-Cl(1A)	164.90(6)	F(6)-C(13)-F(5)	107.21(19)
Cl(1)-Ni(1)-Cl(1A)	82.052(18)	F(6)-C(13)-C(12)	108.98(19)
Ni(1)-Cl(1)-Ni(1A)	97.950(18)	F(5)-C(13)-C(12)	111.4(2)
C(1)-N(1)-C(5)	118.71(19)	F(6)-C(13)-C(14)	109.50(19)
C(1)-N(1)-Ni(1)	124.64(15)	F(5)-C(13)-C(14)	112.87(19)
C(5)-N(1)-Ni(1)	116.57(15)	C(12)-C(13)-C(14)	106.85(18)
C(10)-N(2)-C(6)	118.1(2)	F(8)-C(14)-F(7)	105.84(16)
C(10)-N(2)-Ni(1)	128.87(17)	F(8)-C(14)-C(13)	107.98(18)
C(6)-N(2)-Ni(1)	112.93(16)	F(7)-C(14)-C(13)	107.97(17)
N(1)-C(1)-C(2)	122.6(2)	F(8)-C(14)-Ni(1)	112.50(13)
C(3)-C(2)-C(1)	119.0(3)	F(7)-C(14)-Ni(1)	109.60(14)
C(2)-C(3)-C(4)	119.0(2)	C(13)-C(14)-Ni(1)	112.63(14)
C(3)-C(4)-C(5)	120.0(2)	C(15)-O(1)-C(18)	103.0(19)
N(1)-C(5)-C(4)	120.7(2)	O(1)-C(15)-C(16)	106(3)
N(1)-C(5)-C(6)	115.98(19)	C(15)-C(16)-C(17)	94.6(9)

C(4)-C(5)-C(6)	123.4(2)	C(18)-C(17)-C(16)	109.3(9)
N(2)-C(6)-C(7)	121.7(3)	C(17)-C(18)-O(1)	113.1(13)
N(2)-C(6)-C(5)	115.47(19)	C(15')-O(1')-C(18')	98(2)
C(7)-C(6)-C(5)	122.9(2)	O(1')-C(15')-C(16')	102(4)
C(8)-C(7)-C(6)	119.3(3)	C(17')-C(16')-C(15')	90.4(11)
C(7)-C(8)-C(9)	119.7(3)	C(18')-C(17')-C(16')	106.6(11)
C(8)-C(9)-C(10)	118.7(3)	C(17')-C(18')-O(1')	117.1(14)

Table B6. Bond distances (Å) in [Ni(C_4F_8)Cl(bipy)($NCCH_3$)] (**39**).

Bond	**Distance (Å)**	**Bond**	**Distance (Å)**
Ni(1)-C(14)	1.962(7)	F(8)-C(14)	1.357(8)
Ni(1)-C(11)	1.996(8)	C(1)-C(2)	1.382(11)
Ni(1)-N(2)	2.021(6)	C(2)-C(3)	1.394(12)
Ni(1)-N(3)	2.180(7)	C(3)-C(4)	1.387(12)
Ni(1)-N(1)	2.196(6)	C(4)-C(5)	1.390(11)
Ni(1)-Cl(1)	2.281(2)	C(5)-C(6)	1.458(11)
N(1)-C(1)	1.327(10)	C(6)-C(7)	1.414(10)
N(1)-C(5)	1.373(10)	C(7)-C(8)	1.363(11)
F(2)-C(11)	1.379(10)	C(8)-C(9)	1.362(12)
F(3)-C(12)	1.358(9)	C(9)-C(10)	1.382(11)
F(4)-C(12)	1.343(10)	C(11)-C(12)	1.527(12)
F(5)-C(13)	1.342(10)	C(12)-C(13)	1.526(12)
F(6)-C(13)	1.332(9)	C(13)-C(14)	1.535(11)
F(7)-C(14)	1.393(8)	C(15)-C(16)	1.442(12)

Table B7. Bond angles (°) in [Ni(C_4F_8)Cl(bipy)($NCCH_3$)] (**39**).

Bond	**Angle (°)**	**Bond**	**Angle (°)**
C(14)-Ni(1)-C(11)	84.8(3)	C(7)-C(6)-C(5)	121.4(7)
C(14)-Ni(1)-N(2)	91.8(3)	C(8)-C(7)-C(6)	119.5(8)
C(11)-Ni(1)-N(2)	176.3(3)	C(7)-C(8)-C(9)	120.0(8)
C(14)-Ni(1)-N(3)	90.6(3)	C(8)-C(9)-C(10)	118.2(8)
C(11)-Ni(1)-N(3)	87.4(3)	N(2)-C(10)-C(9)	123.7(8)
N(2)-Ni(1)-N(3)	91.1(3)	F(1)-C(11)-F(2)	105.7(6)
C(14)-Ni(1)-N(1)	90.1(3)	F(1)-C(11)-C(12)	107.6(7)
C(11)-Ni(1)-N(1)	102.8(3)	F(2)-C(11)-C(12)	108.0(6)
N(2)-Ni(1)-N(1)	78.7(2)	F(1)-C(11)-Ni(1)	111.8(5)
N(3)-Ni(1)-N(1)	169.8(2)	F(2)-C(11)-Ni(1)	112.7(5)

C(14)-Ni(1)-Cl(1)	175.4(2)	C(12)-C(11)-Ni(1)	110.7(5)
C(11)-Ni(1)-Cl(1)	90.6(2)	F(4)-C(12)-F(3)	106.5(7)
N(2)-Ni(1)-Cl(1)	92.7(2)	F(4)-C(12)-C(13)	109.2(7)
N(3)-Ni(1)-Cl(1)	89.8(2)	F(3)-C(12)-C(13)	110.4(7)
N(1)-Ni(1)-Cl(1)	90.32(18)	F(4)-C(12)-C(11)	110.2(7)
C(1)-N(1)-C(5)	118.8(7)	F(3)-C(12)-C(11)	112.5(7)
C(1)-N(1)-Ni(1)	129.7(6)	C(13)-C(12)-C(11)	108.0(7)
C(5)-N(1)-Ni(1)	111.4(5)	F(6)-C(13)-F(5)	108.1(7)
C(6)-N(2)-C(10)	117.9(7)	F(6)-C(13)-C(12)	111.3(7)
C(6)-N(2)-Ni(1)	116.6(5)	F(5)-C(13)-C(12)	109.0(7)
C(10)-N(2)-Ni(1)	125.4(6)	F(6)-C(13)-C(14)	113.8(6)
C(15)-N(3)-Ni(1)	166.4(7)	F(5)-C(13)-C(14)	108.6(7)
N(1)-C(1)-C(2)	123.6(8)	C(12)-C(13)-C(14)	105.9(7)
C(1)-C(2)-C(3)	118.1(8)	F(8)-C(14)-F(7)	103.3(6)
C(2)-C(3)-C(4)	119.1(8)	F(8)-C(14)-C(13)	108.3(6)
C(3)-C(4)-C(5)	119.7(8)	F(7)-C(14)-C(13)	106.9(6)
N(1)-C(5)-C(4)	120.6(7)	F(8)-C(14)-Ni(1)	113.8(5)
N(1)-C(5)-C(6)	115.1(7)	F(7)-C(14)-Ni(1)	111.5(5)
C(4)-C(5)-C(6)	124.3(7)	C(13)-C(14)-Ni(1)	112.4(5)
N(2)-C(6)-C(7)	120.6(7)	N(3)-C(15)-C(16)	177.6(9)
N(2)-C(6)-C(5)	118.0(6)		

Appendix C. Coordinates of DFT-Optimized Structures.

Table C1. Coordinates of [Ni(C_4F_8)(bipy)(μ-Cl)] (**37**) in S = 1 (Å).

Atom	**X**	**y**	**z**
Cl	1.27628	-1.0005	-0.2282
F	-0.8705	-0.5228	-3.3643
F	-1.1104	-0.052	2.65735
F	-1.5914	-2.8851	2.79842
H	0.15178	-2.6284	-1.4483
H	-5.3851	-0.1656	-3.773
H	-2.9465	0.16754	-3.495
Ni	0.96232	-1.18	1.10577
N	1.89119	-2.1164	-0.4904
N	3.09586	-1.0788	1.65921
F	1.33247	-1.8139	4.42587
F	-0.7653	-1.3853	4.88744
F	-0.1048	-4.0295	3.92755
F	1.7651	-3.6103	2.16208
F	-0.0379	-3.7952	0.94264
C	1.22795	-2.7008	-1.4918
C	1.8724	-3.3465	-2.5363
H	1.28812	-3.7975	-3.3262
C	3.2569	-3.3893	-2.5377
H	3.79742	-3.8853	-3.334
C	3.94637	-2.7877	-1.4962
H	5.02502	-2.8239	-1.4735
C	3.23837	-2.1511	-0.4786
C	3.90402	-1.5042	0.67241
C	5.28718	-1.3346	0.74413

H	5.92537	-1.6566	-0.065
C	5.84185	-0.7324	1.86211
H	6.91313	-0.5917	1.93099
C	5.00137	-0.3094	2.88048
C	3.63417	-0.4977	2.73327
C	0.15501	-0.5185	2.82094
C	0.09595	-1.6489	3.87692
C	-0.2828	-2.9432	3.13589
C	0.58343	-2.9962	1.85172
Ni	-0.9623	1.18004	-1.1058
N	-1.8912	2.11639	0.49037
N	-3.0959	1.07884	-1.6592
F	-1.3325	1.81393	-4.4259
F	0.76534	1.38531	-4.8874
F	0.10482	4.02955	-3.9275
F	-1.7651	3.61032	-2.1621
F	0.03791	3.79516	-0.9426
C	-1.2279	2.70082	1.49184
C	-1.8724	3.34653	2.53633
H	-1.2881	3.79749	3.32619
C	-3.2569	3.38932	2.53772
H	-3.7974	3.88529	3.33399
C	-3.9464	2.78773	1.4962
H	-5.025	2.82395	1.4735
C	-3.2384	2.15111	0.4786
C	-3.904	1.50423	-0.6724
C	-5.2872	1.33464	-0.7441
H	-5.9254	1.65663	0.06504
C	-5.8419	0.73241	-1.8621
H	-6.9131	0.5917	-1.931

C	-5.0014	0.30939	-2.8805
C	-3.6342	0.49775	-2.7333
C	-0.155	0.51852	-2.8209
C	-0.0959	1.64894	-3.8769
C	0.28284	2.94321	-3.1359
C	-0.5834	2.99623	-1.8517
Cl	1.27628	1.00053	0.2282
F	0.87051	0.52278	3.36432
F	1.11037	0.052	-2.6573
F	1.59136	2.8851	-2.7984
H	-0.1518	2.6284	1.44832
H	5.38514	0.1656	3.77298
H	2.94647	-0.1675	3.49497

Table C2. Coordinates of [Ni(C_4F_8)(bipy)(μ-Cl)] (**37**) in S = 0 (Å).

Atom	**X**	**y**	**z**
Cl	1.27734	-0.9985	-0.2285
F	-0.8762	-0.5244	-3.3654
F	-1.1044	-0.0515	2.65878
F	-1.587	-2.8838	2.80421
H	0.15427	-2.6259	-1.4452
H	-5.3889	-0.1594	-3.7783
H	-2.9499	0.16566	-3.4964
Ni	0.96808	-1.181	1.1089
N	1.89439	-2.1159	-0.4876
N	3.09904	-1.0783	1.66125
F	1.33902	-1.8126	4.42771
F	-0.7582	-1.3824	4.89068
F	-0.0992	-4.0276	3.93228
F	1.76764	-3.6125	2.1631
F	-0.0374	-3.7937	0.94592
C	1.23041	-2.6982	-1.4898
C	1.87428	-3.3415	-2.5361
H	1.28951	-3.7908	-3.3265
C	3.25878	-3.3836	-2.5388
H	3.79885	-3.8773	-3.3368
C	3.94896	-2.7842	-1.4965
H	5.02765	-2.8197	-1.4752
C	3.2416	-2.1505	-0.4767
C	3.90745	-1.5063	0.67561
C	5.29106	-1.3418	0.74996
H	5.92966	-1.6667	-0.0577
C	5.84594	-0.7412	1.86872
H	6.91762	-0.6047	1.93955

C	5.00516	-0.3147	2.88531
C	3.63759	-0.4985	2.73592
C	0.16113	-0.5175	2.82294
C	0.10206	-1.6472	3.87962
C	-0.278	-2.942	3.13989
C	0.58654	-2.9961	1.85447
Ni	-0.9681	1.18097	-1.1089
N	-1.8944	2.11587	0.48757
N	-3.099	1.07827	-1.6612
F	-1.339	1.81264	-4.4277
F	0.75817	1.38237	-4.8907
F	0.09916	4.02763	-3.9323
F	-1.7676	3.61254	-2.1631
F	0.03738	3.79369	-0.9459
C	-1.2304	2.69821	1.48977
C	-1.8743	3.34146	2.53614
H	-1.2895	3.79082	3.32655
C	-3.2588	3.3836	2.53883
H	-3.7988	3.87728	3.33684
C	-3.949	2.78421	1.49648
H	-5.0277	2.81971	1.47522
C	-3.2416	2.15048	0.47669
C	-3.9074	1.50632	-0.6756
C	-5.2911	1.34181	-0.75
H	-5.9297	1.66673	0.05769
C	-5.8459	0.74124	-1.8687
H	-6.9176	0.60466	-1.9395
C	-5.0052	0.31468	-2.8853
C	-3.6376	0.49851	-2.7359
C	-0.1611	0.51746	-2.8229

C	-0.1021	1.6472	-3.8796
C	0.27799	2.94197	-3.1399
C	-0.5865	2.99613	-1.8545
Cl	1.27734	0.9985	0.22853
F	0.87617	0.52435	3.36543
F	1.10443	0.0515	-2.6588
F	1.58696	2.88382	-2.8042
H	-0.1543	2.62592	1.44521
H	5.38891	0.1594	3.77829
H	2.94986	-0.1657	3.49637

Table C3. Coordinates of mixed-valent [Ni(III)/Ni(IV)] radical cation derived from $[Ni(C_4F_8)(bipy)(\mu\text{-}Cl)]_2$ (**37**) (Å).

Atom	**X**	**y**	**z**
Cl	1.18553	-1.0461	-0.0929
F	-0.7697	-0.5753	-3.2437
F	-1.1889	-0.1033	2.62098
F	-1.5565	-2.9243	2.79314
H	0.0807	-2.736	-1.4977
H	-5.1721	-0.2453	-3.7381
H	-2.7572	0.00321	-3.3673
Ni	0.92212	-1.1853	1.04351
N	1.80512	-2.1408	-0.5491
N	2.93634	-0.9905	1.56475
F	1.36398	-1.7413	4.34581
F	-0.7339	-1.3792	4.85799
F	-0.0242	-4.0118	3.91877
F	1.80581	-3.5656	2.10628
F	-0.0088	-3.8224	0.9325
C	1.15807	-2.759	-1.5425
C	1.82291	-3.3905	-2.5817
H	1.25454	-3.8766	-3.3622
C	3.20892	-3.378	-2.5907
H	3.76355	-3.8569	-3.3871
C	3.88095	-2.7462	-1.5553
H	4.96013	-2.7389	-1.5426
C	3.1531	-2.1365	-0.5365
C	3.77745	-1.4786	0.6228
C	5.15804	-1.3612	0.76567
H	5.81855	-1.748	0.00479
C	5.6864	-0.7413	1.88619

H	6.75796	-0.6466	2.00466
C	4.8162	-0.2464	2.84354
C	3.45166	-0.387	2.64276
C	0.08755	-0.5054	2.77308
C	0.10842	-1.6325	3.84004
C	-0.2489	-2.9485	3.12391
C	0.6026	-3.0212	1.82312
Ni	-0.9221	1.18526	-1.0435
N	-1.8051	2.14084	0.54914
N	-2.9363	0.99051	-1.5647
F	-1.364	1.74133	-4.3458
F	0.73389	1.37915	-4.858
F	0.02418	4.01183	-3.9188
F	-1.8058	3.56563	-2.1063
F	0.00879	3.82241	-0.9325
C	-1.1581	2.75904	1.54245
C	-1.8229	3.39045	2.58174
H	-1.2545	3.87656	3.36223
C	-3.2089	3.37796	2.59065
H	-3.7635	3.85686	3.38713
C	-3.881	2.74617	1.55532
H	-4.9601	2.73888	1.54263
C	-3.1531	2.13652	0.53654
C	-3.7775	1.47863	-0.6228
C	-5.158	1.36118	-0.7657
H	-5.8185	1.74801	-0.0048
C	-5.6864	0.74133	-1.8862
H	-6.758	0.64662	-2.0047
C	-4.8162	0.2464	-2.8435
C	-3.4517	0.38702	-2.6428

C	-0.0876	0.50543	-2.7731
C	-0.1084	1.63246	-3.84
C	0.24886	2.9485	-3.1239
C	-0.6026	3.0212	-1.8231
Cl	1.18553	1.04606	0.0929
F	0.76974	0.57526	3.24368
F	1.18889	0.1033	-2.621
F	1.55645	2.92428	-2.7931
H	-0.0807	2.73595	1.49765
H	5.17212	0.24525	3.7381
H	2.75718	-0.0032	3.36728

Table C4. Coordinates of [Ni(C_4F_8)Cl(bipy)] (Å).

Atom	**X**	**y**	**z**
F	2.531954	-0.64484	1.830232
F	2.894748	-1.927609	-0.674398
H	-1.319369	-2.998063	0.745443
Ni	0.058846	-0.314448	0.672029
N	-1.754737	-1.070487	0.178275
N	-0.919447	1.425578	0.015225
F	2.345058	1.534743	-0.913805
F	4.049206	0.439642	-0.076135
F	2.766039	-0.633599	-2.437824
F	0.220154	-0.231616	-2.116407
F	0.444254	-2.251252	-1.292489
C	-2.088202	-2.351202	0.345905
C	-3.349666	-2.830506	0.030792
H	-3.582362	-3.875706	0.179541
C	-4.288265	-1.940445	-0.474378
H	-5.283283	-2.277909	-0.734847
C	-3.941112	-0.607778	-0.636399
H	-4.664775	0.09587	-1.020461
C	-2.654823	-0.191435	-0.296147
C	-2.187835	1.209285	-0.38522
C	-2.995303	2.260082	-0.815019
H	-4.00954	2.079213	-1.139224
C	-2.485662	3.550275	-0.818416
H	-3.100413	4.37749	-1.149514
C	-1.185787	3.761856	-0.383883
C	-0.434571	2.668283	0.024853
C	1.908495	0.266073	1.041136
C	2.715167	0.385869	-0.276258

C	2.320489	-0.805211	-1.171326
C	0.7769	-0.935788	-1.084008
Cl	-0.492069	-0.297051	2.842917
F	1.960524	1.46959	1.680145
H	-0.750069	4.751086	-0.359499
H	0.58019	2.78513	0.374003

Appendix D. HPL Chromatogram

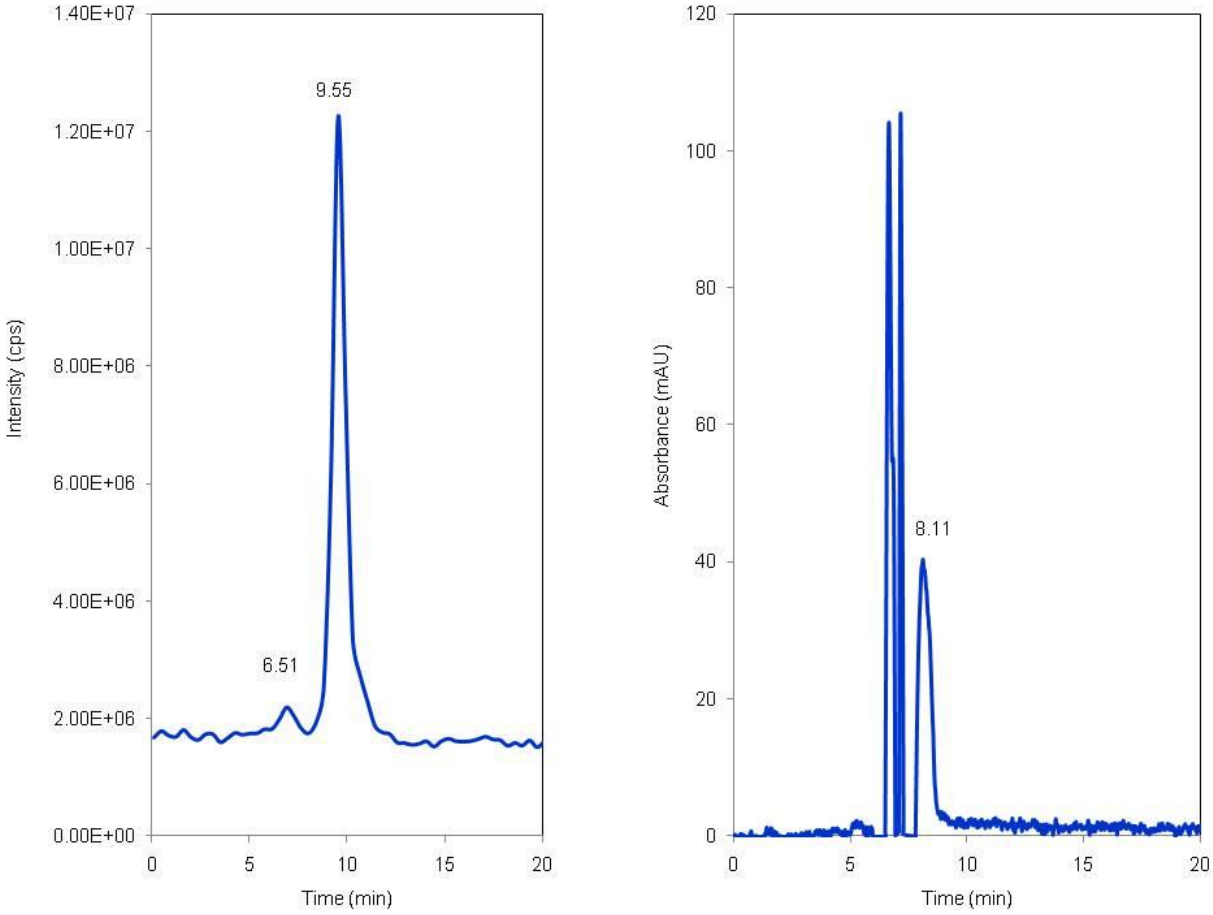

Figure D1. (a) HPL chromatogram of C_4F_6 (9.55 min) (+) ESI-MS detection (b) HPL chromatogram of C_4F_6 (+) UV detection (370 nm).

Appendix E. Contributions to Knowledge

‘High-Valent Polyfluorometallacycles: Intermediates for Green Routes to Hydrofluorocarbons’ Hunter, N. M., Farhat, A., Pell, W., Korobkov, I., Baker, R. T. 93rd Canadian Chemistry Conference and Exhibition, Toronto, ON, Canada, May 28-June 1, 2010. *(Poster presentation)*

‘Toward "Green" Routes to Fluorocarbons: New Chemistry of Iron- and Nickel Organofluorometallacycles’ Baker, R. T., Ahn, S. H., Farhat, A., Granville, S. L., Hunter, N. M., Pell, W., Korobkov, I., Harmjanz, M., Morris, D. E., Scott, B. L., *et al.*, 239th ACS National Meeting, San Francisco, CA, United States, March 21-25, 2010.